



Search for heavy neutrinos and W bosons with right-handed couplings in proton-proton collisions at $\sqrt{s} = 8 \text{ TeV}$

The CMS Collaboration*

Abstract

A search for heavy, right-handed neutrinos, N_ℓ ($\ell = e, \mu$), and right-handed W_R bosons, which arise in the left-right symmetric extensions of the standard model, has been performed by the CMS experiment. The search was based on a sample of two lepton plus two jet events collected in proton-proton collisions at a center-of-mass energy of 8 TeV corresponding to an integrated luminosity of 19.7 fb^{-1} . For models with strict left-right symmetry, and assuming only one N_ℓ flavor contributes significantly to the W_R decay width, the region in the two-dimensional (M_{W_R}, M_{N_ℓ}) mass plane excluded at a 95% confidence level extends to approximately $M_{W_R} = 3.0 \text{ TeV}$ and covers a large range of neutrino masses below the W_R boson mass, depending on the value of M_{W_R} . This search significantly extends the (M_{W_R}, M_{N_ℓ}) exclusion region beyond previous results.

Published in the European Physical Journal C as doi:10.1140/epjc/s10052-014-3149-z.

1 Introduction

The standard model (SM) [1–3] explicitly incorporates the parity violation observed in weak interactions through the use of a left-handed chiral $SU_L(2)$ gauge group which includes the left-handed gauge bosons W_L^\pm and Z_L . One of the attractive features of left-right (LR) symmetric extensions [4–7] to the standard model is that these models explain parity violation in the SM as the consequence of spontaneous symmetry breaking of a larger gauge group to $SU_L(2) \times SU_R(2)$ at a multi-TeV mass scale. The LR extensions introduce an additional right-handed $SU_R(2)$ symmetry group to the SM, which includes heavy charged (W_R^\pm) and neutral (Z_R) gauge bosons that could be produced at LHC energies.

In addition to addressing parity non-conservation in weak interactions, LR theories also provide an explanation for the mass of SM neutrinos. The observation of neutrino oscillations [8, 9] requires that neutrinos have mass, and the fact that the neutrino mass scale [10] is far below that of quarks and charged leptons suggests that the origin of neutrino mass may be distinct from the origin of mass for the other SM fermions. Heavy right-handed Majorana neutrinos ($N_e, N_\mu,$ and N_τ), which are naturally present in LR models, provide a possible explanation for the mass of SM neutrinos through the see-saw mechanism [11, 12].

We search for W_R bosons produced in a sample of proton-proton collisions at a center-of-mass energy $\sqrt{s} = 8$ TeV and collected by the CMS detector at the CERN LHC. This search, which expands upon a previous search using $\sqrt{s} = 7$ TeV data [13], assumes the production of a W_R boson that decays to a charged lepton (we consider $\ell = e, \mu$) and to a right-handed neutrino N_ℓ . The decay of the right-handed neutrino produces a second charged lepton of the same flavor together with a virtual right-handed charged boson W_R^* . When the W_R^* decays to a pair of quarks, we arrive at the decay chain:

$$W_R \rightarrow \ell_1 N_\ell \rightarrow \ell_1 \ell_2 W_R^* \rightarrow \ell_1 \ell_2 q \bar{q}.$$

The quarks hadronize into jets (j), resulting in an observable final state containing two same-flavor charged leptons and two jets. Although the potential Majorana nature of the right-handed neutrinos implies the final-state charged leptons can have the same sign, we do not impose any charge requirements on the final-state electrons or muons in this analysis.

This search is characterized by the masses of the W_R boson (M_{W_R}) and the right-handed neutrino N_ℓ (M_{N_ℓ}), which are allowed to vary independently. Although $M_{N_\ell} > M_{W_R}$ is allowed in the LR symmetric model, it is not considered in this analysis in favor of the dominant $q\bar{q}' \rightarrow W_R$ production mechanism. As the branching fraction for $W_R \rightarrow \ell N_\ell$ depends on the number of heavy-neutrino flavors accessible at LHC energies, results are first interpreted assuming that only one neutrino flavor, namely N_e or N_μ , is light enough to contribute significantly to the W_R boson decay width. Results are then interpreted assuming degenerate $N_e, N_\mu,$ and N_τ masses.

For given W_R boson and N_ℓ mass assumptions, the signal cross section can be predicted from the value of the coupling constant g_R , which denotes the strength of the gauge interactions of W_R bosons. We assume strict LR symmetry, such that g_R is equal to the (left-handed) weak interaction coupling strength g_L at M_{W_R} , and we also assume identical quark and neutrino mixing matrices for the left- and right-handed interactions. The W_R boson production cross section can then be calculated by the FEWZ program [14] using the left-handed W' model [15]. Finally, the left-right boson and lepton mixing angles are assumed to be small [16].

The theoretical lower limit on W_R mass of $M_{W_R} \gtrsim 2.5$ TeV [17, 18] is estimated from the measured size of the K_L – K_S mass difference. Searches for $W_R \rightarrow t\bar{b}$ decays at the LHC using $\sqrt{s} = 7$

and 8 TeV data [19–21] have excluded W_R boson masses below 2.05 TeV at 95% confidence level (CL), and previous searches for $W_R \rightarrow \ell N_\ell$ at the LHC excluded at 95% CL a region in the two-dimensional parameter space (M_{W_R}, M_{N_ℓ}) extending to nearly $M_{W_R} = 2.5$ TeV [13, 22]. This paper describes the first direct search that is sensitive to M_{W_R} values beyond the theoretical lower mass limit.

2 The CMS detector

The central feature of the CMS apparatus is a superconducting solenoid, of 6 m internal diameter, providing a field of 3.8 T. Within the field volume are the silicon pixel and strip tracker, the PbWO_4 crystal electromagnetic calorimeter (ECAL) and the brass and scintillator hadron calorimeter (HCAL). Muons are measured in gas-ionization detectors embedded in the steel flux-return yoke. The ECAL has an energy resolution of better than 0.5% for unconverted photons with transverse energies $E_T \equiv E/\cosh\eta > 100$ GeV. The muons are measured in the pseudorapidity window $|\eta| < 2.4$, where $\eta = -\ln[\tan(\theta/2)]$ and θ is the polar angle with respect to the counterclockwise-beam direction. The muon system detection planes are made of three technologies: drift tubes, cathode strip chambers, and resistive-plate chambers. Matching the muons to the tracks measured in the silicon tracker results in a transverse momentum ($p_T \equiv |p|/\cosh\eta$) resolution between 1 and 10% for $p_T < 1$ TeV. The inner tracker measures charged particles within the range $|\eta| < 2.5$ and provides an impact parameter resolution of ~ 15 μm and a p_T resolution of about 1.5% for 100 GeV particles. The first level of the CMS trigger system, composed of custom hardware processors, uses information from the calorimeters and muon detectors to select up to 100 kHz of events of interest. The high-level trigger (HLT) processor farm uses information from all CMS subdetectors to further decrease the event rate to about 400 Hz before data storage. A more detailed description of the CMS detector, together with a definition of the coordinate system used and the relevant kinematic variables, can be found elsewhere [23].

The particle-flow event reconstruction technique [24, 25] used to reconstruct jets in this analysis consists in reconstructing and identifying each single particle with an optimized combination of all subdetector information. The energy of photons is directly obtained from the ECAL measurement, corrected for zero-suppression effects. The energy of electrons is determined from a combination of the track momentum at the main interaction vertex, the corresponding ECAL cluster energy, and the energy sum of all bremsstrahlung photons attached to the track. The energy of muons is obtained from the corresponding track momentum. The energy of charged hadrons is determined from a combination of the track momentum and the corresponding ECAL and HCAL energy, corrected for zero-suppression effects and for the response function of the calorimeters to hadronic showers. Finally, the energy of neutral hadrons is obtained from the corresponding corrected ECAL and HCAL energy.

3 Data and Monte Carlo samples

The search for W_R boson production described in this paper is performed using pp collision data collected with the CMS detector at $\sqrt{s} = 8$ TeV in 2012. The data sample corresponds to an integrated luminosity of 19.7 fb^{-1} . Candidate $W_R \rightarrow eN_e$ events are collected using a double-electron trigger that requires two clusters in ECAL with $E_T > 33$ GeV each. These ECAL clusters are loosely matched at the HLT stage to tracks formed from hits in the pixel detector. To reject hadronic backgrounds, only a small amount of energy in the HCAL may be associated with the HLT electron candidates. Muon channel events are selected with a single-

muon trigger that requires at least one candidate muon with $p_T > 40 \text{ GeV}$ and $|\eta| < 2.1$, as reconstructed by the HLT.

Simulated $W_R \rightarrow \ell N_\ell$ signal samples are generated assuming $M_{N_\ell} = \frac{1}{2} M_{W_R}$ using PYTHIA 6.4.26 [26], a tree-level Monte Carlo (MC) generator, with CTEQ6L1 parton distribution functions (PDF) [27] and underlying event tune Z2* [28]. The MC generator includes the LR symmetric model with the assumptions previously mentioned. The final state leptons and jets in these signal events are sufficiently energetic to allow reconstruction effects to be addressed apart from the kinematic requirements discussed below. With this separation, the extension from $M_{N_\ell} = \frac{1}{2} M_{W_R}$ to the full two-dimensional (M_{W_R}, M_{N_ℓ}) mass plane for signal events is straight-forward, as is discussed in Section 7. The dominant backgrounds to W_R boson production include SM processes with at least two charged leptons with large transverse momentum, namely $t\bar{t} \rightarrow bW^+ \bar{b}W^-$ and Drell–Yan (DY)+jets processes. All remaining SM background events, which collectively contribute less than 10% to the total background level, are dominated by diboson and single top quark processes. The $t\bar{t}$ background is estimated using control samples in data and a simulated sample of fully leptonic $t\bar{t}$ decays, which are generated using the tree-level matrix element MC generator MADGRAPH 5.1.4.8 [29]. The DY+jets background is estimated using exclusive DY+n jets ($n = 0, 1, 2, 3, 4$) simulated samples generated with MADGRAPH 5.1.3.30. For the above MADGRAPH samples, parton showering, fragmentation, and the underlying event are handled by PYTHIA. A statistically comparable sample of DY+jets events generated with the tree-level MC event generator SHERPA 1.4.2 [30], which incorporates parton showering and other effects in addition to the hard process, is used to help quantify the systematic uncertainty in the DY+jets background estimation. Simulated diboson (WW, WZ, and ZZ) events are generated using PYTHIA 6.4.26, with the additional small contributions from diboson scattering processes generated with MADGRAPH 5.1.3.30. The simulated single top quark (namely, tW) background sample is generated via the next-to-leading-order MC generator POWHEG 1.0 [31–34]. Parton showering and other effects are handled by PYTHIA for the diboson and single top quark background samples.

The generated signal and SM background events pass through a full CMS detector simulation based on GEANT4 [35], and are reconstructed with the same software used to reconstruct collision data, unless otherwise noted. The simulation is compared to data using various control samples, and when necessary the simulation is adjusted to account for slight deviations seen with respect to data. Additional pp collisions in the same beam crossing (pileup) are also included for each simulated event to realistically describe the $\sqrt{s} = 8 \text{ TeV}$ collision environment.

4 Event selection and object reconstruction

We assemble W_R boson candidates from the two highest- p_T (leading) jets and two highest- p_T same-flavor leptons (electrons or muons) reconstructed in collision data or simulation events. Candidate events are first selected by the CMS trigger system using the lepton triggers described previously. The electron and muon trigger efficiencies are determined using the “tag and probe” techniques applied to $Z \rightarrow \ell\ell$ candidates [36–38]. Simple triggers, requiring a single ECAL cluster with $E_T > 300 \text{ GeV}$, collected events with high- p_T electrons to help evaluate the trigger efficiency for electron channel events with high dielectron mass [39]. Following the application of object and event selection requirements mentioned below, the trigger efficiency for $W_R \rightarrow \ell N_\ell$ candidate events is greater than 99% (98%) in the electron (muon) channel.

Because of the large expected mass of the W_R boson, electron and muon reconstruction and identification are performed using algorithms optimized for objects with large transverse momentum [36, 39]. Non-isolated muon backgrounds are suppressed by computing the transverse

momentum sum of all additional tracks within a cone of $\Delta R < 0.3$ about the muon direction, where $\Delta R = \sqrt{(\Delta\eta)^2 + (\Delta\phi)^2}$ (azimuthal angle ϕ in radians), and requiring the p_T sum to be less than 10% of the muon transverse momentum. This isolation requirement is only weakly dependent on the number of pileup collisions in the event, as tracks with a large Δz separation from the muon, i.e., tracks from other pp collisions, are not included in the isolation sum. Electrons are expected to have minimal associated HCAL energy and also to appear isolated in both calorimeters and in the tracker. To minimize the effects of pileup, electrons must be associated with the primary vertex, which is the collision vertex with the highest $\sum p_T^2$ of all associated tracks. As pileup collisions also produce extra energy in the calorimeters and can make the electron appear non-isolated, calorimeter isolation for electron candidates is corrected for the average energy density in the event [40].

Jets are reconstructed using the anti- k_T clustering algorithm [41] with a distance parameter of 0.5. Charged and neutral hadrons, photons, and leptons reconstructed with the CMS particle-flow technique are used as input to the jet clustering algorithm. To reduce the contribution to jet energy from pileup collisions, charged hadrons that do not originate from the primary vertex in the event are not used in jet clustering. After jet clustering, the pileup calorimeter energy contribution from neutral particles is removed by applying a residual average area-based correction [40, 42]. Jet identification requirements [43] suppress jets from calorimeter noise and beam halo, and the event is rejected if either of the two highest- p_T jet candidates fails the identification criteria. The jet four-momenta are corrected for zero-suppression effects and for the response function of the calorimeters to hadronic showers based on studies with simulation and data [44]. As the electrons and muons from W_R boson decay are likely to be spatially separated from jets in the detector, we reject any lepton found within a cone of radius $\Delta R < 0.5$ from the jet axis for either of the two leading jets.

After selecting jets and isolated electrons or muons in the event, $W_R \rightarrow \ell N_\ell$ candidates are formed using the two leading same-flavor leptons and the two leading jets that satisfy the selection criteria. The leading (subleading) lepton is required to have $p_T > 60$ (40) GeV, while the p_T of each jet candidate must exceed 40 GeV. Electrons and jets are reconstructed within the tracker acceptance ($|\eta| < 2.5$). Muon acceptance extends to $|\eta| < 2.4$, although at least one muon is restricted to $|\eta| < 2.1$ in order to be selected by the trigger.

We perform a shape-based analysis, searching for evidence of W_R boson production using the four-object mass distribution ($M_{\ell\ell jj}$), where we consider events with $M_{\ell\ell jj} > 600$ GeV. To reduce the contribution from DY+jets and other SM backgrounds, we also impose a requirement of $M_{\ell\ell} > 200$ GeV on the mass of the lepton pair associated with the W_R boson candidate.

The decay of a W_R boson tends to produce final-state objects that have high p_T and are separated in the detector. We define the signal acceptance to include the kinematic and detector acceptance requirements for the leptons and jets, lepton-jet separation, and the minimum $M_{\ell\ell}$ and $M_{\ell\ell jj}$ requirements. This signal acceptance, typically near 80% at $M_{N_\ell} \sim M_{W_R}/2$, varies by less than 1% between the electron and muon channels because of differences in detector acceptance for leptons. Provided that the W_R boson decay satisfies acceptance requirements, the ability to reconstruct all four final-state particles is near 75% 2.8 (85%) for the electron (muon) channel, with some dependence on W_R boson and N_ℓ masses. However, if the mass of the W_R boson is sufficiently heavy compared to that of the right-handed neutrino, the $N_\ell \rightarrow \ell jj$ decay products tend to overlap and it becomes difficult to reconstruct two distinct jets or find leptons outside of the jet cone. As a result, the signal acceptance as a function of M_{N_ℓ} decreases rapidly as M_{N_ℓ} drops below about 10% of the W_R boson mass.

5 Standard model backgrounds

The $t\bar{t}$ background contribution to the $eejj$ and $\mu\mu jj$ final states is estimated using a control sample of $e\mu jj$ events reconstructed in data. Studies of simulated $t\bar{t} \rightarrow eejj$, $\mu\mu jj$, and $e\mu jj$ decays confirm that the M_{eejj} and $M_{\mu\mu jj}$ distributions can be modeled by the $M_{e\mu jj}$ distribution, so we apply selection requirements to $e\mu jj$ events that parallel those applied to electron and muon channel events. The $e\mu jj$ events are collected using the same HLT selection as $\mu\mu jj$ events, although in this case only one muon is available for selection by the trigger. This sample is dominated by $t\bar{t}$ events, and small contributions from other SM processes are subtracted using simulation. The relative fractions of $t\bar{t} \rightarrow eejj$, $\mu\mu jj$, and $e\mu jj$ events that pass the selection criteria are determined from simulation. Using this information, the $M_{e\mu jj}$ distribution for the $e\mu jj$ control sample from data is scaled to match the expected $t\bar{t}$ background contribution to the M_{eejj} and $M_{\mu\mu jj}$ distributions. The scale factor derived from simulation is determined after requiring $M_{e\mu} > 200 \text{ GeV}$ and $M_{e\mu jj} > 600 \text{ GeV}$, which is equivalent to the third and final selection stage in Table 1. The scale factors for the $t\bar{t}$ background sample are 0.524 ± 0.007 and 0.632 ± 0.008 in the electron and muon channels, respectively, where the uncertainty in the values reflects the number of simulated $t\bar{t}$ events that satisfy all object and event requirements. The trigger efficiency for $e\mu jj$ events is over 90% for events with central muons ($|\eta| < 0.9$) and decreases for events with more forward muons. Consequently, both the electron and muon scale factors are larger than the expected value of 0.5, given the relative branching fractions for $t\bar{t} \rightarrow eejj$, $\mu\mu jj$, and $e\mu jj$ decays.

The $t\bar{t}$ scale factors, determined from simulation, are checked using control regions in data. We first consider events in both simulation and data where one or both jets are identified as originating from a bottom quark. After all selection requirements are applied, reconstructed $t\bar{t}$ decays dominate the event samples. Accounting for contributions from other SM processes using simulation, we compute scale factors for $e\mu jj$ events in data with $60 < M_{e\mu} < 200 \text{ GeV}$ to estimate the $t\bar{t}$ contribution to the SM background when one or both jets are tagged as b jets using the medium working point of the combined secondary vertex tagging algorithm [45]. The M_{ee} and $M_{\mu\mu}$ distributions in b-tagged data agree with expectations based on simulation and the $e\mu jj$ control sample, and the derived scale factors agree with those obtained from simulation within statistical precision. For another cross-check, we compute the scale factor based on the expectation that $t\bar{t} \rightarrow e\mu jj$ should be twice the rate of $t\bar{t} \rightarrow eejj$ or $t\bar{t} \rightarrow \mu\mu jj$. Deviation from this expected ratio depends primarily on the differences in electron and muon reconstruction and identification efficiencies. The number of electron and muon channel events in data in the $120 < M_{\ell\ell} < 200 \text{ GeV}$ control region are thus used to derive the relative efficiency difference between electrons and muons and then extract the $t\bar{t}$ scale factors. The scale factors determined from this control region in data are consistent with those derived from simulation, and the larger statistical uncertainty (2%) of this cross-check is taken as the systematic uncertainty in the $t\bar{t}$ normalization.

The DY+jets background contribution is estimated from $Z/\gamma^* \rightarrow \ell\ell$ decays reconstructed in simulation and data. The simulated DY+jets background contribution is normalized to data using events in the dilepton mass region $60 < M_{\ell\ell} < 120 \text{ GeV}$ after kinematic requirements are applied on the leptons and jets, which is the first selection stage indicated in Table 1. After removing the small contribution from other SM background processes, the simulated DY+jets distributions are normalized to data using scale factors of 1.000 ± 0.007 and 1.027 ± 0.006 for the electron and muon channels, respectively, relative to inclusive next-to-next-to-leading-order cross section calculations. The uncertainty in this value reflects the number of events from data with $60 < M_{\ell\ell} < 120 \text{ GeV}$. The shape of the $M_{\ell\ell}$ distribution in data is in agreement with SM expectations for $M_{\ell\ell} > 60 \text{ GeV}$, as shown in Fig. 1.

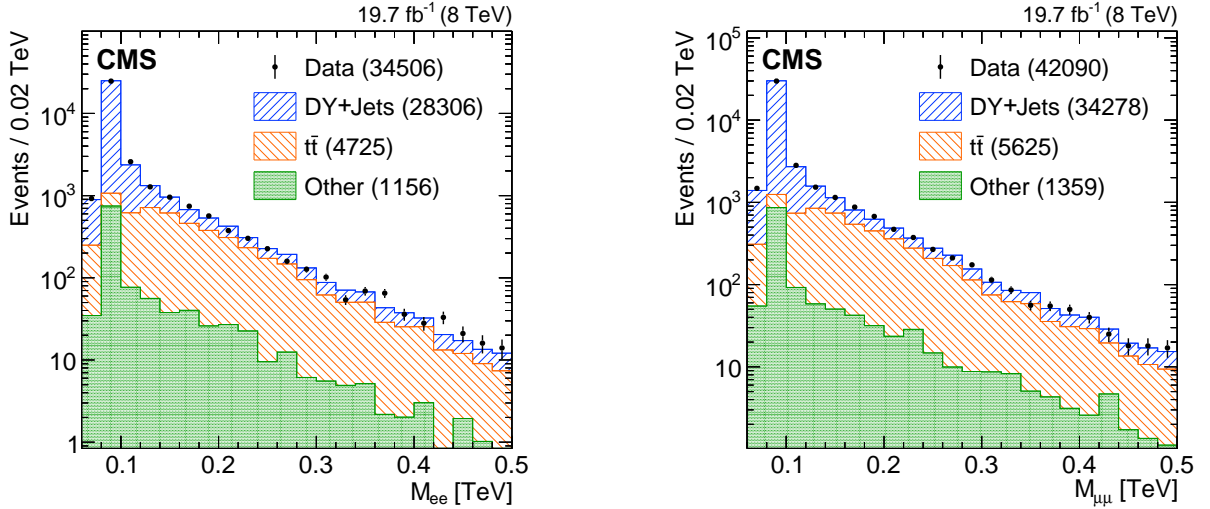


Figure 1: Distribution of the invariant mass M_{ee} (left) and $M_{\mu\mu}$ (right) for events in data (points with error bars) with $p_T > 60$ (40) GeV for the leading (subleading) lepton and at least two jets with $p_T > 40$ GeV, and for background contributions (hatched stacked histograms) from data control samples ($t\bar{t}$) and simulation. The numbers of events from each SM process are included in parentheses in the legend, where the contributions from diboson and single top quark processes have been collected in the “Other” background category.

The diboson and single top quark contributions to the total background are estimated from simulation, based on next-to-leading-order [46] and approximate next-to-next-to-leading-order [47] production cross sections, respectively. The background from W +jets processes, also estimated from simulation, is negligible starting from the earliest selection stage. Finally, the background contribution from multijet processes is estimated using control samples in data and is also found to be negligible at every selection stage.

The observed and expected numbers of events surviving the selections are summarized in Table 1, which explicitly lists the contributions from $t\bar{t}$ and DY +jets processes while including all other SM background contributions in a single column. The yields reflect the numbers of background events surviving each selection stage, with normalization factors obtained from simulation and control sample studies or taken directly from simulation. The numbers of events observed at each selection stage agree with SM expectations in both channels.

6 The M_{W_R} distribution and systematic uncertainties

Once all object and event selection criteria are applied, the $M_{\ell\ell jj}$ distributions in data and simulation are used to search for evidence of W_R boson production, where the expected SM $M_{\ell\ell jj}$ distribution is computed as the sum of the individual background $M_{\ell\ell jj}$ distributions. The $M_{\ell\ell jj}$ distribution is measured in 200 GeV wide bins up to 1.8 TeV, as this bin width is comparable to the mass resolution of the W_R boson for $M_{W_R} < 2.5$ TeV. Beyond 1.8 TeV, events are summed in two bins, $1.8 < M_{\ell\ell jj} < 2.2$ TeV and $M_{\ell\ell jj} > 2.2$ TeV, to account for the small number of background events in the simulated and data control samples at high mass. The $M_{\ell\ell jj}$ distributions for DY +jets, diboson, and single top quark processes are taken from simulation, with the normalization of each distribution as discussed previously. The $M_{e\mu jj}$ distribution from data is used to model the $t\bar{t}$ background contribution in the electron and muon channels.

In our previous search for $W_R \rightarrow \mu N_\mu$ production using 7 TeV collision data [13], we mod-

Table 1: The total numbers of events reconstructed in data, and the expected contributions from signal and background samples, after successive stages of the selection requirements are applied. For the first selection stage, all kinematic and identification requirements are imposed on the leptons and jets as described in the text. The ‘‘Signal’’ column indicates the expected contribution for $M_{W_R} = 2.5$ TeV, with $M_{N_\ell} = 1.25$ TeV. The ‘‘Other’’ column represents the combined background contribution from diboson and single top quark processes. The uncertainties in the background expectation are derived for the final stage of selection and more details are given in Section 6. The total experimental uncertainty is summarized in the first signal uncertainty, and the second signal uncertainty represents the PDF cross section uncertainty. The yields from earlier stages of the selection have greater relative uncertainty than that for the final $M_{\ell\ell jj} > 600$ GeV selection stage.

	Data	Signal	SM Backgrounds			
			Total	t \bar{t}	DY+jets	Other
Two electrons, two jets	34506	30	34154	4725	28273	1156
$M_{ee} > 200$ GeV	1717	29	1747	1164	475	108
$M_{eejj} > 600$ GeV	817	$29 \pm 1 \pm 3$	783 ± 51	476 ± 42	252 ± 24	55 ± 12
Two muons, two jets	42090	35	41204	5625	34220	1359
$M_{\mu\mu} > 200$ GeV	2042	35	2064	1382	549	133
$M_{\mu\mu jj} > 600$ GeV	951	$35 \pm 1 \pm 4$	913 ± 58	562 ± 50	287 ± 26	64 ± 12

eled the shape of each background $M_{\mu\mu jj}$ distribution using an exponential lineshape. For this search, we again find that an exponential function can be used to describe each background $M_{\ell\ell jj}$ distribution below 2 TeV, but these $M_{\ell\ell jj}$ distributions begin to deviate from the assumed exponential shape at high mass. As a result, in this updated search we use the $M_{\ell\ell jj}$ distributions from each background process directly instead of relying on exponential fits to model the shape of the SM backgrounds.

As the $t\bar{t}$ background shape is taken from a control sample of $e\mu jj$ events in data, we examine the shape of the $t\bar{t}$ background $M_{e\mu jj}$ distributions in both simulation and data. Based on the method to extract the background shape in our earlier search, we fit each $M_{e\mu jj}$ distribution to an exponential lineshape for events surviving all selection criteria for $e\mu jj$ events. The $t\bar{t}$ background distribution is again expected to decrease exponentially as $M_{\ell\ell jj}$ increases, although we allow for deviations at high mass (beyond 2 TeV) where the DY+jets background is more significant. The simulated $M_{e\mu jj}$ distribution agrees with the exponential lineshape for $M_{e\mu jj} < 2$ TeV, as expected, while we find that the $M_{e\mu jj}$ distribution in the data control sample noticeably deviates from fit expectations for $1.0 < M_{e\mu jj} < 1.2$ TeV. While the fit expects 94 events, only 78 events are found in data in this region. As a result, we correct the $M_{e\mu jj}$ distribution from the data control sample to the expected number of events from the exponential fit for $1.0 < M_{e\mu jj} < 1.2$ TeV, and this correction is reflected in Table 1. The size of the correction is taken as a systematic uncertainty in the shape of the $t\bar{t}$ $M_{\ell\ell jj}$ distribution.

The $M_{\ell\ell jj}$ distributions for events satisfying all selection criteria appear in Fig. 2. A comparison of the observed data to SM expectations yields a normalized χ^2 of 1.4 (0.9) for electron (muon) channel events. We observe an excess in the electron channel in the region $1.8 < M_{eejj} < 2.2$ TeV, where 14 events are observed compared to 4 events expected from SM backgrounds. This excess has a local significance of 2.8σ estimated using the method discussed in Section 7. This excess does not appear to be consistent with $W_R \rightarrow eN_e$ decay. We examined additional distributions for events with $1.8 < M_{eejj} < 2.2$ TeV, including the mass distributions M_{eij} (for both the leading and subleading electrons), M_{ee} , and M_{jj} , as well as the p_T distributions for each of the final state particles. In this examination, we find no compelling evidence in favor of

the signal hypothesis over the assumption of an excess of SM background events in this region. Examining the charge of the electrons used to build W_R boson candidates in data events with $1.8 < M_{eejj} < 2.2$ TeV, we find same-sign electrons in one of the 14 reconstructed events. In this region, the same-sign SM background is expected to be on the order of half an event due to SM diboson processes and charge misidentification in DY+jets events. No same-sign events are observed in the same mass region of the distribution for the muon channel. For comparison, making plausible assumptions for the properties of a signal contributing in this region, one would expect half of the additional events to have electrons with the same sign.

The uncertainties in modeling the shape of the background $M_{\ell\ell jj}$ distributions dominate the background systematic uncertainty, as shown in Fig. 2. The background $M_{\ell\ell jj}$ uncertainty is determined in each mass bin based on the number of events surviving all selection criteria for each background sample. For the two dominant backgrounds, an additional shape uncertainty is included as part of the background shape uncertainty.

The additional $t\bar{t}$ shape uncertainty is included for the $1.0 < M_{\ell\ell jj} < 1.2$ TeV mass region based on the previously discussed correction to the $M_{e\mu jj}$ distribution for $1.0 < M_{e\mu jj} < 1.2$ TeV. No additional $t\bar{t}$ shape uncertainty is applied at other $M_{\ell\ell jj}$ values as the $M_{e\mu jj}$ distributions in both data and simulation agree with the assumed exponential lineshape below 1.8 TeV, and the statistical uncertainty of the $e\mu jj$ control sample dominates at high mass. For the DY+jets background, the $M_{\ell\ell jj}$ shape uncertainty is determined using simulated samples from two different MC generators, MADGRAPH and SHERPA. The difference between these two $M_{\ell\ell jj}$ distributions, computed as a function of mass, is taken as an additional systematic uncertainty in the DY+jets shape.

The uncertainty associated with the background normalization is taken as the quadratic sum of the uncertainty in the scale factors determined from the cross-check for $t\bar{t}$ background performed on a control region in data, the uncertainty estimated from the difference in the values obtained for DY+jets scale factors in the electron and muon channels, and the combined cross section and luminosity uncertainties for the remaining backgrounds. This overall background normalization uncertainty is small compared to the uncertainties determined for the background shape.

Lepton reconstruction and identification uncertainties, which also contribute to the total signal and background systematic uncertainty, are determined using $Z \rightarrow ee, \mu\mu$ events reconstructed in both data and simulation. Uncertainties in the jet and lepton energy scales and resolutions also contribute to the systematic uncertainty. These uncertainties dominate the signal efficiency uncertainty, resulting in a total systematic uncertainty of up to 10% for the signal efficiency, depending on the W_R boson mass assumption. The combination of lepton and jet energy scale, resolution, and efficiency uncertainties is less than 5% for the background estimates taken from simulation.

The systematic uncertainties related to pileup, uncertainties in the proton PDFs, and initial- or final-state radiation are computed for the simulated background samples and are found to be small when compared to the background shape uncertainty. Additional theoretical uncertainties for the SM background processes are covered by the shape uncertainty. The total uncertainty for signal and background is determined for the final selection stage and presented in Table 1. Figure 2 summarizes the background uncertainty as a function of $M_{\ell\ell jj}$ and displays the dominant background shape uncertainty relative to the total background uncertainty.

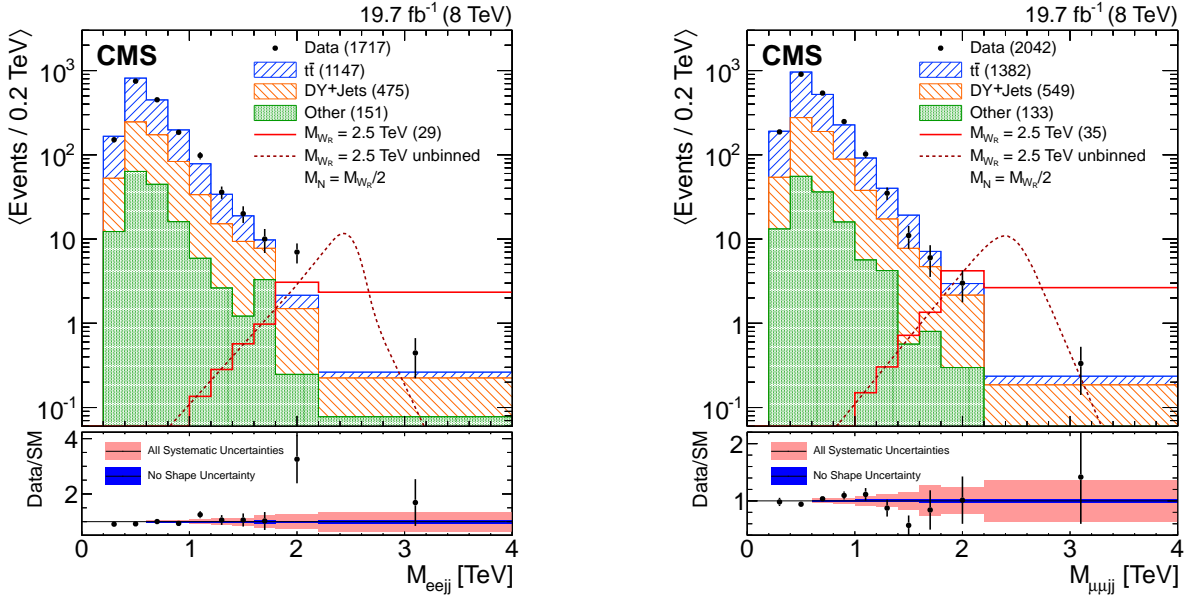


Figure 2: Distribution of the invariant mass M_{eejj} (left) and $M_{\mu\mu jj}$ (right) for events in data (points with error bars) with $M_{\ell\ell} > 200$ GeV and for background contributions (hatched stacked histograms) from data control samples ($t\bar{t}$) and simulation. The signal mass point $M_{W_R} = 2.5$ TeV, $M_{N_\ell} = 1.25$ TeV, is included for comparison (open red histogram, and also as a dotted line for the unbinned signal shape). The numbers of events from each background process (and the expected number of signal events) are included in parentheses in the legend, where the contributions from diboson and single top quark processes have been collected in the “Other” background category. The data are compared with SM expectations in the lower portion of the figure. The total background uncertainty (light red band) and the background uncertainty after neglecting the uncertainty due to background modeling (dark blue band) are included as a function of $M_{\ell\ell jj}$ for $M_{\ell\ell jj} > 600$ GeV (dashed line).

7 Limits on W_R boson production

We estimate limits on W_R boson production using a multibin CL_S limit setting technique [48–50]. The $M_{\ell\ell jj}$ distributions obtained from signal MC, each of the SM backgrounds, and the observed data all serve as limit inputs. The systematic uncertainties mentioned previously are included as nuisance parameters in the limit calculations. We estimate the 95% CL upper limit on the W_R boson cross section multiplied by the $W_R \rightarrow \ell\ell jj$ branching fraction as a function of M_{W_R} and M_{N_ℓ} . These results (available in tabular form in Appendix A) can be used for the evaluation of models other than those considered in this paper.

The limits are computed for a set of W_R boson and N_ℓ mass assumptions, where M_{W_R} starts at 1 TeV and increases in 100 GeV steps and the N_ℓ mass is taken to be half the W_R boson mass. For these determinations, the W_R boson signal samples include the full CMS detector simulation.

The procedure to determine the limits on W_R boson production for a range of N_ℓ mass assumptions ($M_{N_\ell} < M_{W_R}$) proceeds as follows. For a fixed value of M_{W_R} , the limits on $W_R \rightarrow \ell N_\ell \rightarrow \ell\ell jj$ are determined as a function of M_{N_ℓ} (up to M_{W_R}) based on differences in kinematic acceptance, lepton-jet overlap, and $M_{\ell\ell jj}$ shape relative to $M_{N_\ell} = \frac{1}{2}M_{W_R}$. As mentioned previously, the combined reconstruction and identification efficiency for the W_R boson and N_ℓ decay products varies by $\mathcal{O}(1\%)$ as a function of M_{W_R} once acceptance requirements are satisfied. Consequently, for M_{N_ℓ} values other than $M_{N_\ell} = \frac{1}{2}M_{W_R}$, the W_R boson production cross section limits are computed using information from signal samples that do not include the simulated detector response.

The cross section limit calculation based on the kinematic acceptance is compared with the results for fully simulated samples using a spectrum of N_ℓ mass assumptions for $M_{W_R} = 1, 1.5, 2,$ and 3 TeV. The difference between the two methods is at the percent level or smaller for M_{N_ℓ} masses greater than 10–20% of the generated W_R boson mass. Differences grow to $\mathcal{O}(10)\%$ for lighter right-handed neutrinos. The ratio of the products of efficiency and acceptance for the two approaches is computed as a function of M_{N_ℓ}/M_{W_R} , and a global fit to this distribution is used to correct the cross section limits determined as a function of M_{N_ℓ} for all M_{W_R} values.

The uncertainty in this correction is computed using the maximum difference in the efficiency times acceptance ratio for the set of simulated samples as a function of M_{N_ℓ}/M_{W_R} , unless the statistical uncertainty in the ratio calculation dominates. The impact of this uncertainty on signal acceptance is propagated to the cross section limit calculations. The overall effect on the limits from this uncertainty is negligible for most M_{N_ℓ} values, but can degrade the cross section limit by 5–10% for N_ℓ masses below 10% of M_{W_R} .

Finally, we account for variations in the shape of the $M_{\ell\ell jj}$ distribution. As $M_{N_\ell} \rightarrow 0$, neutrino production via a virtual W_R boson becomes more significant. As a result, the shape of the signal $M_{\ell\ell jj}$ distribution is expected to vary as a function of both M_{W_R} and M_{N_ℓ} . This effect is included in the limit calculations.

The largest uncertainty related to the $W_R \rightarrow \ell N_\ell$ production estimation arises from the variation in the predicted signal production cross section as a result of the uncertainties in the proton PDFs, where we use the CTEQ6L1 PDF set for signal events. The cross section uncertainty, which is not considered in the limit calculations, ranges from 5% for $M_{W_R} = 1$ TeV to 26% for $M_{W_R} = 3$ TeV and is computed following the PDF4LHC prescriptions [51, 52] for the CT10 [53], MSTW2008 [54], and NNPDF2.1 [55] PDF sets. The PDF uncertainties in the signal acceptance, which are small compared to the systematic uncertainties for signal events mentioned previously, are included in the limit calculations.

For the results presented in Fig. 3, we indicate a range of N_ℓ masses that are excluded as a function of M_{W_R} assuming that only one heavy neutrino flavor (electron or muon) is accessible from 8 TeV pp collisions, with the other $N_{\ell'}$ ($\ell' = e, \mu, \tau$, with $\ell' \neq \ell$) too heavy to be produced. These (M_{W_R}, M_{N_ℓ}) limits are obtained by comparing the observed and expected cross section upper limits with the expected cross section for each mass point. The limits extend to roughly $M_{W_R} = 3.0$ TeV in each channel and exclude a wide range of heavy neutrino masses for W_R boson mass assumptions below this maximal value. The inclusion of the results from the previous iteration of this analysis [13], which searched for W_R boson production in the $\mu\mu jj$ final state using 7 TeV data, does not significantly affect the limit results. The excess in the electron channel at approximately 2 TeV has a local significance of 2.8σ for a W_R boson candidate with a mass of 2.1 TeV. Assuming contributions from SM backgrounds only, the p-value for the local excess in the M_{eejj} distribution is 0.0050. We also present limits as a function of W_R boson mass for a right-handed neutrino with $M_{N_\ell} = \frac{1}{2}M_{W_R}$ in Fig. 4. For the electron (muon) channel, we exclude W_R bosons with $M_{W_R} < 2.87$ (3.00) TeV, with an expected exclusion of 2.99 (3.04) TeV.

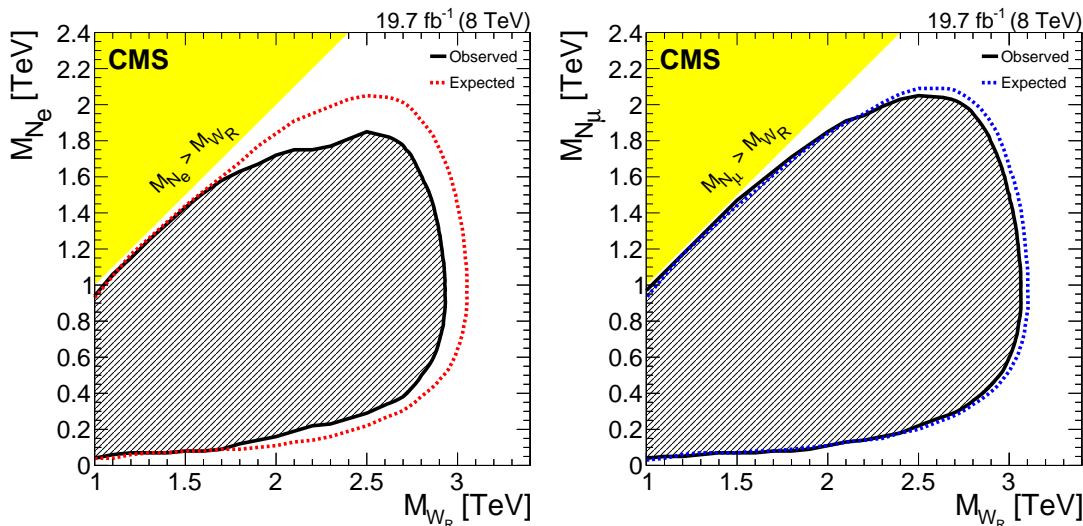


Figure 3: The 95% CL exclusion region (hatched) in the (M_{W_R}, M_{N_ℓ}) plane, assuming the model described in the text (see Section 1), for the electron (left) and muon (right) channels. Neutrino masses greater than M_{W_R} (yellow shaded region) are not considered in this search.

We additionally consider the case where all N_ℓ masses are degenerate and can be produced via W_R boson production and decay in 8 TeV pp collisions. In this case, the electron and muon results can be combined as shown in Fig. 5. The (M_{W_R}, M_{N_ℓ}) exclusion for the combination extends slightly further than the single-channel exclusion limits, with an observed (expected) exclusion for the combined channel of $M_{W_R} < 3.01$ (3.10) TeV for $M_{N_\ell} = \frac{1}{2}M_{W_R}$.

8 Summary

A search for right-handed bosons (W_R) and heavy right-handed neutrinos (N_ℓ) in the left-right symmetric extension of the standard model has been presented. The data sample is in agreement with expectations from standard model processes in the $\mu\mu jj$ final state. An excess is observed in the electron channel with a local significance of 2.8σ at $M_{eejj} \approx 2.1$ TeV. The excess does not appear to be consistent with expectations from left-right symmetric theory. Considering $W_R \rightarrow eN_e$ and $W_R \rightarrow \mu N_\mu$ searches separately, regions in the (M_{W_R}, M_{N_ℓ}) mass space are excluded at 95% confidence level that extend up to $M_{W_R} < 3.0$ TeV for both channels. Assuming $W_R \rightarrow \ell N_\ell$ with degenerate N_ℓ mass for $\ell = e, \mu$, W_R boson production is excluded at 95%

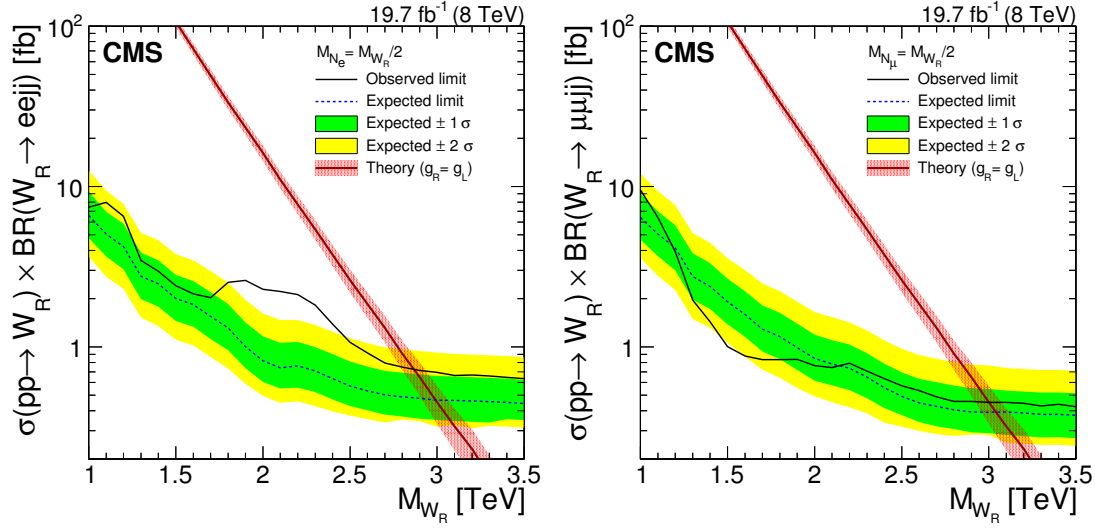


Figure 4: The 95% CL exclusion for W_R boson production cross section times branching fraction, computed as a function of M_{W_R} assuming the right-handed neutrino has half the mass of the W_R boson, for the electron (left) and muon (right) channels. The signal cross section PDF uncertainties (red band surrounding the theoretical W_R -boson production cross section curve) are included for illustration purposes only.

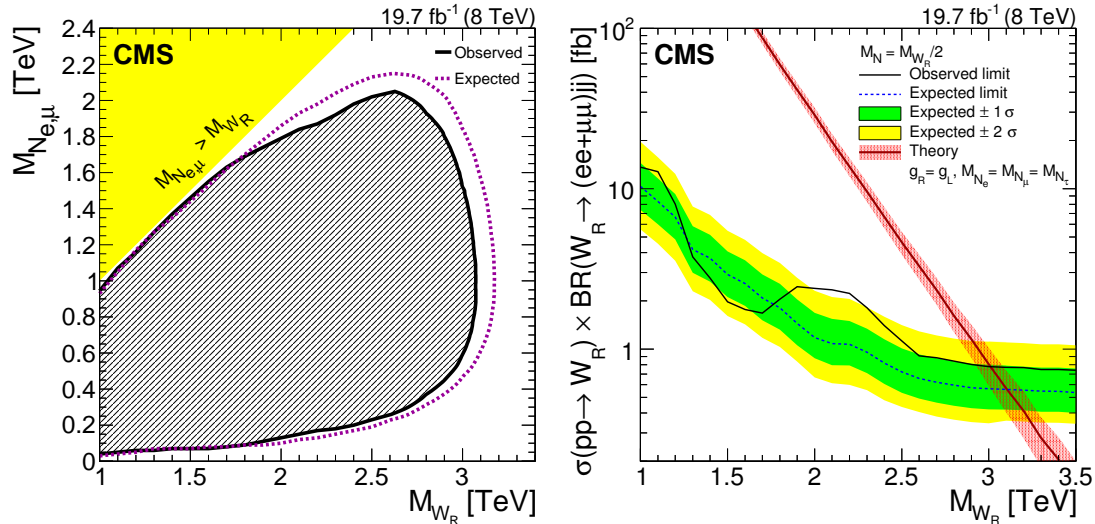


Figure 5: The 95% CL exclusion region in the (M_{W_R}, M_{N_ℓ}) plane (left), and as a function of W_R boson mass with $M_N = \frac{1}{2}M_{W_R}$ (right) obtained combining the electron and muon channels. The signal cross section PDF uncertainties (red band surrounding the theoretical W_R -boson production cross section curve) are included for illustration purposes only. Neutrino masses greater than M_{W_R} (yellow shaded region in the left figure) are not considered in this search.

confidence level up to $M_{W_R} < 3.0$ TeV. This search has significantly extended the exclusion region in the two-dimensional (M_{W_R}, M_{N_ℓ}) mass plane compared to previous searches, and for the first time this search has excluded M_{W_R} values beyond the theoretical lower mass limit of $M_{W_R} \gtrsim 2.5$ TeV.

Acknowledgments

We congratulate our colleagues in the CERN accelerator departments for the excellent performance of the LHC and thank the technical and administrative staffs at CERN and at other CMS institutes for their contributions to the success of the CMS effort. In addition, we gratefully acknowledge the computing centres and personnel of the Worldwide LHC Computing Grid for delivering so effectively the computing infrastructure essential to our analyses. Finally, we acknowledge the enduring support for the construction and operation of the LHC and the CMS detector provided by the following funding agencies: BMWFW and FWF (Austria); FNRS and FWO (Belgium); CNPq, CAPES, FAPERJ, and FAPESP (Brazil); MES (Bulgaria); CERN; CAS, MoST, and NSFC (China); COLCIENCIAS (Colombia); MSES and CSF (Croatia); RPF (Cyprus); MoER, ERC IUT and ERDF (Estonia); Academy of Finland, MEC, and HIP (Finland); CEA and CNRS/IN2P3 (France); BMBF, DFG, and HGF (Germany); GSRT (Greece); OTKA and NIH (Hungary); DAE and DST (India); IPM (Iran); SFI (Ireland); INFN (Italy); NRF and WCU (Republic of Korea); LAS (Lithuania); MOE and UM (Malaysia); CINVESTAV, CONACYT, SEP, and UASLP-FAI (Mexico); MBIE (New Zealand); PAEC (Pakistan); MSHE and NSC (Poland); FCT (Portugal); JINR (Dubna); MON, RosAtom, RAS and RFBR (Russia); MESTD (Serbia); SEIDI and CPAN (Spain); Swiss Funding Agencies (Switzerland); MST (Taipei); ThEPCenter, IPST, STAR and NSTDA (Thailand); TUBITAK and TAEK (Turkey); NASU and SFFR (Ukraine); STFC (United Kingdom); DOE and NSF (USA).

Individuals have received support from the Marie-Curie programme and the European Research Council and EPLANET (European Union); the Leventis Foundation; the A. P. Sloan Foundation; the Alexander von Humboldt Foundation; the Belgian Federal Science Policy Office; the Fonds pour la Formation à la Recherche dans l'Industrie et dans l'Agriculture (FRIA-Belgium); the Agentschap voor Innovatie door Wetenschap en Technologie (IWT-Belgium); the Ministry of Education, Youth and Sports (MEYS) of the Czech Republic; the Council of Science and Industrial Research, India; the HOMING PLUS programme of Foundation for Polish Science, cofinanced from European Union, Regional Development Fund; the Compagnia di San Paolo (Torino); the Consorzio per la Fisica (Trieste); MIUR project 20108T4XTM (Italy); the Thalís and Aristeia programmes cofinanced by EU-ESF and the Greek NSRF; and the National Priorities Research Program by Qatar National Research Fund.

References

- [1] S. L. Glashow, "Partial-symmetries of weak interactions", *Nucl. Phys.* **22** (1961) 579, doi:10.1016/0029-5582(61)90469-2.
- [2] S. Weinberg, "A Model of Leptons", *Phys. Rev. Lett.* **19** (1967) 1264, doi:10.1103/PhysRevLett.19.1264.
- [3] A. Salam, "Weak and electromagnetic interactions", in *Elementary particle physics: relativistic groups and analyticity*, N. Svartholm, ed., p. 367. Almqvist & Wiskell, 1968. Proceedings of the eighth Nobel symposium.

- [4] J. C. Pati and A. Salam, "Lepton number as the fourth 'color'", *Phys. Rev. D* **10** (1974) 275, doi:10.1103/PhysRevD.10.275.
- [5] R. N. Mohapatra and J. C. Pati, "A Natural Left-Right Symmetry", *Phys. Rev. D* **11** (1975) 2558, doi:10.1103/PhysRevD.11.2558.
- [6] G. Senjanović and R. N. Mohapatra, "Exact left-right symmetry and spontaneous violation of parity", *Phys. Rev. D* **12** (1975) 1502, doi:10.1103/PhysRevD.12.1502.
- [7] W.-Y. Keung and G. Senjanović, "Majorana Neutrinos and the Production of the Right-Handed Charged Gauge Boson", *Phys. Rev. Lett.* **50** (1983) 1427, doi:10.1103/PhysRevLett.50.1427.
- [8] W. M. Alberico and S. M. Bilenky, "Neutrino Oscillations, Masses and Mixing", *Phys. Part. Nucl.* **35** (2003) 297, arXiv:hep-ph/0306239.
- [9] C. Giunti and M. Laveder, "Neutrino mixing", in *Developments in Quantum Physics – 2004*, F. Columbus and V. Krasnoholovets, eds. Nova Science Publishers, Inc., 2003. arXiv:hep-ph/0310238.
- [10] Particle Data Group, J. Beringer et al., "Review of Particle Physics", *Phys. Rev. D* **86** (2012) 010001, doi:10.1103/PhysRevD.86.010001.
- [11] R. N. Mohapatra and G. Senjanović, "Neutrino Mass and Spontaneous Parity Nonconservation", *Phys. Rev. Lett.* **44** (1980) 912, doi:10.1103/PhysRevLett.44.912.
- [12] M. Gell-Mann, P. Ramond, and R. Slansky, "Complex Spinors and Unified Theories", in *Supergravity*, P. van Nieuwenhuizen and D. Z. Freedman, eds. North Holland Publishing Co., 1979. arXiv:1306.4669.
- [13] CMS Collaboration, "Search for heavy neutrinos and W_R bosons with right-handed couplings in a left-right symmetric model in pp collisions at $\sqrt{s} = 7\text{ TeV}$ ", *Phys. Rev. Lett.* **109** (2012) 261802, doi:10.1103/PhysRevLett.109.261802, arXiv:1210.2402.
- [14] R. Gavin, Y. Li, F. Petriello, and S. Quackenbush, "FEWZ 2.0: A code for hadronic Z production at next-to-next-to-leading order", *Comput. Phys. Commun.* **182** (2011) 2388, doi:10.1016/j.cpc.2011.06.008, arXiv:1011.3540.
- [15] R. Hamberg, W. van Neerven, and T. Matsuura, "A complete calculation of the order α_s^2 correction to the Drell-Yan K-factor", *Nucl. Phys. B* **359** (1991) 343, doi:10.1016/0550-3213(91)90064-5. See also the erratum at doi:10.1016/S0550-3213(02)00814-3.
- [16] E. Nardi, E. Roulet, and D. Tommasini, "New Neutral Gauge Bosons and New Heavy Fermions in the Light of the New LEP Data", *Phys. Lett. B* **344** (1995) 225, doi:10.1016/0370-2693(95)91542-M, arXiv:hep-ph/9409310.
- [17] G. Beall, M. Bander, and A. Soni, "Constraint on the Mass Scale of a Left-Right-Symmetric Electroweak Theory from the $K_L - K_S$ Mass Difference", *Phys. Rev. Lett.* **48** (1982) 848, doi:10.1103/PhysRevLett.48.848.
- [18] A. Maiezza, M. Nemevšek, F. Nesti, and G. Senjanović, "Left-right symmetry at LHC", *Phys. Rev. D* **82** (2010) 055022, doi:10.1103/PhysRevD.82.055022, arXiv:1005.5160.

- [19] ATLAS Collaboration, "Search for $t\bar{b}$ resonances in proton-proton collisions at $\sqrt{s} = 7$ TeV with the ATLAS detector", *Phys. Rev. Lett.* **109** (2012) 081801, doi:10.1103/PhysRevLett.109.081801, arXiv:1205.1016.
- [20] CMS Collaboration, "Search for a W' boson decaying to a bottom quark and a top quark in pp collisions at $\sqrt{s} = 7$ TeV", *Phys. Lett. B* **718** (2013) 1229, doi:10.1016/j.physletb.2012.12.008, arXiv:1208.0956.
- [21] CMS Collaboration, "Search for $W' \rightarrow t\bar{b}$ decays in the lepton+jets final state at $\sqrt{s} = 8$ TeV", *JHEP* **1405** (2014) 108, doi:10.1007/JHEP05(2014)108, arXiv:1402.2176.
- [22] ATLAS Collaboration, "Search for heavy neutrinos and right-handed W bosons in events with two leptons and jets in pp collisions at $\sqrt{s} = 7$ TeV with the ATLAS detector", *Eur. Phys. J. C* **72** (2012) 2056, doi:10.1140/epjc/s10052-012-2056-4, arXiv:1203.5420.
- [23] CMS Collaboration, "The CMS experiment at the CERN LHC", *JINST* **03** (2008) S08004, doi:10.1088/1748-0221/3/08/S08004.
- [24] CMS Collaboration, "Commissioning of the Particle-Flow Event Reconstruction with the first LHC collisions recorded in the CMS detector", CMS Physics Analysis Summary CMS-PAS-PFT-10-001, 2010.
- [25] CMS Collaboration, "Particle-Flow Event Reconstruction in CMS and Performance for Jets, Taus, and MET", CMS Physics Analysis Summary CMS-PAS-PFT-09-001, 2009.
- [26] T. Sjöstrand, S. Mrenna, and P. Skands, "PYTHIA 6.4 physics and manual", *JHEP* **05** (2006) 026, doi:10.1088/1126-6708/2006/05/026, arXiv:hep-ph/0603175.
- [27] J. Botts et al., "CTEQ parton distributions and flavor dependence of sea quarks", *Phys. Lett. B* **304** (1993) 159, doi:10.1016/0370-2693(93)91416-K, arXiv:hep-ph/9303255.
- [28] R. Field, "Early LHC Underlying Event Data - Findings and Surprises", (2010). arXiv:1010.3558.
- [29] J. Alwall et al., "The automated computation of tree-level and next-to-leading order differential cross sections, and their matching to parton shower simulations", (2014). arXiv:1405.0301.
- [30] T. Gleisberg et al., "Event generation with SHERPA 1.1", *JHEP* **02** (2009) 007, doi:10.1088/1126-6708/2009/02/007, arXiv:0811.4622.
- [31] P. Nason, "A New method for combining NLO QCD with shower Monte Carlo algorithms", *JHEP* **11** (2004) 040, doi:10.1088/1126-6708/2004/11/040, arXiv:hep-ph/0409146.
- [32] S. Frixione, P. Nason, and C. Oleari, "Matching NLO QCD computations with Parton Shower simulations: the POWHEG method", *JHEP* **11** (2007) 070, doi:10.1088/1126-6708/2007/11/070, arXiv:0709.2092.
- [33] S. Alioli, P. Nason, C. Oleari, and E. Re, "A general framework for implementing NLO calculations in shower Monte Carlo programs: the POWHEG BOX", *JHEP* **06** (2010) 043, doi:10.1007/JHEP06(2010)043, arXiv:1002.2581.

- [34] E. Re, “Single-top Wt-channel production matched with parton showers using the POWHEG method”, *Eur. Phys. J. C* **71** (2011) 1547, doi:10.1140/epjc/s10052-011-1547-z, arXiv:1009.2450.
- [35] GEANT4 Collaboration, “GEANT4—a simulation toolkit”, *Nucl. Instrum. Meth. A* **506** (2003) 250, doi:10.1016/S0168-9002(03)01368-8.
- [36] CMS Collaboration, “Search for narrow resonances in dilepton mass spectra in pp collisions at $\sqrt{s} = 7$ TeV”, *Phys. Lett. B* **714** (2012) 158, doi:10.1016/j.physletb.2012.06.051.
- [37] CMS Collaboration, “Performance of CMS muon reconstruction in pp collision events at $\sqrt{s} = 7$ TeV”, *J. Instrum.* **7** (2012) P10002, doi:10.1088/1748-0221/7/10/P10002.
- [38] CMS Collaboration, “Electron Reconstruction and Identification at $\sqrt{s} = 7$ TeV”, CMS Physics Analysis Summary CMS-PAS-EGM-10-004, 2010.
- [39] CMS Collaboration, “Search for heavy narrow dilepton resonances in pp collisions at $\sqrt{s} = 7$ TeV and $\sqrt{s} = 8$ TeV”, *Phys. Lett. B* **720** (2012) 63, doi:10.1016/j.physletb.2013.02.003.
- [40] M. Cacciari and G. P. Salam, “Pileup subtraction using jet areas”, *Phys. Lett. B* **659** (2008) 119, doi:10.1016/j.physletb.2007.09.077, arXiv:0707.1378.
- [41] M. Cacciari, G. P. Salam, and G. Soyez, “The anti- k_r jet clustering algorithm”, *JHEP* **04** (2008) 063, doi:10.1088/1126-6708/2008/04/063, arXiv:0802.1189.
- [42] M. Cacciari, G. P. Salam, and G. Soyez, “The Catchment Area of Jets”, *JHEP* **04** (2008) 005, doi:10.1088/1126-6708/2008/04/005, arXiv:0802.1188.
- [43] CMS Collaboration, “Jet Performance in pp Collisions at $\sqrt{s} = 7$ TeV”, CMS Physics Analysis Summary CMS-PAS-JME-10-003, 2010.
- [44] CMS Collaboration, “Determination of jet energy calibration and transverse momentum resolution in CMS”, *J. Instrum.* **6** (2011) P11002, doi:10.1088/1748-0221/6/11/P11002.
- [45] CMS Collaboration, “Performance of b tagging at $\sqrt{s} = 8$ TeV in multijet, $t\bar{t}$ and boosted topology events”, CMS Physics Analysis Summary CMS-PAS-BTV-13-001, 2013.
- [46] J. M. Campbell, R. K. Ellis, and C. Williams, “Vector boson pair production at the LHC”, *JHEP* **07** (2011) 018, doi:10.1007/JHEP07(2011)018, arXiv:1105.0020.
- [47] N. Kidonakis, “Differential and total cross sections for top pair and single top production”, (2012). arXiv:1205.3453.
- [48] A. L. Read, “Presentation of search results: the CL_s technique”, *J. Phys. G* **28** (2002) 2693, doi:10.1088/0954-3899/28/10/313.
- [49] T. Junk, “Confidence level computation for combining searches with small statistics”, *Nucl. Instrum. Meth. A* **434** (1999) 435, doi:10.1016/S0168-9002(99)00498-2, arXiv:hep-ex/9902006.
- [50] L. Moneta et al., “The RooStats Project”, in *13th International Workshop on Advanced Computing and Analysis Techniques in Physics Research*. SISSA, 2010. arXiv:1009.1003.

-
- [51] PDF4LHC Working Group, “PDF4LHC Recommendations”, (2011).
arXiv:1101.0536.
- [52] PDF4LHC Working Group, “The PDF4LHC Working Group Interim Recommendations”, (2011). arXiv:1101.0538.
- [53] H.-L. Lai et al., “New parton distributions for collider physics”, *Phys. Rev. D* **82** (2010) 074024, doi:10.1103/PhysRevD.82.074024, arXiv:1007.2241.
- [54] A. D. Martin, W. J. Stirling, R. S. Thorne, and G. Watt, “Uncertainties on α_s in global PDF analyses and implications for predicted hadronic cross sections”, *Eur. Phys. J. C* **64** (2009) 653, doi:10.1140/epjc/s10052-009-1164-2, arXiv:0905.3531.
- [55] NNPDF Collaboration, “Unbiased global determination of parton distributions and their uncertainties at NNLO and at LO”, *Nucl. Phys. B* **855** (2012) 153, doi:10.1016/j.nuclphysb.2011.09.024, arXiv:1107.2652.

A 95% CL exclusion limits as a function of W_R and N_ℓ mass (tabular format)

Table A1: The 95% CL observed (Obs.) and expected (Exp.) exclusion limits (in fb) on the W_R production cross section times branching fraction for $W_R \rightarrow eejj$ as a function of W_R and N_e mass (in GeV) for $1000 \leq M_{W_R} \leq 1600$ GeV. The signal acceptance (Acc.) is also included for each (M_{W_R}, M_{N_e}) entry.

M_{W_R}	M_{N_e}	Obs.	Exp.	Acc.	M_{W_R}	M_{N_e}	Obs.	Exp.	Acc.
1000	100	65.7	58.5	0.073 ± 0.110	1400	100	60.1	50.2	0.043 ± 0.164
1000	200	14.6	13.0	0.298 ± 0.031	1400	200	9.07	7.57	0.241 ± 0.061
1000	300	9.77	8.69	0.447 ± 0.014	1400	300	4.91	4.09	0.428 ± 0.027
1000	400	8.17	7.27	0.549 ± 0.011	1400	400	3.76	3.13	0.549 ± 0.015
1000	500	7.44	6.63	0.596 ± 0.009	1400	500	3.29	2.75	0.630 ± 0.011
1000	600	7.14	6.35	0.620 ± 0.009	1400	600	3.09	2.58	0.688 ± 0.010
1000	700	7.16	6.38	0.617 ± 0.009	1400	700	2.97	2.48	0.711 ± 0.011
1000	800	7.71	6.86	0.573 ± 0.009	1400	800	2.89	2.41	0.729 ± 0.009
1000	900	10.2	9.05	0.435 ± 0.010	1400	900	2.89	2.41	0.729 ± 0.009
1100	100	97.0	61.6	0.062 ± 0.124	1400	1000	2.90	2.42	0.725 ± 0.009
1100	200	17.6	11.2	0.290 ± 0.038	1400	1100	2.96	2.47	0.712 ± 0.009
1100	300	10.3	6.56	0.441 ± 0.016	1400	1200	3.17	2.64	0.664 ± 0.009
1100	400	8.61	5.47	0.548 ± 0.011	1400	1300	3.77	3.15	0.558 ± 0.010
1100	500	8.05	5.11	0.609 ± 0.010	1500	100	59.4	49.4	0.038 ± 0.176
1100	600	7.69	4.89	0.655 ± 0.010	1500	200	8.23	6.86	0.221 ± 0.070
1100	700	7.59	4.82	0.663 ± 0.009	1500	300	3.97	3.31	0.411 ± 0.031
1100	800	7.82	4.96	0.644 ± 0.010	1500	400	3.00	2.50	0.545 ± 0.017
1100	900	8.30	5.27	0.606 ± 0.009	1500	500	2.64	2.20	0.625 ± 0.012
1100	1000	10.6	6.75	0.473 ± 0.010	1500	600	2.49	2.07	0.686 ± 0.010
1200	100	91.5	59.2	0.052 ± 0.139	1500	700	2.41	2.01	0.716 ± 0.010
1200	200	16.2	10.5	0.275 ± 0.045	1500	800	2.37	1.98	0.739 ± 0.011
1200	300	9.76	6.32	0.442 ± 0.019	1500	900	2.35	1.95	0.746 ± 0.009
1200	400	7.81	5.05	0.556 ± 0.012	1500	1000	2.32	1.93	0.755 ± 0.009
1200	500	6.98	4.52	0.627 ± 0.010	1500	1100	2.37	1.97	0.739 ± 0.009
1200	600	6.53	4.23	0.671 ± 0.009	1500	1200	2.46	2.05	0.711 ± 0.009
1200	700	6.39	4.14	0.684 ± 0.009	1500	1300	2.59	2.16	0.675 ± 0.009
1200	800	6.36	4.12	0.687 ± 0.009	1500	1400	3.06	2.55	0.573 ± 0.009
1200	900	6.48	4.20	0.674 ± 0.009	1600	100	58.8	50.4	0.033 ± 0.187
1200	1000	6.98	4.52	0.626 ± 0.009	1600	200	8.08	6.93	0.212 ± 0.078
1200	1100	8.71	5.64	0.502 ± 0.009	1600	300	3.91	3.35	0.402 ± 0.036
1300	100	61.7	49.2	0.047 ± 0.152	1600	400	2.89	2.48	0.536 ± 0.019
1300	200	9.48	7.55	0.254 ± 0.054	1600	500	2.49	2.13	0.627 ± 0.017
1300	300	4.99	3.97	0.446 ± 0.023	1600	600	2.27	1.95	0.680 ± 0.010
1300	400	3.95	3.14	0.558 ± 0.013	1600	700	2.21	1.89	0.723 ± 0.009
1300	500	3.60	2.86	0.635 ± 0.010	1600	800	2.14	1.84	0.747 ± 0.010
1300	600	3.46	2.76	0.684 ± 0.010	1600	900	2.10	1.80	0.760 ± 0.009
1300	700	3.41	2.72	0.699 ± 0.009	1600	1000	2.09	1.79	0.763 ± 0.009
1300	800	3.32	2.65	0.716 ± 0.009	1600	1100	2.10	1.80	0.761 ± 0.009
1300	900	3.35	2.67	0.710 ± 0.009	1600	1200	2.13	1.83	0.749 ± 0.009
1300	1000	3.41	2.72	0.698 ± 0.009	1600	1300	2.18	1.87	0.732 ± 0.009
1300	1100	3.66	2.92	0.650 ± 0.009	1600	1400	2.30	1.97	0.695 ± 0.012
1300	1200	4.43	3.53	0.536 ± 0.009	1600	1500	2.70	2.31	0.592 ± 0.009

Table A2: The 95% CL observed (Obs.) and expected (Exp.) exclusion limits (in fb) on the W_R production cross section times branching fraction for $W_R \rightarrow eejj$ as a function of W_R and N_ℓ mass (in GeV) for $1700 \leq M_{W_R} \leq 2000$ GeV. The signal acceptance (Acc.) is also included for each (M_{W_R}, M_{N_ℓ}) entry.

M_{W_R}	M_{N_ℓ}	Obs.	Exp.	Acc.	M_{W_R}	M_{N_ℓ}	Obs.	Exp.	Acc.
1700	100	76.5	58.3	0.032 ± 0.197	1900	100	131	50.7	0.025 ± 0.216
1700	200	9.12	6.95	0.195 ± 0.086	1900	200	14.3	5.51	0.161 ± 0.103
1700	300	3.87	2.95	0.383 ± 0.040	1900	300	5.83	2.25	0.348 ± 0.055
1700	400	2.71	2.07	0.526 ± 0.022	1900	400	3.91	1.51	0.502 ± 0.028
1700	500	2.30	1.75	0.616 ± 0.015	1900	500	3.23	1.25	0.605 ± 0.025
1700	600	2.14	1.63	0.676 ± 0.011	1900	600	2.89	1.12	0.674 ± 0.013
1700	700	2.09	1.59	0.719 ± 0.010	1900	700	2.74	1.06	0.715 ± 0.011
1700	800	2.02	1.54	0.751 ± 0.011	1900	800	2.67	1.03	0.747 ± 0.010
1700	900	2.00	1.52	0.767 ± 0.009	1900	900	2.61	1.01	0.769 ± 0.009
1700	1000	1.98	1.51	0.774 ± 0.009	1900	1000	2.56	0.987	0.782 ± 0.011
1700	1100	1.97	1.50	0.776 ± 0.009	1900	1100	2.55	0.983	0.784 ± 0.011
1700	1200	1.98	1.51	0.770 ± 0.009	1900	1200	2.54	0.980	0.787 ± 0.009
1700	1300	2.01	1.53	0.762 ± 0.011	1900	1300	2.53	0.978	0.788 ± 0.009
1700	1400	2.07	1.58	0.739 ± 0.009	1900	1400	2.54	0.979	0.787 ± 0.009
1700	1500	2.18	1.66	0.702 ± 0.009	1900	1500	2.60	1.00	0.770 ± 0.009
1700	1600	2.51	1.91	0.609 ± 0.010	1900	1600	2.64	1.02	0.756 ± 0.009
1800	100	105	54.5	0.027 ± 0.207	1900	1700	2.79	1.08	0.715 ± 0.009
1800	200	13.0	6.74	0.178 ± 0.095	1900	1800	3.19	1.23	0.626 ± 0.010
1800	300	5.61	2.91	0.363 ± 0.045	2000	100	139	49.5	0.023 ± 0.225
1800	400	3.86	2.00	0.514 ± 0.026	2000	200	15.7	5.62	0.150 ± 0.110
1800	500	3.14	1.63	0.605 ± 0.016	2000	300	6.08	2.17	0.328 ± 0.056
1800	600	2.82	1.46	0.671 ± 0.012	2000	400	3.87	1.38	0.483 ± 0.031
1800	700	2.66	1.38	0.720 ± 0.010	2000	500	3.03	1.08	0.593 ± 0.020
1800	800	2.56	1.33	0.748 ± 0.009	2000	600	2.66	0.952	0.665 ± 0.014
1800	900	2.53	1.31	0.765 ± 0.009	2000	700	2.50	0.892	0.709 ± 0.011
1800	1000	2.49	1.29	0.776 ± 0.009	2000	800	2.38	0.850	0.743 ± 0.010
1800	1100	2.46	1.28	0.784 ± 0.015	2000	900	2.33	0.832	0.766 ± 0.009
1800	1200	2.46	1.28	0.784 ± 0.009	2000	1000	2.29	0.820	0.784 ± 0.009
1800	1300	2.47	1.28	0.783 ± 0.009	2000	1100	2.27	0.811	0.791 ± 0.009
1800	1400	2.51	1.30	0.769 ± 0.009	2000	1200	2.24	0.800	0.802 ± 0.009
1800	1500	2.58	1.34	0.749 ± 0.010	2000	1300	2.23	0.798	0.803 ± 0.009
1800	1600	2.73	1.41	0.709 ± 0.015	2000	1400	2.25	0.805	0.796 ± 0.009
1800	1700	3.15	1.63	0.613 ± 0.009	2000	1500	2.27	0.812	0.789 ± 0.009
					2000	1600	2.30	0.822	0.779 ± 0.009
					2000	1700	2.35	0.838	0.764 ± 0.009
					2000	1800	2.49	0.889	0.720 ± 0.011
					2000	1900	2.84	1.02	0.631 ± 0.010

Table A3: The 95% CL observed (Obs.) and expected (Exp.) exclusion limits (in fb) on the W_R production cross section times branching fraction for $W_R \rightarrow eejj$ as a function of W_R and N_e mass (in GeV) for $2100 \leq M_{W_R} \leq 2300$ GeV. The signal acceptance (Acc.) is also included for each (M_{W_R}, M_{N_e}) entry.

M_{W_R}	M_{N_e}	Obs.	Exp.	Acc.	M_{W_R}	M_{N_e}	Obs.	Exp.	Acc.
2100	100	173	57.8	0.024 ± 0.233	2300	100	158	61.5	0.022 ± 0.251
2100	200	18.1	6.07	0.142 ± 0.117	2300	200	15.5	6.00	0.134 ± 0.133
2100	300	6.94	2.32	0.315 ± 0.061	2300	300	5.76	2.24	0.297 ± 0.072
2100	400	4.26	1.42	0.469 ± 0.034	2300	400	3.42	1.33	0.438 ± 0.042
2100	500	3.25	1.09	0.586 ± 0.021	2300	500	2.62	1.02	0.554 ± 0.026
2100	600	2.77	0.927	0.657 ± 0.015	2300	600	2.26	0.879	0.651 ± 0.018
2100	700	2.52	0.843	0.710 ± 0.012	2300	700	2.06	0.798	0.691 ± 0.014
2100	800	2.38	0.796	0.745 ± 0.010	2300	800	1.96	0.759	0.736 ± 0.011
2100	900	2.29	0.767	0.759 ± 0.010	2300	900	1.90	0.738	0.760 ± 0.010
2100	1000	2.24	0.750	0.785 ± 0.009	2300	1000	1.85	0.716	0.779 ± 0.010
2100	1100	2.21	0.738	0.791 ± 0.009	2300	1100	1.82	0.704	0.793 ± 0.010
2100	1200	2.19	0.732	0.797 ± 0.011	2300	1200	1.81	0.703	0.801 ± 0.012
2100	1300	2.16	0.724	0.806 ± 0.011	2300	1300	1.79	0.695	0.809 ± 0.032
2100	1400	2.17	0.726	0.802 ± 0.011	2300	1400	1.78	0.691	0.813 ± 0.009
2100	1500	2.18	0.728	0.800 ± 0.009	2300	1500	1.78	0.689	0.815 ± 0.009
2100	1600	2.20	0.734	0.793 ± 0.009	2300	1600	1.78	0.692	0.812 ± 0.009
2100	1700	2.24	0.748	0.779 ± 0.011	2300	1700	1.80	0.697	0.806 ± 0.010
2100	1800	2.29	0.767	0.759 ± 0.010	2300	1800	1.81	0.701	0.801 ± 0.030
2100	1900	2.39	0.801	0.727 ± 0.009	2300	1900	1.83	0.711	0.790 ± 0.010
2100	2000	2.71	0.906	0.643 ± 0.010	2300	2000	1.89	0.734	0.765 ± 0.009
2200	100	161	57.9	0.024 ± 0.242	2300	2100	1.98	0.767	0.732 ± 0.013
2200	200	17.3	6.23	0.135 ± 0.125	2300	2200	2.21	0.856	0.656 ± 0.011
2200	300	6.67	2.40	0.300 ± 0.067					
2200	400	4.17	1.50	0.459 ± 0.038					
2200	500	3.23	1.16	0.568 ± 0.023					
2200	600	2.75	0.990	0.647 ± 0.016					
2200	700	2.48	0.894	0.704 ± 0.013					
2200	800	2.33	0.838	0.735 ± 0.012					
2200	900	2.24	0.804	0.765 ± 0.011					
2200	1000	2.17	0.780	0.784 ± 0.009					
2200	1100	2.12	0.763	0.793 ± 0.010					
2200	1200	2.10	0.757	0.799 ± 0.009					
2200	1300	2.07	0.744	0.812 ± 0.009					
2200	1400	2.10	0.754	0.801 ± 0.010					
2200	1500	2.08	0.747	0.808 ± 0.010					
2200	1600	2.08	0.749	0.806 ± 0.009					
2200	1700	2.10	0.756	0.798 ± 0.009					
2200	1800	2.13	0.768	0.786 ± 0.009					
2200	1900	2.19	0.786	0.768 ± 0.009					
2200	2000	2.30	0.826	0.730 ± 0.010					
2200	2100	2.57	0.925	0.653 ± 0.030					

Table A4: The 95% CL observed (Obs.) and expected (Exp.) exclusion limits (in fb) on the W_R production cross section times branching fraction for $W_R \rightarrow eejj$ as a function of W_R and N_e mass (in GeV) for $2400 \leq M_{W_R} \leq 2500$ GeV. The signal acceptance (Acc.) is also included for each (M_{W_R}, M_{N_e}) entry.

M_{W_R}	M_{N_e}	Obs.	Exp.	Acc.	M_{W_R}	M_{N_e}	Obs.	Exp.	Acc.
2400	100	160	73.2	0.025 ± 0.262	2500	100	157	83.8	0.027 ± 0.270
2400	200	14.3	6.57	0.127 ± 0.139	2500	200	13.6	7.27	0.125 ± 0.149
2400	300	5.09	2.33	0.278 ± 0.078	2500	300	4.63	2.47	0.265 ± 0.085
2400	400	2.93	1.34	0.429 ± 0.060	2500	400	2.60	1.39	0.414 ± 0.059
2400	500	2.16	0.990	0.548 ± 0.028	2500	500	1.82	0.972	0.539 ± 0.032
2400	600	1.79	0.821	0.634 ± 0.019	2500	600	1.50	0.800	0.622 ± 0.021
2400	700	1.63	0.745	0.691 ± 0.015	2500	700	1.32	0.705	0.683 ± 0.015
2400	800	1.52	0.696	0.732 ± 0.012	2500	800	1.22	0.651	0.729 ± 0.013
2400	900	1.54	0.706	0.757 ± 0.011	2500	900	1.15	0.613	0.750 ± 0.011
2400	1000	1.49	0.683	0.778 ± 0.010	2500	1000	1.12	0.598	0.776 ± 0.010
2400	1100	1.43	0.654	0.794 ± 0.009	2500	1100	1.09	0.581	0.790 ± 0.010
2400	1200	1.39	0.636	0.807 ± 0.010	2500	1200	1.08	0.574	0.803 ± 0.010
2400	1300	1.38	0.630	0.813 ± 0.012	2500	1300	1.07	0.569	0.809 ± 0.010
2400	1400	1.38	0.631	0.811 ± 0.009	2500	1400	1.06	0.565	0.814 ± 0.009
2400	1500	1.37	0.629	0.814 ± 0.009	2500	1500	1.05	0.560	0.820 ± 0.011
2400	1600	1.37	0.626	0.817 ± 0.009	2500	1600	1.04	0.555	0.827 ± 0.009
2400	1700	1.37	0.626	0.817 ± 0.011	2500	1700	1.06	0.563	0.815 ± 0.012
2400	1800	1.38	0.634	0.807 ± 0.011	2500	1800	1.06	0.565	0.812 ± 0.009
2400	1900	1.39	0.638	0.801 ± 0.009	2500	1900	1.06	0.563	0.814 ± 0.019
2400	2000	1.41	0.646	0.792 ± 0.009	2500	2000	1.07	0.569	0.806 ± 0.009
2400	2100	1.44	0.660	0.775 ± 0.009	2500	2100	1.08	0.576	0.797 ± 0.009
2400	2200	1.51	0.693	0.738 ± 0.011	2500	2200	1.12	0.594	0.772 ± 0.012
2400	2300	1.69	0.772	0.662 ± 0.014	2500	2300	1.16	0.620	0.740 ± 0.011
					2500	2400	1.30	0.691	0.664 ± 0.011

Table A5: The 95% CL observed (Obs.) and expected (Exp.) exclusion limits (in fb) on the W_R production cross section times branching fraction for $W_R \rightarrow eejj$ as a function of W_R and N_e mass (in GeV) for $2600 \leq M_{W_R} \leq 2700$ GeV. The signal acceptance (Acc.) is also included for each (M_{W_R}, M_{N_e}) entry.

M_{W_R}	M_{N_e}	Obs.	Exp.	Acc.	M_{W_R}	M_{N_e}	Obs.	Exp.	Acc.
2600	100	148	86.1	0.023 ± 0.276	2700	100	131	83.0	0.026 ± 0.288
2600	200	13.9	8.07	0.122 ± 0.157	2700	200	13.2	8.35	0.127 ± 0.165
2600	300	4.60	2.67	0.256 ± 0.090	2700	300	4.36	2.76	0.257 ± 0.098
2600	400	2.46	1.43	0.404 ± 0.054	2700	400	2.29	1.45	0.394 ± 0.059
2600	500	1.71	0.993	0.521 ± 0.034	2700	500	1.56	0.986	0.513 ± 0.037
2600	600	1.37	0.794	0.616 ± 0.024	2700	600	1.22	0.770	0.613 ± 0.025
2600	700	1.19	0.689	0.682 ± 0.018	2700	700	1.07	0.678	0.674 ± 0.018
2600	800	1.09	0.632	0.722 ± 0.013	2700	800	0.993	0.628	0.719 ± 0.015
2600	900	1.03	0.596	0.744 ± 0.013	2700	900	0.918	0.580	0.748 ± 0.012
2600	1000	0.977	0.568	0.771 ± 0.010	2700	1000	0.851	0.538	0.774 ± 0.012
2600	1100	0.941	0.547	0.783 ± 0.010	2700	1100	0.824	0.521	0.785 ± 0.011
2600	1200	0.947	0.550	0.803 ± 0.010	2700	1200	0.776	0.491	0.799 ± 0.010
2600	1300	0.918	0.534	0.807 ± 0.010	2700	1300	0.781	0.494	0.810 ± 0.009
2600	1400	0.912	0.530	0.812 ± 0.010	2700	1400	0.794	0.502	0.814 ± 0.010
2600	1500	0.907	0.527	0.816 ± 0.012	2700	1500	0.787	0.498	0.820 ± 0.014
2600	1600	0.897	0.521	0.825 ± 0.011	2700	1600	0.781	0.494	0.826 ± 0.014
2600	1700	0.896	0.521	0.825 ± 0.019	2700	1700	0.784	0.496	0.823 ± 0.034
2600	1800	0.901	0.523	0.821 ± 0.010	2700	1800	0.781	0.494	0.826 ± 0.016
2600	1900	0.903	0.525	0.819 ± 0.011	2700	1900	0.783	0.495	0.823 ± 0.010
2600	2000	0.908	0.528	0.814 ± 0.010	2700	2000	0.783	0.495	0.823 ± 0.010
2600	2100	0.914	0.531	0.808 ± 0.011	2700	2100	0.787	0.498	0.819 ± 0.016
2600	2200	0.927	0.539	0.797 ± 0.017	2700	2200	0.801	0.506	0.805 ± 0.011
2600	2300	0.950	0.552	0.778 ± 0.009	2700	2300	0.811	0.513	0.795 ± 0.013
2600	2400	1.00	0.581	0.739 ± 0.010	2700	2400	0.830	0.525	0.776 ± 0.009
2600	2500	1.11	0.645	0.666 ± 0.013	2700	2500	0.872	0.551	0.739 ± 0.010
					2700	2600	0.954	0.603	0.676 ± 0.012

Table A6: The 95% CL observed (Obs.) and expected (Exp.) exclusion limits (in fb) on the W_R production cross section times branching fraction for $W_R \rightarrow eejj$ as a function of W_R and N_e mass (in GeV) for $2800 \leq M_{W_R} \leq 2900$ GeV. The signal acceptance (Acc.) is also included for each (M_{W_R}, M_{N_e}) entry.

M_{W_R}	M_{N_e}	Obs.	Exp.	Acc.	M_{W_R}	M_{N_e}	Obs.	Exp.	Acc.
2800	100	138	90.4	0.028 ± 0.300	2900	100	136	91.3	0.030 ± 0.307
2800	200	15.2	9.93	0.130 ± 0.175	2900	200	16.8	11.2	0.130 ± 0.187
2800	300	5.01	3.27	0.255 ± 0.108	2900	300	5.42	3.62	0.247 ± 0.115
2800	400	2.56	1.67	0.385 ± 0.064	2900	400	2.71	1.81	0.391 ± 0.071
2800	500	1.69	1.10	0.507 ± 0.041	2900	500	1.74	1.16	0.498 ± 0.045
2800	600	1.30	0.851	0.601 ± 0.027	2900	600	1.32	0.880	0.595 ± 0.029
2800	700	1.09	0.713	0.666 ± 0.020	2900	700	1.10	0.735	0.658 ± 0.022
2800	800	1.00	0.655	0.708 ± 0.015	2900	800	0.966	0.646	0.701 ± 0.016
2800	900	0.900	0.587	0.739 ± 0.012	2900	900	0.882	0.590	0.737 ± 0.014
2800	1000	0.851	0.556	0.765 ± 0.012	2900	1000	0.830	0.555	0.758 ± 0.013
2800	1100	0.814	0.531	0.779 ± 0.018	2900	1100	0.790	0.528	0.778 ± 0.027
2800	1200	0.785	0.512	0.799 ± 0.013	2900	1200	0.761	0.509	0.795 ± 0.013
2800	1300	0.762	0.497	0.808 ± 0.010	2900	1300	0.737	0.493	0.810 ± 0.011
2800	1400	0.751	0.490	0.816 ± 0.010	2900	1400	0.721	0.482	0.815 ± 0.010
2800	1500	0.743	0.485	0.823 ± 0.010	2900	1500	0.714	0.478	0.817 ± 0.011
2800	1600	0.738	0.482	0.828 ± 0.011	2900	1600	0.706	0.472	0.826 ± 0.011
2800	1700	0.735	0.480	0.830 ± 0.011	2900	1700	0.705	0.472	0.826 ± 0.012
2800	1800	0.736	0.480	0.829 ± 0.010	2900	1800	0.698	0.467	0.834 ± 0.019
2800	1900	0.738	0.481	0.827 ± 0.009	2900	1900	0.699	0.468	0.833 ± 0.011
2800	2000	0.739	0.482	0.826 ± 0.009	2900	2000	0.698	0.467	0.834 ± 0.037
2800	2100	0.740	0.483	0.824 ± 0.012	2900	2100	0.710	0.475	0.819 ± 0.010
2800	2200	0.750	0.489	0.813 ± 0.012	2900	2200	0.706	0.472	0.824 ± 0.010
2800	2300	0.757	0.494	0.806 ± 0.010	2900	2300	0.712	0.476	0.817 ± 0.010
2800	2400	0.764	0.498	0.799 ± 0.010	2900	2400	0.718	0.480	0.811 ± 0.018
2800	2500	0.783	0.511	0.779 ± 0.009	2900	2500	0.727	0.486	0.801 ± 0.010
2800	2600	0.821	0.536	0.743 ± 0.017	2900	2600	0.748	0.500	0.778 ± 0.015
2800	2700	0.898	0.586	0.680 ± 0.013	2900	2700	0.782	0.523	0.744 ± 0.010
					2900	2800	0.846	0.566	0.688 ± 0.016

Table A7: The 95% CL observed (Obs.) and expected (Exp.) exclusion limits (in fb) on the W_R production cross section times branching fraction for $W_R \rightarrow eejj$ as a function of W_R and N_e mass (in GeV) for $3000 \leq M_{W_R} \leq 3100$ GeV. The signal acceptance (Acc.) is also included for each (M_{W_R}, M_{N_e}) entry.

M_{W_R}	M_{N_e}	Obs.	Exp.	Acc.	M_{W_R}	M_{N_e}	Obs.	Exp.	Acc.
3000	100	134	90.2	0.030 ± 0.314	3100	100	134	94.2	0.036 ± 0.318
3000	200	18.8	12.6	0.131 ± 0.196	3100	200	20.6	14.4	0.145 ± 0.204
3000	300	5.90	3.96	0.256 ± 0.124	3100	300	6.52	4.57	0.261 ± 0.136
3000	400	2.94	1.97	0.382 ± 0.082	3100	400	3.12	2.19	0.387 ± 0.089
3000	500	1.86	1.25	0.496 ± 0.052	3100	500	1.97	1.38	0.489 ± 0.057
3000	600	1.37	0.923	0.586 ± 0.033	3100	600	1.42	0.996	0.578 ± 0.037
3000	700	1.13	0.756	0.648 ± 0.022	3100	700	1.15	0.806	0.646 ± 0.028
3000	800	0.984	0.661	0.695 ± 0.019	3100	800	0.989	0.693	0.695 ± 0.018
3000	900	0.891	0.598	0.729 ± 0.017	3100	900	0.888	0.622	0.733 ± 0.019
3000	1000	0.831	0.558	0.765 ± 0.013	3100	1000	0.823	0.576	0.752 ± 0.013
3000	1100	0.786	0.528	0.779 ± 0.017	3100	1100	0.771	0.540	0.774 ± 0.012
3000	1200	0.755	0.506	0.790 ± 0.013	3100	1200	0.740	0.518	0.792 ± 0.028
3000	1300	0.730	0.490	0.799 ± 0.018	3100	1300	0.713	0.499	0.803 ± 0.020
3000	1400	0.711	0.477	0.813 ± 0.012	3100	1400	0.689	0.482	0.813 ± 0.033
3000	1500	0.695	0.466	0.825 ± 0.010	3100	1500	0.671	0.470	0.815 ± 0.010
3000	1600	0.693	0.465	0.826 ± 0.015	3100	1600	0.664	0.465	0.827 ± 0.010
3000	1700	0.687	0.461	0.833 ± 0.009	3100	1700	0.659	0.461	0.833 ± 0.010
3000	1800	0.688	0.462	0.831 ± 0.011	3100	1800	0.658	0.461	0.833 ± 0.010
3000	1900	0.688	0.462	0.831 ± 0.022	3100	1900	0.659	0.461	0.832 ± 0.013
3000	2000	0.684	0.459	0.836 ± 0.011	3100	2000	0.654	0.458	0.838 ± 0.017
3000	2100	0.686	0.460	0.833 ± 0.010	3100	2100	0.659	0.461	0.831 ± 0.024
3000	2200	0.691	0.464	0.827 ± 0.040	3100	2200	0.657	0.460	0.834 ± 0.018
3000	2300	0.691	0.464	0.826 ± 0.011	3100	2300	0.659	0.462	0.830 ± 0.011
3000	2400	0.696	0.467	0.821 ± 0.013	3100	2400	0.664	0.465	0.825 ± 0.011
3000	2500	0.704	0.473	0.811 ± 0.015	3100	2500	0.670	0.469	0.817 ± 0.011
3000	2600	0.714	0.479	0.800 ± 0.009	3100	2600	0.674	0.472	0.813 ± 0.009
3000	2700	0.729	0.489	0.784 ± 0.010	3100	2700	0.683	0.478	0.801 ± 0.010
3000	2800	0.764	0.513	0.747 ± 0.011	3100	2800	0.701	0.491	0.781 ± 0.012
3000	2900	0.826	0.555	0.691 ± 0.013	3100	2900	0.730	0.511	0.750 ± 0.010
					3100	3000	0.789	0.553	0.693 ± 0.019

Table A8: The 95% CL observed (Obs.) and expected (Exp.) exclusion limits (in fb) on the W_R production cross section times branching fraction for $W_R \rightarrow eejj$ as a function of W_R and N_e mass (in GeV) for $M_{W_R} = 3200$ GeV. The signal acceptance (Acc.) is also included for each (M_{W_R}, M_{N_e}) entry.

M_{W_R}	M_{N_e}	Obs.	Exp.	Acc.
3200	100	139	95.7	0.039 ± 0.320
3200	200	23.5	16.3	0.147 ± 0.210
3200	300	7.35	5.08	0.277 ± 0.143
3200	400	3.56	2.46	0.391 ± 0.096
3200	500	2.19	1.51	0.485 ± 0.066
3200	600	1.57	1.08	0.574 ± 0.041
3200	700	1.25	0.861	0.639 ± 0.032
3200	800	1.06	0.731	0.690 ± 0.022
3200	900	0.936	0.646	0.721 ± 0.025
3200	1000	0.860	0.594	0.749 ± 0.019
3200	1100	0.804	0.555	0.774 ± 0.016
3200	1200	0.760	0.524	0.787 ± 0.012
3200	1300	0.731	0.504	0.800 ± 0.017
3200	1400	0.705	0.487	0.809 ± 0.021
3200	1500	0.684	0.472	0.818 ± 0.014
3200	1600	0.669	0.462	0.827 ± 0.014
3200	1700	0.667	0.461	0.828 ± 0.011
3200	1800	0.662	0.457	0.834 ± 0.019
3200	1900	0.661	0.456	0.835 ± 0.011
3200	2000	0.659	0.455	0.837 ± 0.033
3200	2100	0.664	0.459	0.831 ± 0.010
3200	2200	0.658	0.454	0.838 ± 0.018
3200	2300	0.662	0.457	0.833 ± 0.011
3200	2400	0.666	0.460	0.828 ± 0.010
3200	2500	0.671	0.463	0.822 ± 0.011
3200	2600	0.676	0.467	0.816 ± 0.010
3200	2700	0.678	0.468	0.813 ± 0.015
3200	2800	0.690	0.476	0.800 ± 0.010
3200	2900	0.709	0.489	0.778 ± 0.013
3200	3000	0.730	0.504	0.755 ± 0.012
3200	3100	0.794	0.548	0.695 ± 0.028

Table A9: The 95% CL observed (Obs.) and expected (Exp.) exclusion limits (in fb) on the W_R production cross section times branching fraction for $W_R \rightarrow \mu\mu jj$ as a function of W_R and N_μ mass (in GeV) for $1000 \leq M_{W_R} \leq 1600$ GeV. This signal acceptance (Acc.) is also included for each (M_{W_R}, M_{N_μ}) entry.

M_{W_R}	M_{N_μ}	Obs.	Exp.	Acc.	M_{W_R}	M_{N_μ}	Obs.	Exp.	Acc.
1000	100	79.0	53.1	0.0664 ± 0.0685	1400	100	26.9	44.7	0.037 ± 0.140
1000	200	18.1	12.1	0.283 ± 0.017	1400	200	4.17	6.93	0.224 ± 0.029
1000	300	12.4	8.31	0.435 ± 0.014	1400	300	2.31	3.83	0.410 ± 0.016
1000	400	10.4	7.00	0.539 ± 0.014	1400	400	1.79	2.97	0.533 ± 0.015
1000	500	9.53	6.40	0.586 ± 0.015	1400	500	1.58	2.63	0.618 ± 0.015
1000	600	9.12	6.13	0.612 ± 0.014	1400	600	1.49	2.48	0.676 ± 0.014
1000	700	9.16	6.15	0.609 ± 0.014	1400	700	1.43	2.38	0.702 ± 0.014
1000	800	9.83	6.61	0.567 ± 0.014	1400	800	1.40	2.32	0.720 ± 0.014
1000	900	13.0	8.71	0.430 ± 0.015	1400	900	1.40	2.32	0.721 ± 0.014
1100	100	72.9	57.5	0.0550 ± 0.0851	1400	1000	1.40	2.33	0.717 ± 0.014
1100	200	13.7	10.8	0.275 ± 0.020	1400	1100	1.43	2.37	0.705 ± 0.014
1100	300	8.18	6.46	0.428 ± 0.015	1400	1200	1.53	2.54	0.658 ± 0.015
1100	400	6.88	5.43	0.536 ± 0.014	1400	1300	1.82	3.02	0.553 ± 0.014
1100	500	6.47	5.10	0.599 ± 0.014	1500	100	22.8	43.5	0.033 ± 0.160
1100	600	6.17	4.87	0.647 ± 0.014	1500	200	3.26	6.20	0.205 ± 0.035
1100	700	6.10	4.82	0.654 ± 0.014	1500	300	1.60	3.05	0.391 ± 0.018
1100	800	6.29	4.96	0.635 ± 0.014	1500	400	1.23	2.34	0.528 ± 0.014
1100	900	6.67	5.26	0.599 ± 0.014	1500	500	1.09	2.08	0.611 ± 0.014
1100	1000	8.53	6.73	0.468 ± 0.015	1500	600	1.03	1.97	0.675 ± 0.014
1200	100	51.3	54.3	0.047 ± 0.103	1500	700	1.01	1.91	0.707 ± 0.014
1200	200	9.38	9.92	0.259 ± 0.022	1500	800	0.988	1.88	0.731 ± 0.014
1200	300	5.76	6.10	0.426 ± 0.015	1500	900	0.978	1.86	0.738 ± 0.014
1200	400	4.66	4.93	0.543 ± 0.014	1500	1000	0.968	1.84	0.746 ± 0.014
1200	500	4.19	4.43	0.617 ± 0.014	1500	1100	0.986	1.88	0.732 ± 0.014
1200	600	3.93	4.16	0.661 ± 0.014	1500	1200	1.02	1.95	0.705 ± 0.015
1200	700	3.86	4.08	0.674 ± 0.014	1500	1300	1.08	2.05	0.670 ± 0.014
1200	800	3.82	4.04	0.680 ± 0.014	1500	1400	1.27	2.42	0.568 ± 0.014
1200	900	3.90	4.13	0.666 ± 0.014	1600	100	22.1	40.2	0.029 ± 0.179
1200	1000	4.19	4.43	0.621 ± 0.014	1600	200	3.13	5.68	0.196 ± 0.041
1200	1100	5.23	5.53	0.498 ± 0.014	1600	300	1.55	2.81	0.382 ± 0.018
1300	100	32.5	45.4	0.042 ± 0.121	1600	400	1.16	2.11	0.517 ± 0.015
1300	200	5.13	7.18	0.239 ± 0.026	1600	500	1.01	1.83	0.612 ± 0.015
1300	300	2.76	3.86	0.428 ± 0.015	1600	600	0.924	1.68	0.668 ± 0.014
1300	400	2.21	3.09	0.543 ± 0.014	1600	700	0.901	1.64	0.713 ± 0.014
1300	500	2.03	2.84	0.622 ± 0.015	1600	800	0.877	1.59	0.737 ± 0.014
1300	600	1.96	2.74	0.674 ± 0.014	1600	900	0.861	1.57	0.751 ± 0.014
1300	700	1.93	2.71	0.688 ± 0.014	1600	1000	0.855	1.56	0.755 ± 0.014
1300	800	1.88	2.63	0.707 ± 0.015	1600	1100	0.857	1.56	0.754 ± 0.014
1300	900	1.90	2.65	0.702 ± 0.014	1600	1200	0.870	1.58	0.743 ± 0.014
1300	1000	1.93	2.70	0.690 ± 0.015	1600	1300	0.890	1.62	0.726 ± 0.014
1300	1100	2.07	2.89	0.644 ± 0.014	1600	1400	0.936	1.70	0.690 ± 0.014
1300	1200	2.51	3.51	0.531 ± 0.017	1600	1500	1.10	2.00	0.588 ± 0.014

Table A10: The 95% CL observed (Obs.) and expected (Exp.) exclusion limits (in fb) on the W_R production cross section times branching fraction for $W_R \rightarrow \mu\mu jj$ as a function of W_R and N_μ mass (in GeV) for $1700 \leq M_{W_R} \leq 2000$ GeV. This signal acceptance (Acc.) is also included for each (M_{W_R}, M_{N_μ}) entry.

M_{W_R}	M_{N_μ}	Obs.	Exp.	Acc.	M_{W_R}	M_{N_μ}	Obs.	Exp.	Acc.
1700	100	28.6	44.3	0.028 ± 0.198	1900	100	38.2	45.2	0.020 ± 0.235
1700	200	3.53	5.46	0.179 ± 0.048	1900	200	4.32	5.11	0.148 ± 0.063
1700	300	1.53	2.36	0.364 ± 0.020	1900	300	1.80	2.12	0.327 ± 0.028
1700	400	1.09	1.68	0.507 ± 0.016	1900	400	1.22	1.45	0.482 ± 0.023
1700	500	0.929	1.44	0.601 ± 0.014	1900	500	1.02	1.21	0.587 ± 0.014
1700	600	0.869	1.35	0.664 ± 0.015	1900	600	0.922	1.09	0.659 ± 0.016
1700	700	0.853	1.32	0.709 ± 0.014	1900	700	0.879	1.04	0.703 ± 0.015
1700	800	0.827	1.28	0.743 ± 0.014	1900	800	0.857	1.01	0.738 ± 0.014
1700	900	0.815	1.26	0.759 ± 0.014	1900	900	0.838	0.991	0.759 ± 0.014
1700	1000	0.809	1.25	0.765 ± 0.014	1900	1000	0.824	0.974	0.774 ± 0.016
1700	1100	0.806	1.25	0.768 ± 0.015	1900	1100	0.820	0.970	0.777 ± 0.014
1700	1200	0.812	1.26	0.762 ± 0.014	1900	1200	0.818	0.967	0.780 ± 0.014
1700	1300	0.819	1.27	0.755 ± 0.014	1900	1300	0.816	0.964	0.782 ± 0.016
1700	1400	0.844	1.31	0.733 ± 0.014	1900	1400	0.817	0.966	0.781 ± 0.014
1700	1500	0.887	1.37	0.698 ± 0.015	1900	1500	0.835	0.987	0.763 ± 0.014
1700	1600	1.02	1.58	0.605 ± 0.014	1900	1600	0.848	1.00	0.752 ± 0.014
1800	100	31.5	43.8	0.023 ± 0.216	1900	1700	0.896	1.06	0.711 ± 0.015
1800	200	4.03	5.61	0.163 ± 0.055	1900	1800	1.02	1.21	0.622 ± 0.015
1800	300	1.77	2.46	0.343 ± 0.022	2000	100	41.5	46.1	0.019 ± 0.253
1800	400	1.24	1.72	0.494 ± 0.015	2000	200	4.92	5.46	0.137 ± 0.068
1800	500	1.02	1.42	0.589 ± 0.019	2000	300	1.93	2.15	0.308 ± 0.028
1800	600	0.922	1.28	0.657 ± 0.014	2000	400	1.25	1.39	0.461 ± 0.017
1800	700	0.872	1.21	0.709 ± 0.014	2000	500	0.992	1.10	0.573 ± 0.015
1800	800	0.841	1.17	0.738 ± 0.014	2000	600	0.878	0.975	0.648 ± 0.014
1800	900	0.833	1.16	0.756 ± 0.014	2000	700	0.826	0.918	0.696 ± 0.014
1800	1000	0.820	1.14	0.768 ± 0.015	2000	800	0.790	0.878	0.733 ± 0.014
1800	1100	0.810	1.13	0.777 ± 0.014	2000	900	0.775	0.861	0.757 ± 0.014
1800	1200	0.811	1.13	0.777 ± 0.014	2000	1000	0.764	0.849	0.776 ± 0.014
1800	1300	0.812	1.13	0.775 ± 0.014	2000	1100	0.755	0.839	0.785 ± 0.018
1800	1400	0.825	1.15	0.764 ± 0.014	2000	1200	0.746	0.829	0.794 ± 0.014
1800	1500	0.848	1.18	0.743 ± 0.014	2000	1300	0.744	0.827	0.796 ± 0.015
1800	1600	0.894	1.24	0.704 ± 0.014	2000	1400	0.752	0.835	0.788 ± 0.014
1800	1700	1.03	1.44	0.610 ± 0.015	2000	1500	0.758	0.842	0.782 ± 0.015
					2000	1600	0.767	0.852	0.772 ± 0.014
					2000	1700	0.781	0.868	0.758 ± 0.015
					2000	1800	0.828	0.920	0.715 ± 0.015
					2000	1900	0.946	1.05	0.627 ± 0.014

Table A11: The 95% CL observed (Obs.) and expected (Exp.) exclusion limits (in fb) on the W_R production cross section times branching fraction for $W_R \rightarrow \mu\mu jj$ as a function of W_R and N_μ mass (in GeV) for $2100 \leq M_{W_R} \leq 2300$ GeV. This signal acceptance (Acc.) is also included for each (M_{W_R}, M_{N_μ}) entry.

M_{W_R}	M_{N_μ}	Obs.	Exp.	Acc.	M_{W_R}	M_{N_μ}	Obs.	Exp.	Acc.
2100	100	51.7	54.3	0.020 ± 0.271	2300	100	54.0	49.5	0.018 ± 0.306
2100	200	5.70	5.99	0.129 ± 0.076	2300	200	5.59	5.12	0.121 ± 0.095
2100	300	2.22	2.33	0.294 ± 0.029	2300	300	2.11	1.94	0.275 ± 0.037
2100	400	1.38	1.45	0.448 ± 0.018	2300	400	1.27	1.17	0.413 ± 0.020
2100	500	1.07	1.12	0.566 ± 0.025	2300	500	0.987	0.905	0.533 ± 0.016
2100	600	0.917	0.964	0.640 ± 0.014	2300	600	0.862	0.791	0.632 ± 0.015
2100	700	0.839	0.881	0.696 ± 0.014	2300	700	0.788	0.722	0.675 ± 0.014
2100	800	0.794	0.835	0.733 ± 0.015	2300	800	0.752	0.690	0.723 ± 0.014
2100	900	0.767	0.806	0.749 ± 0.014	2300	900	0.734	0.673	0.750 ± 0.014
2100	1000	0.751	0.789	0.775 ± 0.014	2300	1000	0.714	0.654	0.769 ± 0.014
2100	1100	0.740	0.777	0.783 ± 0.014	2300	1100	0.703	0.644	0.784 ± 0.014
2100	1200	0.734	0.771	0.789 ± 0.014	2300	1200	0.701	0.643	0.794 ± 0.014
2100	1300	0.725	0.762	0.798 ± 0.014	2300	1300	0.693	0.636	0.802 ± 0.014
2100	1400	0.728	0.764	0.796 ± 0.014	2300	1400	0.690	0.633	0.806 ± 0.014
2100	1500	0.729	0.766	0.794 ± 0.014	2300	1500	0.690	0.632	0.806 ± 0.015
2100	1600	0.735	0.773	0.787 ± 0.014	2300	1600	0.690	0.633	0.806 ± 0.015
2100	1700	0.749	0.787	0.773 ± 0.014	2300	1700	0.695	0.637	0.800 ± 0.014
2100	1800	0.768	0.807	0.754 ± 0.014	2300	1800	0.700	0.642	0.795 ± 0.014
2100	1900	0.801	0.841	0.723 ± 0.014	2300	1900	0.709	0.650	0.785 ± 0.014
2100	2000	0.906	0.952	0.639 ± 0.014	2300	2000	0.731	0.671	0.760 ± 0.016
2200	100	53.2	49.5	0.018 ± 0.288	2300	2100	0.764	0.700	0.728 ± 0.014
2200	200	6.05	5.62	0.123 ± 0.085	2300	2200	0.853	0.782	0.652 ± 0.014
2200	300	2.36	2.20	0.279 ± 0.033					
2200	400	1.50	1.40	0.435 ± 0.019					
2200	500	1.17	1.09	0.547 ± 0.016					
2200	600	1.01	0.941	0.629 ± 0.015					
2200	700	0.919	0.854	0.689 ± 0.014					
2200	800	0.865	0.804	0.721 ± 0.014					
2200	900	0.832	0.774	0.754 ± 0.014					
2200	1000	0.808	0.751	0.775 ± 0.014					
2200	1100	0.791	0.736	0.783 ± 0.015					
2200	1200	0.782	0.727	0.792 ± 0.040					
2200	1300	0.770	0.716	0.804 ± 0.015					
2200	1400	0.780	0.725	0.794 ± 0.015					
2200	1500	0.774	0.719	0.801 ± 0.015					
2200	1600	0.775	0.720	0.800 ± 0.015					
2200	1700	0.782	0.727	0.792 ± 0.014					
2200	1800	0.795	0.739	0.780 ± 0.017					
2200	1900	0.814	0.756	0.762 ± 0.016					
2200	2000	0.854	0.794	0.725 ± 0.015					
2200	2100	0.955	0.888	0.649 ± 0.016					

Table A12: The 95% CL observed (Obs.) and expected (Exp.) exclusion limits (in fb) on the W_R production cross section times branching fraction for $W_R \rightarrow \mu\mu jj$ as a function of W_R and N_μ mass (in GeV) for $2400 \leq M_{W_R} \leq 2500$ GeV. This signal acceptance (Acc.) is also included for each (M_{W_R}, M_{N_μ}) entry.

M_{W_R}	M_{N_μ}	Obs.	Exp.	Acc.	M_{W_R}	M_{N_μ}	Obs.	Exp.	Acc.
2400	100	63.9	56.1	0.020 ± 0.325	2500	100	72.8	62.7	0.021 ± 0.345
2400	200	6.12	5.36	0.116 ± 0.105	2500	200	6.78	5.83	0.112 ± 0.116
2400	300	2.20	1.93	0.258 ± 0.041	2500	300	2.33	2.01	0.245 ± 0.047
2400	400	1.29	1.13	0.407 ± 0.022	2500	400	1.33	1.14	0.389 ± 0.024
2400	500	0.961	0.843	0.526 ± 0.016	2500	500	0.944	0.813	0.515 ± 0.017
2400	600	0.804	0.705	0.614 ± 0.015	2500	600	0.784	0.675	0.602 ± 0.016
2400	700	0.735	0.645	0.675 ± 0.014	2500	700	0.697	0.600	0.665 ± 0.014
2400	800	0.690	0.605	0.718 ± 0.014	2500	800	0.647	0.557	0.714 ± 0.014
2400	900	0.702	0.616	0.745 ± 0.016	2500	900	0.611	0.526	0.738 ± 0.014
2400	1000	0.681	0.597	0.768 ± 0.014	2500	1000	0.597	0.514	0.766 ± 0.014
2400	1100	0.653	0.572	0.784 ± 0.014	2500	1100	0.581	0.500	0.781 ± 0.014
2400	1200	0.635	0.557	0.800 ± 0.014	2500	1200	0.574	0.494	0.794 ± 0.014
2400	1300	0.631	0.553	0.805 ± 0.015	2500	1300	0.569	0.490	0.802 ± 0.014
2400	1400	0.632	0.554	0.804 ± 0.014	2500	1400	0.565	0.486	0.807 ± 0.014
2400	1500	0.630	0.552	0.806 ± 0.014	2500	1500	0.561	0.483	0.813 ± 0.015
2400	1600	0.626	0.549	0.811 ± 0.015	2500	1600	0.556	0.479	0.820 ± 0.016
2400	1700	0.627	0.550	0.810 ± 0.022	2500	1700	0.564	0.485	0.809 ± 0.019
2400	1800	0.634	0.556	0.802 ± 0.021	2500	1800	0.566	0.487	0.806 ± 0.018
2400	1900	0.639	0.561	0.795 ± 0.014	2500	1900	0.564	0.485	0.810 ± 0.016
2400	2000	0.646	0.566	0.786 ± 0.014	2500	2000	0.570	0.491	0.800 ± 0.014
2400	2100	0.660	0.579	0.769 ± 0.014	2500	2100	0.576	0.496	0.791 ± 0.014
2400	2200	0.692	0.607	0.734 ± 0.014	2500	2200	0.595	0.512	0.766 ± 0.016
2400	2300	0.771	0.676	0.659 ± 0.017	2500	2300	0.621	0.534	0.735 ± 0.015
					2500	2400	0.691	0.594	0.661 ± 0.015

Table A13: The 95% CL observed (Obs.) and expected (Exp.) exclusion limits (in fb) on the W_R production cross section times branching fraction for $W_R \rightarrow \mu\mu jj$ as a function of W_R and N_μ mass (in GeV) for $2600 \leq M_{W_R} \leq 2700$ GeV. This signal acceptance (Acc.) is also included for each (M_{W_R}, M_{N_μ}) entry.

M_{W_R}	M_{N_μ}	Obs.	Exp.	Acc.	M_{W_R}	M_{N_μ}	Obs.	Exp.	Acc.
2600	100	74.3	62.3	0.019 ± 0.359	2700	100	68.8	59.9	0.021 ± 0.378
2600	200	7.52	6.30	0.110 ± 0.127	2700	200	7.51	6.55	0.114 ± 0.142
2600	300	2.53	2.12	0.236 ± 0.053	2700	300	2.52	2.20	0.237 ± 0.060
2600	400	1.37	1.15	0.379 ± 0.029	2700	400	1.34	1.17	0.369 ± 0.032
2600	500	0.963	0.807	0.498 ± 0.018	2700	500	0.923	0.805	0.487 ± 0.019
2600	600	0.777	0.651	0.594 ± 0.015	2700	600	0.728	0.635	0.589 ± 0.015
2600	700	0.680	0.570	0.663 ± 0.014	2700	700	0.646	0.564	0.652 ± 0.015
2600	800	0.627	0.526	0.707 ± 0.014	2700	800	0.602	0.525	0.701 ± 0.014
2600	900	0.593	0.497	0.732 ± 0.014	2700	900	0.558	0.487	0.733 ± 0.014
2600	1000	0.567	0.475	0.760 ± 0.014	2700	1000	0.519	0.453	0.761 ± 0.014
2600	1100	0.547	0.458	0.773 ± 0.015	2700	1100	0.504	0.439	0.775 ± 0.019
2600	1200	0.551	0.462	0.794 ± 0.014	2700	1200	0.475	0.414	0.789 ± 0.016
2600	1300	0.535	0.448	0.799 ± 0.014	2700	1300	0.479	0.417	0.802 ± 0.016
2600	1400	0.531	0.445	0.805 ± 0.015	2700	1400	0.487	0.424	0.806 ± 0.025
2600	1500	0.529	0.443	0.808 ± 0.014	2700	1500	0.482	0.421	0.813 ± 0.014
2600	1600	0.522	0.438	0.818 ± 0.017	2700	1600	0.479	0.418	0.818 ± 0.014
2600	1700	0.522	0.438	0.819 ± 0.014	2700	1700	0.481	0.419	0.816 ± 0.014
2600	1800	0.525	0.440	0.814 ± 0.035	2700	1800	0.479	0.417	0.820 ± 0.015
2600	1900	0.526	0.441	0.812 ± 0.014	2700	1900	0.480	0.419	0.817 ± 0.014
2600	2000	0.529	0.444	0.807 ± 0.014	2700	2000	0.480	0.419	0.816 ± 0.014
2600	2100	0.533	0.446	0.802 ± 0.014	2700	2100	0.482	0.420	0.813 ± 0.016
2600	2200	0.540	0.452	0.792 ± 0.016	2700	2200	0.491	0.428	0.799 ± 0.014
2600	2300	0.553	0.464	0.772 ± 0.015	2700	2300	0.497	0.433	0.790 ± 0.022
2600	2400	0.582	0.487	0.735 ± 0.015	2700	2400	0.509	0.444	0.771 ± 0.014
2600	2500	0.645	0.541	0.662 ± 0.015	2700	2500	0.533	0.465	0.736 ± 0.015
					2700	2600	0.583	0.508	0.673 ± 0.017

Table A14: The 95% CL observed (Obs.) and expected (Exp.) exclusion limits (in fb) on the W_R production cross section times branching fraction for $W_R \rightarrow \mu\mu jj$ as a function of W_R and N_μ mass (in GeV) for $2800 \leq M_{W_R} \leq 2900$ GeV. This signal acceptance (Acc.) is also included for each (M_{W_R}, M_{N_μ}) entry.

M_{W_R}	M_{N_μ}	Obs.	Exp.	Acc.	M_{W_R}	M_{N_μ}	Obs.	Exp.	Acc.
2800	100	71.6	63.4	0.023 ± 0.398	2900	100	73.4	63.2	0.024 ± 0.412
2800	200	8.59	7.62	0.116 ± 0.154	2900	200	9.90	8.53	0.117 ± 0.169
2800	300	2.87	2.55	0.235 ± 0.066	2900	300	3.25	2.80	0.227 ± 0.079
2800	400	1.49	1.32	0.360 ± 0.036	2900	400	1.65	1.42	0.365 ± 0.045
2800	500	0.992	0.879	0.482 ± 0.021	2900	500	1.07	0.919	0.471 ± 0.040
2800	600	0.774	0.686	0.576 ± 0.016	2900	600	0.817	0.703	0.570 ± 0.017
2800	700	0.654	0.580	0.645 ± 0.015	2900	700	0.688	0.593	0.637 ± 0.015
2800	800	0.604	0.535	0.691 ± 0.014	2900	800	0.608	0.524	0.683 ± 0.014
2800	900	0.544	0.482	0.724 ± 0.014	2900	900	0.558	0.481	0.721 ± 0.014
2800	1000	0.516	0.458	0.752 ± 0.017	2900	1000	0.527	0.454	0.744 ± 0.014
2800	1100	0.494	0.438	0.768 ± 0.015	2900	1100	0.503	0.433	0.767 ± 0.014
2800	1200	0.478	0.424	0.789 ± 0.015	2900	1200	0.485	0.417	0.784 ± 0.018
2800	1300	0.464	0.412	0.800 ± 0.014	2900	1300	0.470	0.405	0.800 ± 0.014
2800	1400	0.457	0.406	0.807 ± 0.014	2900	1400	0.461	0.397	0.807 ± 0.015
2800	1500	0.453	0.402	0.815 ± 0.015	2900	1500	0.455	0.392	0.810 ± 0.014
2800	1600	0.450	0.399	0.820 ± 0.014	2900	1600	0.450	0.387	0.820 ± 0.015
2800	1700	0.448	0.397	0.824 ± 0.014	2900	1700	0.450	0.388	0.820 ± 0.015
2800	1800	0.449	0.398	0.823 ± 0.014	2900	1800	0.446	0.384	0.827 ± 0.028
2800	1900	0.450	0.399	0.821 ± 0.016	2900	1900	0.447	0.385	0.825 ± 0.017
2800	2000	0.450	0.399	0.820 ± 0.014	2900	2000	0.445	0.383	0.828 ± 0.017
2800	2100	0.451	0.400	0.818 ± 0.014	2900	2100	0.454	0.391	0.813 ± 0.014
2800	2200	0.457	0.406	0.807 ± 0.015	2900	2200	0.451	0.388	0.819 ± 0.016
2800	2300	0.461	0.409	0.801 ± 0.015	2900	2300	0.454	0.391	0.812 ± 0.016
2800	2400	0.465	0.412	0.794 ± 0.015	2900	2400	0.458	0.395	0.805 ± 0.014
2800	2500	0.477	0.423	0.774 ± 0.014	2900	2500	0.464	0.399	0.796 ± 0.014
2800	2600	0.500	0.443	0.739 ± 0.015	2900	2600	0.477	0.411	0.773 ± 0.014
2800	2700	0.546	0.484	0.676 ± 0.016	2900	2700	0.499	0.429	0.740 ± 0.014
					2900	2800	0.539	0.464	0.684 ± 0.020

Table A15: The 95% CL observed (Obs.) and expected (Exp.) exclusion limits (in fb) on the W_R production cross section times branching fraction for $W_R \rightarrow \mu\mu jj$ as a function of W_R and N_μ mass (in GeV) for $3000 \leq M_{W_R} \leq 3100$ GeV. This signal acceptance (Acc.) is also included for each (M_{W_R}, M_{N_μ}) entry.

M_{W_R}	M_{N_μ}	Obs.	Exp.	Acc.	M_{W_R}	M_{N_μ}	Obs.	Exp.	Acc.
3000	100	72.8	63.2	0.024 ± 0.428	3100	100	75.6	65.9	0.029 ± 0.439
3000	200	11.3	9.79	0.117 ± 0.185	3100	200	12.9	11.2	0.130 ± 0.197
3000	300	3.59	3.12	0.234 ± 0.094	3100	300	4.15	3.62	0.240 ± 0.104
3000	400	1.81	1.57	0.356 ± 0.052	3100	400	2.01	1.75	0.359 ± 0.060
3000	500	1.16	1.01	0.469 ± 0.031	3100	500	1.28	1.12	0.461 ± 0.037
3000	600	0.864	0.750	0.561 ± 0.019	3100	600	0.935	0.815	0.552 ± 0.024
3000	700	0.714	0.620	0.627 ± 0.016	3100	700	0.763	0.665	0.623 ± 0.021
3000	800	0.628	0.545	0.675 ± 0.015	3100	800	0.660	0.575	0.674 ± 0.016
3000	900	0.571	0.496	0.713 ± 0.016	3100	900	0.595	0.519	0.715 ± 0.015
3000	1000	0.535	0.465	0.750 ± 0.014	3100	1000	0.554	0.483	0.738 ± 0.015
3000	1100	0.507	0.440	0.767 ± 0.015	3100	1100	0.521	0.454	0.762 ± 0.018
3000	1200	0.488	0.424	0.780 ± 0.020	3100	1200	0.500	0.436	0.781 ± 0.017
3000	1300	0.473	0.410	0.790 ± 0.015	3100	1300	0.483	0.421	0.793 ± 0.015
3000	1400	0.461	0.400	0.805 ± 0.018	3100	1400	0.467	0.407	0.805 ± 0.023
3000	1500	0.451	0.391	0.816 ± 0.016	3100	1500	0.455	0.397	0.808 ± 0.018
3000	1600	0.449	0.390	0.819 ± 0.014	3100	1600	0.451	0.393	0.818 ± 0.032
3000	1700	0.445	0.387	0.826 ± 0.017	3100	1700	0.448	0.390	0.825 ± 0.017
3000	1800	0.446	0.387	0.824 ± 0.018	3100	1800	0.447	0.390	0.825 ± 0.032
3000	1900	0.446	0.387	0.824 ± 0.015	3100	1900	0.448	0.390	0.825 ± 0.018
3000	2000	0.443	0.385	0.829 ± 0.031	3100	2000	0.445	0.387	0.831 ± 0.014
3000	2100	0.444	0.385	0.828 ± 0.015	3100	2100	0.448	0.390	0.825 ± 0.041
3000	2200	0.448	0.389	0.820 ± 0.015	3100	2200	0.446	0.389	0.828 ± 0.015
3000	2300	0.448	0.389	0.821 ± 0.026	3100	2300	0.448	0.390	0.824 ± 0.020
3000	2400	0.451	0.392	0.815 ± 0.014	3100	2400	0.451	0.393	0.819 ± 0.015
3000	2500	0.456	0.396	0.806 ± 0.017	3100	2500	0.455	0.396	0.812 ± 0.015
3000	2600	0.462	0.401	0.795 ± 0.015	3100	2600	0.457	0.399	0.807 ± 0.016
3000	2700	0.471	0.409	0.780 ± 0.014	3100	2700	0.463	0.404	0.797 ± 0.017
3000	2800	0.494	0.429	0.744 ± 0.014	3100	2800	0.475	0.414	0.777 ± 0.014
3000	2900	0.535	0.464	0.688 ± 0.024	3100	2900	0.494	0.431	0.747 ± 0.015
					3100	3000	0.535	0.466	0.690 ± 0.019

Table A16: The 95% CL observed (Obs.) and expected (Exp.) exclusion limits (in fb) on the W_R production cross section times branching fraction for $W_R \rightarrow \mu\mu jj$ as a function of W_R and N_μ mass (in GeV) for $M_{W_R} = 3200$ GeV. This signal acceptance (Acc.) is also included for each (M_{W_R}, M_{N_μ}) entry.

M_{W_R}	M_{N_μ}	Obs.	Exp.	Acc.
3200	100	75.8	66.0	0.031 ± 0.449
3200	200	14.4	12.5	0.131 ± 0.206
3200	300	4.58	3.99	0.254 ± 0.111
3200	400	2.24	1.95	0.363 ± 0.070
3200	500	1.39	1.21	0.458 ± 0.050
3200	600	1.01	0.877	0.546 ± 0.029
3200	700	0.808	0.704	0.614 ± 0.020
3200	800	0.691	0.602	0.668 ± 0.016
3200	900	0.614	0.535	0.703 ± 0.018
3200	1000	0.567	0.494	0.734 ± 0.014
3200	1100	0.531	0.463	0.762 ± 0.027
3200	1200	0.503	0.438	0.776 ± 0.015
3200	1300	0.485	0.422	0.790 ± 0.026
3200	1400	0.468	0.408	0.799 ± 0.015
3200	1500	0.455	0.396	0.808 ± 0.016
3200	1600	0.445	0.388	0.819 ± 0.015
3200	1700	0.444	0.387	0.820 ± 0.030
3200	1800	0.441	0.384	0.827 ± 0.018
3200	1900	0.440	0.383	0.829 ± 0.031
3200	2000	0.438	0.382	0.832 ± 0.023
3200	2100	0.442	0.385	0.825 ± 0.018
3200	2200	0.438	0.382	0.831 ± 0.019
3200	2300	0.441	0.385	0.826 ± 0.019
3200	2400	0.443	0.386	0.822 ± 0.015
3200	2500	0.446	0.389	0.817 ± 0.018
3200	2600	0.449	0.391	0.811 ± 0.017
3200	2700	0.451	0.393	0.808 ± 0.021
3200	2800	0.459	0.399	0.795 ± 0.021
3200	2900	0.471	0.410	0.774 ± 0.022
3200	3000	0.485	0.423	0.751 ± 0.015
3200	3100	0.527	0.459	0.691 ± 0.039

Table A17: The 95% CL observed (Obs.) and expected (Exp.) exclusion limits (in fb) on the W_R production cross section times branching fraction for $W_R \rightarrow (ee + \mu\mu)jj$ as a function of W_R and N_ℓ mass (in GeV) for $1000 \leq M_{W_R} \leq 1600$ GeV. The signal acceptance (Acc.) is also included for each (M_{W_R}, M_{N_ℓ}) entry.

M_{W_R}	M_{N_ℓ}	Obs.	Exp.	Acc.	M_{W_R}	M_{N_ℓ}	Obs.	Exp.	Acc.
1000	100	117	88.5	0.0695 ± 0.0650	1400	100	54.0	71.9	0.040 ± 0.109
1000	200	26.3	19.9	0.291 ± 0.018	1400	200	8.26	11.0	0.232 ± 0.034
1000	300	17.8	13.5	0.441 ± 0.010	1400	300	4.52	6.02	0.419 ± 0.016
1000	400	15.0	11.3	0.544 ± 0.009	1400	400	3.49	4.64	0.541 ± 0.011
1000	500	13.7	10.3	0.591 ± 0.009	1400	500	3.07	4.08	0.624 ± 0.009
1000	600	13.1	9.90	0.616 ± 0.008	1400	600	2.89	3.84	0.682 ± 0.009
1000	700	13.1	9.94	0.613 ± 0.008	1400	700	2.77	3.69	0.707 ± 0.009
1000	800	14.1	10.7	0.570 ± 0.008	1400	800	2.70	3.60	0.725 ± 0.008
1000	900	18.6	14.1	0.433 ± 0.009	1400	900	2.70	3.59	0.725 ± 0.008
1100	100	150	98.2	0.0582 ± 0.0760	1400	1000	2.71	3.61	0.721 ± 0.008
1100	200	27.8	18.1	0.282 ± 0.021	1400	1100	2.76	3.68	0.708 ± 0.008
1100	300	16.4	10.7	0.435 ± 0.011	1400	1200	2.96	3.93	0.661 ± 0.009
1100	400	13.8	9.00	0.542 ± 0.009	1400	1300	3.52	4.68	0.555 ± 0.009
1100	500	12.9	8.43	0.604 ± 0.009	1500	100	46.7	69.1	0.035 ± 0.119
1100	600	12.3	8.04	0.651 ± 0.009	1500	200	6.57	9.72	0.212 ± 0.039
1100	700	12.2	7.95	0.659 ± 0.008	1500	300	3.20	4.74	0.401 ± 0.018
1100	800	12.5	8.19	0.639 ± 0.009	1500	400	2.44	3.61	0.536 ± 0.011
1100	900	13.3	8.68	0.602 ± 0.009	1500	500	2.15	3.19	0.618 ± 0.009
1100	1000	17.0	11.1	0.470 ± 0.009	1500	600	2.04	3.01	0.680 ± 0.009
1200	100	108	89.9	0.0495 ± 0.0869	1500	700	1.98	2.92	0.711 ± 0.009
1200	200	19.5	16.2	0.267 ± 0.025	1500	800	1.94	2.87	0.735 ± 0.009
1200	300	11.9	9.84	0.434 ± 0.012	1500	900	1.92	2.84	0.742 ± 0.008
1200	400	9.54	7.92	0.549 ± 0.009	1500	1000	1.90	2.81	0.750 ± 0.008
1200	500	8.56	7.10	0.622 ± 0.009	1500	1100	1.94	2.87	0.735 ± 0.008
1200	600	8.01	6.65	0.666 ± 0.008	1500	1200	2.01	2.98	0.708 ± 0.009
1200	700	7.86	6.52	0.679 ± 0.008	1500	1300	2.11	3.13	0.673 ± 0.008
1200	800	7.79	6.46	0.684 ± 0.008	1500	1400	2.50	3.69	0.570 ± 0.008
1200	900	7.95	6.60	0.670 ± 0.009	1600	100	46.4	67.3	0.031 ± 0.130
1200	1000	8.53	7.08	0.624 ± 0.009	1600	200	6.48	9.39	0.204 ± 0.044
1200	1100	10.6	8.83	0.500 ± 0.008	1600	300	3.17	4.59	0.392 ± 0.020
1300	100	64.6	72.0	0.0445 ± 0.0977	1600	400	2.36	3.43	0.527 ± 0.012
1300	200	10.1	11.2	0.246 ± 0.030	1600	500	2.04	2.96	0.620 ± 0.011
1300	300	5.36	5.97	0.437 ± 0.014	1600	600	1.87	2.71	0.674 ± 0.009
1300	400	4.26	4.75	0.551 ± 0.010	1600	700	1.82	2.64	0.718 ± 0.008
1300	500	3.90	4.35	0.628 ± 0.009	1600	800	1.77	2.56	0.742 ± 0.009
1300	600	3.76	4.19	0.679 ± 0.009	1600	900	1.74	2.52	0.755 ± 0.008
1300	700	3.71	4.13	0.694 ± 0.008	1600	1000	1.72	2.50	0.759 ± 0.008
1300	800	3.61	4.02	0.712 ± 0.009	1600	1100	1.73	2.50	0.758 ± 0.008
1300	900	3.64	4.05	0.706 ± 0.008	1600	1200	1.75	2.54	0.746 ± 0.008
1300	1000	3.70	4.12	0.694 ± 0.009	1600	1300	1.79	2.60	0.729 ± 0.008
1300	1100	3.96	4.42	0.647 ± 0.008	1600	1400	1.89	2.74	0.692 ± 0.009
1300	1200	4.81	5.36	0.534 ± 0.009	1600	1500	2.22	3.21	0.590 ± 0.009

Table A18: The 95% CL observed (Obs.) and expected (Exp.) exclusion limits (in fb) on the W_R production cross section times branching fraction for $W_R \rightarrow (ee + \mu\mu)jj$ as a function of W_R and N_ℓ mass (in GeV) for $1700 \leq M_{W_R} \leq 2000$ GeV. The signal acceptance (Acc.) is also included for each (M_{W_R}, M_{N_ℓ}) entry.

M_{W_R}	M_{N_ℓ}	Obs.	Exp.	Acc.	M_{W_R}	M_{N_ℓ}	Obs.	Exp.	Acc.
1700	100	60.3	75.0	0.029 ± 0.140	1900	100	117	69.5	0.022 ± 0.159
1700	200	7.31	9.09	0.187 ± 0.049	1900	200	13.0	7.71	0.154 ± 0.061
1700	300	3.13	3.90	0.373 ± 0.023	1900	300	5.37	3.17	0.338 ± 0.031
1700	400	2.21	2.75	0.516 ± 0.014	1900	400	3.63	2.14	0.492 ± 0.018
1700	500	1.88	2.34	0.609 ± 0.010	1900	500	3.01	1.78	0.596 ± 0.015
1700	600	1.76	2.19	0.670 ± 0.009	1900	600	2.71	1.60	0.667 ± 0.010
1700	700	1.72	2.14	0.714 ± 0.009	1900	700	2.58	1.52	0.709 ± 0.009
1700	800	1.67	2.07	0.747 ± 0.009	1900	800	2.51	1.48	0.743 ± 0.009
1700	900	1.64	2.04	0.763 ± 0.008	1900	900	2.45	1.45	0.764 ± 0.009
1700	1000	1.63	2.03	0.770 ± 0.008	1900	1000	2.41	1.42	0.778 ± 0.010
1700	1100	1.62	2.02	0.772 ± 0.009	1900	1100	2.40	1.42	0.781 ± 0.009
1700	1200	1.63	2.03	0.766 ± 0.008	1900	1200	2.39	1.41	0.783 ± 0.008
1700	1300	1.65	2.05	0.758 ± 0.009	1900	1300	2.38	1.41	0.785 ± 0.009
1700	1400	1.70	2.11	0.736 ± 0.008	1900	1400	2.39	1.41	0.784 ± 0.008
1700	1500	1.79	2.22	0.700 ± 0.009	1900	1500	2.44	1.44	0.767 ± 0.008
1700	1600	2.06	2.56	0.607 ± 0.009	1900	1600	2.48	1.47	0.754 ± 0.008
1800	100	81.1	71.6	0.025 ± 0.150	1900	1700	2.62	1.55	0.713 ± 0.009
1800	200	10.2	9.02	0.170 ± 0.055	1900	1800	2.99	1.77	0.624 ± 0.009
1800	300	4.45	3.93	0.353 ± 0.025	2000	100	137	67.6	0.021 ± 0.169
1800	400	3.08	2.72	0.504 ± 0.015	2000	200	15.9	7.84	0.143 ± 0.065
1800	500	2.52	2.23	0.597 ± 0.013	2000	300	6.20	3.06	0.318 ± 0.032
1800	600	2.28	2.01	0.664 ± 0.009	2000	400	3.97	1.96	0.472 ± 0.018
1800	700	2.15	1.90	0.715 ± 0.009	2000	500	3.14	1.55	0.583 ± 0.012
1800	800	2.07	1.83	0.743 ± 0.008	2000	600	2.77	1.36	0.656 ± 0.010
1800	900	2.05	1.81	0.760 ± 0.008	2000	700	2.60	1.28	0.702 ± 0.009
1800	1000	2.02	1.78	0.772 ± 0.009	2000	800	2.48	1.22	0.738 ± 0.009
1800	1100	1.99	1.76	0.781 ± 0.010	2000	900	2.43	1.20	0.762 ± 0.008
1800	1200	1.99	1.76	0.780 ± 0.008	2000	1000	2.40	1.18	0.780 ± 0.008
1800	1300	2.00	1.76	0.779 ± 0.008	2000	1100	2.37	1.17	0.788 ± 0.010
1800	1400	2.03	1.79	0.766 ± 0.008	2000	1200	2.34	1.15	0.798 ± 0.008
1800	1500	2.08	1.84	0.746 ± 0.008	2000	1300	2.33	1.15	0.799 ± 0.009
1800	1600	2.20	1.94	0.706 ± 0.010	2000	1400	2.36	1.16	0.792 ± 0.008
1800	1700	2.54	2.24	0.612 ± 0.009	2000	1500	2.37	1.17	0.785 ± 0.009
					2000	1600	2.40	1.19	0.776 ± 0.008
					2000	1700	2.45	1.21	0.761 ± 0.009
					2000	1800	2.59	1.28	0.718 ± 0.009
					2000	1900	2.96	1.46	0.629 ± 0.009

Table A19: The 95% CL observed (Obs.) and expected (Exp.) exclusion limits (in fb) on the W_R production cross section times branching fraction for $W_R \rightarrow (ee + \mu\mu)jj$ as a function of W_R and N_ℓ mass (in GeV) for $2100 \leq M_{W_R} \leq 2300$ GeV. The signal acceptance (Acc.) is also included for each (M_{W_R}, M_{N_ℓ}) entry.

M_{W_R}	M_{N_ℓ}	Obs.	Exp.	Acc.	M_{W_R}	M_{N_ℓ}	Obs.	Exp.	Acc.
2100	100	172	79.3	0.022 ± 0.178	2300	100	147	77.7	0.020 ± 0.197
2100	200	18.5	8.55	0.135 ± 0.070	2300	200	14.8	7.81	0.127 ± 0.082
2100	300	7.14	3.30	0.305 ± 0.034	2300	300	5.57	2.94	0.286 ± 0.041
2100	400	4.41	2.04	0.458 ± 0.019	2300	400	3.33	1.76	0.425 ± 0.023
2100	500	3.39	1.57	0.576 ± 0.016	2300	500	2.56	1.35	0.543 ± 0.015
2100	600	2.90	1.34	0.648 ± 0.010	2300	600	2.23	1.18	0.641 ± 0.011
2100	700	2.65	1.22	0.703 ± 0.009	2300	700	2.03	1.07	0.683 ± 0.010
2100	800	2.50	1.16	0.739 ± 0.009	2300	800	1.94	1.02	0.730 ± 0.009
2100	900	2.42	1.12	0.754 ± 0.009	2300	900	1.89	0.994	0.755 ± 0.009
2100	1000	2.36	1.09	0.780 ± 0.008	2300	1000	1.83	0.966	0.774 ± 0.008
2100	1100	2.33	1.07	0.787 ± 0.008	2300	1100	1.80	0.950	0.788 ± 0.009
2100	1200	2.31	1.07	0.793 ± 0.009	2300	1200	1.80	0.948	0.797 ± 0.009
2100	1300	2.28	1.05	0.802 ± 0.009	2300	1300	1.78	0.937	0.806 ± 0.017
2100	1400	2.29	1.06	0.799 ± 0.009	2300	1400	1.77	0.933	0.810 ± 0.008
2100	1500	2.29	1.06	0.797 ± 0.008	2300	1500	1.77	0.932	0.811 ± 0.009
2100	1600	2.31	1.07	0.790 ± 0.008	2300	1600	1.77	0.933	0.809 ± 0.009
2100	1700	2.35	1.09	0.776 ± 0.009	2300	1700	1.78	0.939	0.803 ± 0.009
2100	1800	2.41	1.12	0.756 ± 0.009	2300	1800	1.79	0.946	0.798 ± 0.017
2100	1900	2.52	1.16	0.725 ± 0.008	2300	1900	1.82	0.958	0.787 ± 0.009
2100	2000	2.85	1.32	0.641 ± 0.009	2300	2000	1.87	0.988	0.763 ± 0.009
2200	100	159	76.4	0.021 ± 0.187	2300	2100	1.96	1.03	0.730 ± 0.010
2200	200	17.6	8.46	0.129 ± 0.076	2300	2200	2.19	1.15	0.654 ± 0.009
2200	300	6.82	3.28	0.289 ± 0.037					
2200	400	4.30	2.07	0.446 ± 0.021					
2200	500	3.35	1.61	0.557 ± 0.014					
2200	600	2.87	1.38	0.637 ± 0.011					
2200	700	2.60	1.25	0.696 ± 0.010					
2200	800	2.44	1.17	0.728 ± 0.009					
2200	900	2.35	1.13	0.760 ± 0.009					
2200	1000	2.27	1.09	0.780 ± 0.008					
2200	1100	2.23	1.07	0.788 ± 0.009					
2200	1200	2.20	1.06	0.796 ± 0.021					
2200	1300	2.17	1.04	0.808 ± 0.009					
2200	1400	2.19	1.06	0.798 ± 0.009					
2200	1500	2.18	1.05	0.804 ± 0.009					
2200	1600	2.18	1.05	0.803 ± 0.009					
2200	1700	2.20	1.06	0.795 ± 0.008					
2200	1800	2.23	1.07	0.783 ± 0.009					
2200	1900	2.29	1.10	0.765 ± 0.009					
2200	2000	2.40	1.16	0.728 ± 0.009					
2200	2100	2.69	1.29	0.651 ± 0.017					

Table A20: The 95% CL observed (Obs.) and expected (Exp.) exclusion limits (in fb) on the W_R production cross section times branching fraction for $W_R \rightarrow (ee + \mu\mu)jj$ as a function of W_R and N_ℓ mass (in GeV) for $2400 \leq M_{W_R} \leq 2500$ GeV. The signal acceptance (Acc.) is also included for each (M_{W_R}, M_{N_ℓ}) entry.

M_{W_R}	M_{N_ℓ}	Obs.	Exp.	Acc.	M_{W_R}	M_{N_ℓ}	Obs.	Exp.	Acc.
2400	100	151	88.1	0.022 ± 0.207	2500	100	153	98.3	0.024 ± 0.217
2400	200	14.0	8.18	0.121 ± 0.088	2500	200	13.8	8.85	0.119 ± 0.095
2400	300	5.00	2.93	0.268 ± 0.044	2500	300	4.71	3.02	0.254 ± 0.049
2400	400	2.90	1.69	0.418 ± 0.032	2500	400	2.67	1.71	0.401 ± 0.032
2400	500	2.15	1.26	0.537 ± 0.016	2500	500	1.88	1.21	0.527 ± 0.018
2400	600	1.79	1.05	0.624 ± 0.012	2500	600	1.56	0.999	0.612 ± 0.013
2400	700	1.63	0.956	0.683 ± 0.010	2500	700	1.38	0.884	0.674 ± 0.011
2400	800	1.53	0.895	0.725 ± 0.009	2500	800	1.28	0.818	0.722 ± 0.009
2400	900	1.55	0.909	0.751 ± 0.010	2500	900	1.20	0.772	0.744 ± 0.009
2400	1000	1.50	0.880	0.773 ± 0.009	2500	1000	1.17	0.753	0.771 ± 0.009
2400	1100	1.44	0.843	0.789 ± 0.008	2500	1100	1.14	0.733	0.785 ± 0.009
2400	1200	1.40	0.820	0.803 ± 0.009	2500	1200	1.13	0.724	0.798 ± 0.009
2400	1300	1.39	0.815	0.809 ± 0.009	2500	1300	1.12	0.717	0.805 ± 0.008
2400	1400	1.39	0.815	0.807 ± 0.008	2500	1400	1.11	0.712	0.811 ± 0.008
2400	1500	1.39	0.813	0.810 ± 0.008	2500	1500	1.10	0.707	0.816 ± 0.009
2400	1600	1.38	0.809	0.814 ± 0.009	2500	1600	1.09	0.700	0.824 ± 0.009
2400	1700	1.38	0.809	0.813 ± 0.012	2500	1700	1.11	0.710	0.812 ± 0.011
2400	1800	1.40	0.818	0.804 ± 0.012	2500	1800	1.11	0.713	0.809 ± 0.010
2400	1900	1.41	0.825	0.798 ± 0.009	2500	1900	1.11	0.710	0.812 ± 0.012
2400	2000	1.43	0.834	0.789 ± 0.008	2500	2000	1.12	0.718	0.803 ± 0.008
2400	2100	1.46	0.852	0.772 ± 0.008	2500	2100	1.13	0.726	0.794 ± 0.008
2400	2200	1.53	0.894	0.736 ± 0.009	2500	2200	1.17	0.750	0.769 ± 0.010
2400	2300	1.70	0.995	0.660 ± 0.011	2500	2300	1.22	0.781	0.737 ± 0.009
					2500	2400	1.36	0.869	0.662 ± 0.009

Table A21: The 95% CL observed (Obs.) and expected (Exp.) exclusion limits (in fb) on the W_R production cross section times branching fraction for $W_R \rightarrow (ee + \mu\mu)jj$ as a function of W_R and N_ℓ mass (in GeV) for $2600 \leq M_{W_R} \leq 2700$ GeV. The signal acceptance (Acc.) is also included for each (M_{W_R}, M_{N_ℓ}) entry.

M_{W_R}	M_{N_ℓ}	Obs.	Exp.	Acc.	M_{W_R}	M_{N_ℓ}	Obs.	Exp.	Acc.
2600	100	136	98.1	0.021 ± 0.225	2700	100	134	94.6	0.023 ± 0.236
2600	200	13.3	9.58	0.115 ± 0.101	2700	200	14.1	9.94	0.120 ± 0.109
2600	300	4.42	3.19	0.246 ± 0.053	2700	300	4.70	3.31	0.247 ± 0.058
2600	400	2.38	1.72	0.392 ± 0.031	2700	400	2.48	1.75	0.381 ± 0.034
2600	500	1.66	1.20	0.509 ± 0.019	2700	500	1.70	1.20	0.500 ± 0.021
2600	600	1.34	0.966	0.605 ± 0.014	2700	600	1.34	0.940	0.601 ± 0.015
2600	700	1.17	0.842	0.672 ± 0.011	2700	700	1.18	0.831	0.663 ± 0.012
2600	800	1.07	0.774	0.715 ± 0.010	2700	800	1.10	0.772	0.710 ± 0.010
2600	900	1.01	0.731	0.738 ± 0.010	2700	900	1.02	0.715	0.740 ± 0.009
2600	1000	0.965	0.698	0.765 ± 0.009	2700	1000	0.943	0.664	0.768 ± 0.009
2600	1100	0.931	0.672	0.778 ± 0.009	2700	1100	0.914	0.643	0.780 ± 0.011
2600	1200	0.937	0.677	0.799 ± 0.009	2700	1200	0.861	0.606	0.794 ± 0.009
2600	1300	0.909	0.657	0.803 ± 0.009	2700	1300	0.867	0.611	0.806 ± 0.009
2600	1400	0.903	0.652	0.808 ± 0.009	2700	1400	0.882	0.621	0.810 ± 0.013
2600	1500	0.899	0.649	0.812 ± 0.009	2700	1500	0.874	0.615	0.817 ± 0.010
2600	1600	0.888	0.641	0.821 ± 0.010	2700	1600	0.868	0.611	0.822 ± 0.010
2600	1700	0.887	0.641	0.822 ± 0.012	2700	1700	0.870	0.613	0.819 ± 0.019
2600	1800	0.891	0.644	0.818 ± 0.018	2700	1800	0.866	0.610	0.823 ± 0.011
2600	1900	0.894	0.646	0.816 ± 0.009	2700	1900	0.869	0.612	0.820 ± 0.009
2600	2000	0.899	0.650	0.810 ± 0.009	2700	2000	0.870	0.612	0.820 ± 0.008
2600	2100	0.905	0.654	0.805 ± 0.009	2700	2100	0.873	0.614	0.816 ± 0.011
2600	2200	0.917	0.663	0.794 ± 0.011	2700	2200	0.888	0.625	0.802 ± 0.009
2600	2300	0.940	0.679	0.775 ± 0.009	2700	2300	0.899	0.633	0.792 ± 0.013
2600	2400	0.988	0.714	0.737 ± 0.009	2700	2400	0.921	0.648	0.774 ± 0.008
2600	2500	1.10	0.792	0.664 ± 0.010	2700	2500	0.965	0.679	0.738 ± 0.009
					2700	2600	1.05	0.743	0.674 ± 0.010

Table A22: The 95% CL observed (Obs.) and expected (Exp.) exclusion limits (in fb) on the W_R production cross section times branching fraction for $W_R \rightarrow (ee + \mu\mu)jj$ as a function of W_R and N_ℓ mass (in GeV) for $2800 \leq M_{W_R} \leq 2900$ GeV. The signal acceptance (Acc.) is also included for each (M_{W_R}, M_{N_ℓ}) entry.

M_{W_R}	M_{N_ℓ}	Obs.	Exp.	Acc.	M_{W_R}	M_{N_ℓ}	Obs.	Exp.	Acc.
2800	100	143	101	0.025 ± 0.248	2900	100	140	100	0.027 ± 0.255
2800	200	16.5	11.6	0.123 ± 0.117	2900	200	18.1	12.9	0.123 ± 0.126
2800	300	5.46	3.86	0.245 ± 0.063	2900	300	5.90	4.21	0.236 ± 0.070
2800	400	2.81	1.99	0.372 ± 0.037	2900	400	2.97	2.12	0.377 ± 0.042
2800	500	1.86	1.32	0.494 ± 0.023	2900	500	1.91	1.37	0.485 ± 0.030
2800	600	1.45	1.02	0.589 ± 0.016	2900	600	1.46	1.04	0.582 ± 0.017
2800	700	1.22	0.861	0.655 ± 0.013	2900	700	1.22	0.873	0.647 ± 0.014
2800	800	1.12	0.793	0.699 ± 0.010	2900	800	1.08	0.769	0.692 ± 0.011
2800	900	1.01	0.713	0.731 ± 0.010	2900	900	0.986	0.704	0.729 ± 0.010
2800	1000	0.955	0.675	0.758 ± 0.011	2900	1000	0.930	0.664	0.751 ± 0.009
2800	1100	0.913	0.646	0.773 ± 0.011	2900	1100	0.886	0.632	0.772 ± 0.015
2800	1200	0.882	0.624	0.794 ± 0.010	2900	1200	0.853	0.609	0.790 ± 0.011
2800	1300	0.857	0.606	0.804 ± 0.009	2900	1300	0.827	0.590	0.805 ± 0.009
2800	1400	0.844	0.597	0.811 ± 0.009	2900	1400	0.810	0.578	0.811 ± 0.009
2800	1500	0.836	0.591	0.819 ± 0.009	2900	1500	0.800	0.571	0.814 ± 0.009
2800	1600	0.830	0.587	0.824 ± 0.009	2900	1600	0.791	0.565	0.823 ± 0.009
2800	1700	0.826	0.584	0.827 ± 0.009	2900	1700	0.791	0.565	0.823 ± 0.010
2800	1800	0.827	0.585	0.826 ± 0.009	2900	1800	0.783	0.559	0.831 ± 0.017
2800	1900	0.829	0.586	0.824 ± 0.009	2900	1900	0.785	0.561	0.829 ± 0.010
2800	2000	0.830	0.587	0.823 ± 0.009	2900	2000	0.782	0.559	0.831 ± 0.021
2800	2100	0.832	0.588	0.821 ± 0.009	2900	2100	0.797	0.569	0.816 ± 0.009
2800	2200	0.843	0.596	0.810 ± 0.009	2900	2200	0.792	0.565	0.821 ± 0.010
2800	2300	0.850	0.601	0.803 ± 0.009	2900	2300	0.798	0.570	0.815 ± 0.010
2800	2400	0.857	0.606	0.796 ± 0.009	2900	2400	0.805	0.575	0.808 ± 0.011
2800	2500	0.879	0.622	0.776 ± 0.008	2900	2500	0.814	0.581	0.798 ± 0.009
2800	2600	0.921	0.651	0.741 ± 0.011	2900	2600	0.838	0.598	0.776 ± 0.010
2800	2700	1.01	0.711	0.678 ± 0.010	2900	2700	0.876	0.625	0.742 ± 0.009
					2900	2800	0.947	0.676	0.686 ± 0.013

Table A23: The 95% CL observed (Obs.) and expected (Exp.) exclusion limits (in fb) on the W_R production cross section times branching fraction for $W_R \rightarrow (ee + \mu\mu)jj$ as a function of W_R and N_ℓ mass (in GeV) for $3000 \leq M_{W_R} \leq 3100$ GeV. The signal acceptance (Acc.) is also included for each (M_{W_R}, M_{N_ℓ}) entry.

M_{W_R}	M_{N_ℓ}	Obs.	Exp.	Acc.	M_{W_R}	M_{N_ℓ}	Obs.	Exp.	Acc.
3000	100	137	99.7	0.027 ± 0.264	3100	100	141	103	0.032 ± 0.269
3000	200	20.3	14.7	0.124 ± 0.135	3100	200	23.0	16.7	0.137 ± 0.142
3000	300	6.40	4.66	0.245 ± 0.078	3100	300	7.33	5.32	0.250 ± 0.086
3000	400	3.21	2.33	0.369 ± 0.048	3100	400	3.53	2.56	0.373 ± 0.054
3000	500	2.04	1.49	0.482 ± 0.030	3100	500	2.24	1.63	0.475 ± 0.034
3000	600	1.52	1.10	0.573 ± 0.019	3100	600	1.63	1.18	0.565 ± 0.022
3000	700	1.25	0.908	0.637 ± 0.014	3100	700	1.32	0.959	0.634 ± 0.018
3000	800	1.09	0.796	0.685 ± 0.012	3100	800	1.14	0.827	0.685 ± 0.012
3000	900	0.993	0.722	0.721 ± 0.011	3100	900	1.02	0.744	0.724 ± 0.012
3000	1000	0.928	0.675	0.757 ± 0.010	3100	1000	0.952	0.691	0.745 ± 0.010
3000	1100	0.879	0.640	0.773 ± 0.011	3100	1100	0.893	0.648	0.768 ± 0.011
3000	1200	0.845	0.614	0.785 ± 0.012	3100	1200	0.857	0.622	0.787 ± 0.016
3000	1300	0.818	0.595	0.795 ± 0.012	3100	1300	0.827	0.600	0.798 ± 0.013
3000	1400	0.797	0.579	0.809 ± 0.011	3100	1400	0.799	0.580	0.809 ± 0.020
3000	1500	0.779	0.567	0.820 ± 0.009	3100	1500	0.779	0.565	0.812 ± 0.010
3000	1600	0.775	0.564	0.823 ± 0.010	3100	1600	0.772	0.560	0.823 ± 0.017
3000	1700	0.769	0.560	0.829 ± 0.010	3100	1700	0.765	0.556	0.829 ± 0.010
3000	1800	0.771	0.561	0.827 ± 0.011	3100	1800	0.765	0.555	0.829 ± 0.017
3000	1900	0.771	0.561	0.827 ± 0.013	3100	1900	0.765	0.555	0.828 ± 0.011
3000	2000	0.766	0.557	0.833 ± 0.016	3100	2000	0.760	0.552	0.834 ± 0.011
3000	2100	0.767	0.558	0.831 ± 0.009	3100	2100	0.765	0.555	0.828 ± 0.024
3000	2200	0.774	0.563	0.823 ± 0.022	3100	2200	0.762	0.554	0.831 ± 0.012
3000	2300	0.773	0.563	0.824 ± 0.014	3100	2300	0.765	0.556	0.827 ± 0.011
3000	2400	0.779	0.567	0.818 ± 0.010	3100	2400	0.770	0.559	0.822 ± 0.009
3000	2500	0.788	0.573	0.808 ± 0.011	3100	2500	0.777	0.564	0.814 ± 0.009
3000	2600	0.798	0.581	0.798 ± 0.009	3100	2600	0.782	0.567	0.810 ± 0.009
3000	2700	0.814	0.592	0.782 ± 0.009	3100	2700	0.792	0.575	0.799 ± 0.010
3000	2800	0.853	0.621	0.746 ± 0.009	3100	2800	0.812	0.590	0.779 ± 0.009
3000	2900	0.923	0.672	0.689 ± 0.013	3100	2900	0.845	0.613	0.749 ± 0.009
					3100	3000	0.915	0.664	0.692 ± 0.013

Table A24: The 95% CL observed (Obs.) and expected (Exp.) exclusion limits (in fb) on the W_R production cross section times branching fraction for $W_R \rightarrow (ee + \mu\mu)jj$ as a function of W_R and N_ℓ mass (in GeV) for $M_{W_R} = 3200$ GeV. The signal acceptance (Acc.) is also included for each (M_{W_R}, M_{N_ℓ}) entry.

M_{W_R}	M_{N_ℓ}	Obs.	Exp.	Acc.
3200	100	144	104	0.035 ± 0.274
3200	200	25.9	18.7	0.139 ± 0.147
3200	300	8.16	5.90	0.265 ± 0.091
3200	400	3.98	2.88	0.376 ± 0.059
3200	500	2.46	1.78	0.471 ± 0.041
3200	600	1.77	1.28	0.560 ± 0.025
3200	700	1.41	1.02	0.626 ± 0.019
3200	800	1.20	0.871	0.679 ± 0.014
3200	900	1.07	0.772	0.712 ± 0.016
3200	1000	0.983	0.711	0.741 ± 0.012
3200	1100	0.920	0.665	0.768 ± 0.016
3200	1200	0.870	0.629	0.781 ± 0.010
3200	1300	0.838	0.606	0.795 ± 0.016
3200	1400	0.809	0.585	0.804 ± 0.013
3200	1500	0.785	0.568	0.813 ± 0.011
3200	1600	0.769	0.556	0.823 ± 0.010
3200	1700	0.767	0.555	0.824 ± 0.016
3200	1800	0.760	0.550	0.831 ± 0.013
3200	1900	0.758	0.548	0.832 ± 0.016
3200	2000	0.756	0.547	0.834 ± 0.020
3200	2100	0.762	0.551	0.828 ± 0.010
3200	2200	0.756	0.547	0.835 ± 0.013
3200	2300	0.762	0.551	0.829 ± 0.011
3200	2400	0.765	0.553	0.825 ± 0.009
3200	2500	0.770	0.557	0.819 ± 0.010
3200	2600	0.775	0.560	0.814 ± 0.010
3200	2700	0.778	0.563	0.811 ± 0.013
3200	2800	0.791	0.572	0.797 ± 0.012
3200	2900	0.813	0.588	0.776 ± 0.013
3200	3000	0.837	0.605	0.753 ± 0.010
3200	3100	0.909	0.658	0.693 ± 0.024

B The CMS Collaboration

Yerevan Physics Institute, Yerevan, Armenia

V. Khachatryan, A.M. Sirunyan, A. Tumasyan

Institut für Hochenergiephysik der OeAW, Wien, Austria

W. Adam, T. Bergauer, M. Dragicevic, J. Erö, C. Fabjan¹, M. Friedl, R. Frühwirth¹, V.M. Ghete, C. Hartl, N. Hörmann, J. Hrubec, M. Jeitler¹, W. Kiesenhofer, V. Knünz, M. Krammer¹, I. Krätschmer, D. Liko, I. Mikulec, D. Rabady², B. Rahbaran, H. Rohringer, R. Schöfbeck, J. Strauss, A. Taurok, W. Treberer-Treberspurg, W. Waltenberger, C.-E. Wulz¹

National Centre for Particle and High Energy Physics, Minsk, Belarus

V. Mossolov, N. Shumeiko, J. Suarez Gonzalez

Universiteit Antwerpen, Antwerpen, Belgium

S. Alderweireldt, M. Bansal, S. Bansal, T. Cornelis, E.A. De Wolf, X. Janssen, A. Knutsson, S. Luyckx, S. Ochesanu, B. Roland, R. Rougny, M. Van De Klundert, H. Van Haevermaet, P. Van Mechelen, N. Van Remortel, A. Van Spilbeeck

Vrije Universiteit Brussel, Brussel, Belgium

F. Blekman, S. Blyweert, J. D'Hondt, N. Daci, N. Heracleous, J. Keaveney, S. Lowette, M. Maes, A. Olbrechts, Q. Python, D. Strom, S. Tavernier, W. Van Doninck, P. Van Mulders, G.P. Van Onsem, I. Vilella

Université Libre de Bruxelles, Bruxelles, Belgium

C. Caillol, B. Clerbaux, G. De Lentdecker, D. Dobur, L. Favart, A.P.R. Gay, A. Grebenyuk, A. Léonard, A. Mohammadi, L. Perniè², T. Reis, T. Seva, L. Thomas, C. Vander Velde, P. Vanlaer, J. Wang

Ghent University, Ghent, Belgium

V. Adler, K. Beernaert, L. Benucci, A. Cimmino, S. Costantini, S. Crucy, S. Dildick, A. Fagot, G. Garcia, J. McCartin, A.A. Ocampo Rios, D. Ryckbosch, S. Salva Diblen, M. Sigamani, N. Strobbe, F. Thyssen, M. Tytgat, E. Yazgan, N. Zaganidis

Université Catholique de Louvain, Louvain-la-Neuve, Belgium

S. Basesmez, C. Beluffi³, G. Bruno, R. Castello, A. Caudron, L. Ceard, G.G. Da Silveira, C. Delaere, T. du Pree, D. Favart, L. Forthomme, A. Giammanco⁴, J. Hollar, P. Jez, M. Komm, V. Lemaitre, C. Nuttens, D. Pagano, L. Perrini, A. Pin, K. Piotrkowski, A. Popov⁵, L. Quertenmont, M. Selvaggi, M. Vidal Marono, J.M. Vizan Garcia

Université de Mons, Mons, Belgium

N. Bely, T. Caebergs, E. Daubie, G.H. Hammad

Centro Brasileiro de Pesquisas Fisicas, Rio de Janeiro, Brazil

W.L. Aldá Júnior, G.A. Alves, L. Brito, M. Correa Martins Junior, M.E. Pol

Universidade do Estado do Rio de Janeiro, Rio de Janeiro, Brazil

W. Carvalho, J. Chinellato⁶, A. Custódio, E.M. Da Costa, D. De Jesus Damiao, C. De Oliveira Martins, S. Fonseca De Souza, H. Malbouisson, D. Matos Figueiredo, L. Mundim, H. Nogima, W.L. Prado Da Silva, J. Santaolalla, A. Santoro, A. Sznajder, E.J. Tonelli Manganote⁶, A. Vilela Pereira

Universidade Estadual Paulista ^a, Universidade Federal do ABC ^b, São Paulo, Brazil

C.A. Bernardes^b, T.R. Fernandez Perez Tomei^a, E.M. Gregores^b, P.G. Mercadante^b, S.F. Novaes^a, Sandra S. Padula^a

Institute for Nuclear Research and Nuclear Energy, Sofia, Bulgaria

A. Aleksandrov, V. Genchev², P. Iaydjiev, A. Marinov, S. Piperov, M. Rodozov, G. Sultanov, M. Vutova

University of Sofia, Sofia, Bulgaria

A. Dimitrov, I. Glushkov, R. Hadjiiska, V. Kozhuharov, L. Litov, B. Pavlov, P. Petkov

Institute of High Energy Physics, Beijing, China

J.G. Bian, G.M. Chen, H.S. Chen, M. Chen, R. Du, C.H. Jiang, D. Liang, S. Liang, R. Plestina⁷, J. Tao, X. Wang, Z. Wang

State Key Laboratory of Nuclear Physics and Technology, Peking University, Beijing, China

C. Asawatangtrakuldee, Y. Ban, Y. Guo, Q. Li, W. Li, S. Liu, Y. Mao, S.J. Qian, D. Wang, L. Zhang, W. Zou

Universidad de Los Andes, Bogota, Colombia

C. Avila, L.F. Chaparro Sierra, C. Florez, J.P. Gomez, B. Gomez Moreno, J.C. Sanabria

Technical University of Split, Split, Croatia

N. Godinovic, D. Lelas, D. Polic, I. Puljak

University of Split, Split, Croatia

Z. Antunovic, M. Kovac

Institute Rudjer Boskovic, Zagreb, Croatia

V. Brigljevic, K. Kadija, J. Luetic, D. Mekterovic, L. Sudic

University of Cyprus, Nicosia, Cyprus

A. Attikis, G. Mavromanolakis, J. Mousa, C. Nicolaou, F. Ptochos, P.A. Razis

Charles University, Prague, Czech Republic

M. Bodlak, M. Finger, M. Finger Jr.⁸

Academy of Scientific Research and Technology of the Arab Republic of Egypt, Egyptian Network of High Energy Physics, Cairo, Egypt

Y. Assran⁹, S. Elgammal¹⁰, M.A. Mahmoud¹¹, A. Radi^{10,12}

National Institute of Chemical Physics and Biophysics, Tallinn, Estonia

M. Kadastik, M. Murumaa, M. Raidal, A. Tiko

Department of Physics, University of Helsinki, Helsinki, Finland

P. Eerola, G. Fedi, M. Voutilainen

Helsinki Institute of Physics, Helsinki, Finland

J. Härkönen, V. Karimäki, R. Kinnunen, M.J. Kortelainen, T. Lampén, K. Lassila-Perini, S. Lehti, T. Lindén, P. Luukka, T. Mäenpää, T. Peltola, E. Tuominen, J. Tuominiemi, E. Tuovinen, L. Wendland

Lappeenranta University of Technology, Lappeenranta, Finland

T. Tuuva

DSM/IRFU, CEA/Saclay, Gif-sur-Yvette, France

M. Besancon, F. Couderc, M. Dejardin, D. Denegri, B. Fabbro, J.L. Faure, C. Favaro, F. Ferri, S. Ganjour, A. Givernaud, P. Gras, G. Hamel de Monchenault, P. Jarry, E. Locci, J. Malcles, J. Rander, A. Rosowsky, M. Titov

Laboratoire Leprince-Ringuet, Ecole Polytechnique, IN2P3-CNRS, Palaiseau, France

S. Baffioni, F. Beaudette, P. Busson, C. Charlot, T. Dahms, M. Dalchenko, L. Dobrzynski, N. Filipovic, A. Florent, R. Granier de Cassagnac, L. Mastrolorenzo, P. Miné, C. Mironov, I.N. Naranjo, M. Nguyen, C. Ochando, P. Paganini, R. Salerno, J.b. Sauvan, Y. Sirois, C. Veelken, Y. Yilmaz, A. Zabi

Institut Pluridisciplinaire Hubert Curien, Université de Strasbourg, Université de Haute Alsace Mulhouse, CNRS/IN2P3, Strasbourg, France

J.-L. Agram¹³, J. Andrea, A. Aubin, D. Bloch, J.-M. Brom, E.C. Chabert, C. Collard, E. Conte¹³, J.-C. Fontaine¹³, D. Gelé, U. Goerlach, C. Goetzmann, A.-C. Le Bihan, P. Van Hove

Centre de Calcul de l'Institut National de Physique Nucleaire et de Physique des Particules, CNRS/IN2P3, Villeurbanne, France

S. Gadrat

Université de Lyon, Université Claude Bernard Lyon 1, CNRS-IN2P3, Institut de Physique Nucléaire de Lyon, Villeurbanne, France

S. Beauceron, N. Beaupere, G. Boudoul², S. Brochet, C.A. Carrillo Montoya, J. Chasserat, R. Chierici, D. Contardo², P. Depasse, H. El Mamouni, J. Fan, J. Fay, S. Gascon, M. Gouzevitch, B. Ille, T. Kurca, M. Lethuillier, L. Mirabito, S. Perries, J.D. Ruiz Alvarez, D. Sabes, L. Sgandurra, V. Sordini, M. Vander Donckt, P. Verdier, S. Viret, H. Xiao

Institute of High Energy Physics and Informatization, Tbilisi State University, Tbilisi, Georgia

I. Bagaturia

RWTH Aachen University, I. Physikalisches Institut, Aachen, Germany

C. Autermann, S. Beranek, M. Bontenackels, M. Edelhoff, L. Feld, O. Hindrichs, K. Klein, A. Ostapchuk, A. Perieanu, F. Raupach, J. Sammet, S. Schael, H. Weber, B. Wittmer, V. Zhukov⁵

RWTH Aachen University, III. Physikalisches Institut A, Aachen, Germany

M. Ata, E. Dietz-Laursonn, D. Duchardt, M. Erdmann, R. Fischer, A. Güth, T. Hebbeker, C. Heidemann, K. Hoepfner, D. Klingebiel, S. Knutzen, P. Kreuzer, M. Merschmeyer, A. Meyer, P. Millet, M. Olschewski, K. Padeken, P. Papacz, H. Reithler, S.A. Schmitz, L. Sonnenschein, D. Teyssier, S. Thüer, M. Weber

RWTH Aachen University, III. Physikalisches Institut B, Aachen, Germany

V. Cherepanov, Y. Erdogan, G. Flügge, H. Geenen, M. Geisler, W. Haj Ahmad, F. Hoehle, B. Kargoll, T. Kress, Y. Kuessel, J. Lingemann², A. Nowack, I.M. Nugent, L. Perchalla, O. Pooth, A. Stahl

Deutsches Elektronen-Synchrotron, Hamburg, Germany

I. Asin, N. Bartosik, J. Behr, W. Behrenhoff, U. Behrens, A.J. Bell, M. Bergholz¹⁴, A. Bethani, K. Borras, A. Burgmeier, A. Cakir, L. Calligaris, A. Campbell, S. Choudhury, F. Costanza, C. Diez Pardos, S. Dooling, T. Dorland, G. Eckerlin, D. Eckstein, T. Eichhorn, G. Flucke, J. Garay Garcia, A. Geiser, P. Gunnellini, J. Hauk, G. Hellwig, M. Hempel, D. Horton, H. Jung, A. Kalogeropoulos, M. Kasemann, P. Katsas, J. Kieseler, C. Kleinwort, D. Krücker, W. Lange, J. Leonard, K. Lipka, A. Lobanov, W. Lohmann¹⁴, B. Lutz, R. Mankel, I. Marfin, I.-A. Melzer-Pellmann, A.B. Meyer, J. Mnich, A. Mussgiller, S. Naumann-Emme, A. Nayak, O. Novgorodova, F. Nowak, E. Ntomari, H. Perrey, D. Pitzl, R. Placakyte, A. Raspereza, P.M. Ribeiro Cipriano, E. Ron, M.Ö. Sahin, J. Salfeld-Nebgen, P. Saxena, R. Schmidt¹⁴, T. Schoerner-Sadenius, M. Schröder, C. Seitz, S. Spannagel, A.D.R. Vargas Trevino, R. Walsh, C. Wissing

University of Hamburg, Hamburg, Germany

M. Aldaya Martin, V. Blobel, M. Centis Vignali, A.r. Draeger, J. Erfle, E. Garutti, K. Goebel, M. Görner, J. Haller, M. Hoffmann, R.S. Höing, H. Kirschenmann, R. Klanner, R. Kogler, J. Lange, T. Lapsien, T. Lenz, I. Marchesini, J. Ott, T. Peiffer, N. Pietsch, T. Pöhlsen, D. Rathjens, C. Sander, H. Schettler, P. Schleper, E. Schlieckau, A. Schmidt, M. Seidel, J. Sibille¹⁵, V. Sola, H. Stadie, G. Steinbrück, D. Troendle, E. Usai, L. Vanelderen

Institut für Experimentelle Kernphysik, Karlsruhe, Germany

C. Barth, C. Baus, J. Berger, C. Böser, E. Butz, T. Chwalek, W. De Boer, A. Descroix, A. Dierlamm, M. Feindt, F. Frensch, M. Giffels, F. Hartmann², T. Hauth², U. Husemann, I. Katkov⁵, A. Kornmayer², E. Kuznetsova, P. Lobelle Pardo, M.U. Mozer, Th. Müller, A. Nürnberg, G. Quast, K. Rabbertz, F. Ratnikov, S. Röcker, H.J. Simonis, F.M. Stober, R. Ulrich, J. Wagner-Kuhr, S. Wayand, T. Weiler, R. Wolf

Institute of Nuclear and Particle Physics (INPP), NCSR Demokritos, Aghia Paraskevi, Greece

G. Anagnostou, G. Daskalakis, T. Gerasis, V.A. Giakoumopoulou, A. Kyriakis, D. Loukas, A. Markou, C. Markou, A. Psallidas, I. Topsis-Giotis

University of Athens, Athens, Greece

A. Panagiotou, N. Saoulidou, E. Stiliaris

University of Ioánnina, Ioánnina, Greece

X. Aslanoglou, I. Evangelou, G. Flouris, C. Foudas, P. Kokkas, N. Manthos, I. Papadopoulos, E. Paradas

Wigner Research Centre for Physics, Budapest, Hungary

G. Bencze, C. Hajdu, P. Hidas, D. Horvath¹⁶, F. Sikler, V. Veszpremi, G. Vesztergombi¹⁷, A.J. Zsigmond

Institute of Nuclear Research ATOMKI, Debrecen, Hungary

N. Beni, S. Czellar, J. Karancsi¹⁸, J. Molnar, J. Palinkas, Z. Szillasi

University of Debrecen, Debrecen, Hungary

P. Raics, Z.L. Trocsanyi, B. Ujvari

National Institute of Science Education and Research, Bhubaneswar, India

S.K. Swain

Panjab University, Chandigarh, India

S.B. Beri, V. Bhatnagar, N. Dhingra, R. Gupta, U. Bhawandeep, A.K. Kalsi, M. Kaur, M. Mittal, N. Nishu, J.B. Singh

University of Delhi, Delhi, India

Ashok Kumar, Arun Kumar, S. Ahuja, A. Bhardwaj, B.C. Choudhary, A. Kumar, S. Malhotra, M. Naimuddin, K. Ranjan, V. Sharma

Saha Institute of Nuclear Physics, Kolkata, India

S. Banerjee, S. Bhattacharya, K. Chatterjee, S. Dutta, B. Gomber, Sa. Jain, Sh. Jain, R. Khurana, A. Modak, S. Mukherjee, D. Roy, S. Sarkar, M. Sharan

Bhabha Atomic Research Centre, Mumbai, India

A. Abdulsalam, D. Dutta, S. Kailas, V. Kumar, A.K. Mohanty², L.M. Pant, P. Shukla, A. Topkar

Tata Institute of Fundamental Research, Mumbai, India

T. Aziz, S. Banerjee, S. Bhowmik¹⁹, R.M. Chatterjee, R.K. Dewanjee, S. Dugad, S. Ganguly,

S. Ghosh, M. Guchait, A. Gurtu²⁰, G. Kole, S. Kumar, M. Maity¹⁹, G. Majumder, K. Mazumdar, G.B. Mohanty, B. Parida, K. Sudhakar, N. Wickramage²¹

Institute for Research in Fundamental Sciences (IPM), Tehran, Iran

H. Bakhshiansohi, H. Behnamian, S.M. Etesami²², A. Fahim²³, R. Goldouzian, A. Jafari, M. Khakzad, M. Mohammadi Najafabadi, M. Naseri, S. Paktinat Mehdiabadi, B. Safarzadeh²⁴, M. Zeinali

University College Dublin, Dublin, Ireland

M. Felcini, M. Grunewald

INFN Sezione di Bari ^a, Università di Bari ^b, Politecnico di Bari ^c, Bari, Italy

M. Abbrescia^{a,b}, L. Barbone^{a,b}, C. Calabria^{a,b}, S.S. Chhibra^{a,b}, A. Colaleo^a, D. Creanza^{a,c}, N. De Filippis^{a,c}, M. De Palma^{a,b}, L. Fiore^a, G. Iaselli^{a,c}, G. Maggi^{a,c}, M. Maggi^a, S. My^{a,c}, S. Nuzzo^{a,b}, A. Pompili^{a,b}, G. Pugliese^{a,c}, R. Radogna^{a,b,2}, G. Selvaggi^{a,b}, L. Silvestris^{a,2}, G. Singh^{a,b}, R. Venditti^{a,b}, P. Verwilligen^a, G. Zito^a

INFN Sezione di Bologna ^a, Università di Bologna ^b, Bologna, Italy

G. Abbiendi^a, A.C. Benvenuti^a, D. Bonacorsi^{a,b}, S. Braibant-Giacomelli^{a,b}, L. Brigliadori^{a,b}, R. Campanini^{a,b}, P. Capiluppi^{a,b}, A. Castro^{a,b}, F.R. Cavallo^a, G. Codispoti^{a,b}, M. Cuffiani^{a,b}, G.M. Dallavalle^a, F. Fabbri^a, A. Fanfani^{a,b}, D. Fasanella^{a,b}, P. Giacomelli^a, C. Grandi^a, L. Guiducci^{a,b}, S. Marcellini^a, G. Masetti^{a,2}, A. Montanari^a, F.L. Navarria^{a,b}, A. Perrotta^a, F. Primavera^{a,b}, A.M. Rossi^{a,b}, T. Rovelli^{a,b}, G.P. Siroli^{a,b}, N. Tosi^{a,b}, R. Travaglini^{a,b}

INFN Sezione di Catania ^a, Università di Catania ^b, CSFNSM ^c, Catania, Italy

S. Albergo^{a,b}, G. Cappello^a, M. Chiorboli^{a,b}, S. Costa^{a,b}, F. Giordano^{a,c,2}, R. Potenza^{a,b}, A. Tricomi^{a,b}, C. Tuve^{a,b}

INFN Sezione di Firenze ^a, Università di Firenze ^b, Firenze, Italy

G. Barbagli^a, V. Ciulli^{a,b}, C. Civinini^a, R. D'Alessandro^{a,b}, E. Focardi^{a,b}, E. Gallo^a, S. Gonzi^{a,b}, V. Gori^{a,b,2}, P. Lenzi^{a,b}, M. Meschini^a, S. Paoletti^a, G. Sguazzoni^a, A. Tropiano^{a,b}

INFN Laboratori Nazionali di Frascati, Frascati, Italy

L. Benussi, S. Bianco, F. Fabbri, D. Piccolo

INFN Sezione di Genova ^a, Università di Genova ^b, Genova, Italy

F. Ferro^a, M. Lo Vetere^{a,b}, E. Robutti^a, S. Tosi^{a,b}

INFN Sezione di Milano-Bicocca ^a, Università di Milano-Bicocca ^b, Milano, Italy

M.E. Dinardo^{a,b}, P. Dini^a, S. Fiorendi^{a,b,2}, S. Gennai^{a,2}, R. Gerosa², A. Ghezzi^{a,b}, P. Govoni^{a,b}, M.T. Lucchini^{a,b,2}, S. Malvezzi^a, R.A. Manzoni^{a,b}, A. Martelli^{a,b}, B. Marzocchi, D. Menasce^a, L. Moroni^a, M. Paganoni^{a,b}, S. Ragazzi^{a,b}, N. Redaelli^a, T. Tabarelli de Fatis^{a,b}

INFN Sezione di Napoli ^a, Università di Napoli 'Federico II' ^b, Università della Basilicata (Potenza) ^c, Università G. Marconi (Roma) ^d, Napoli, Italy

S. Buontempo^a, N. Cavallo^{a,c}, S. Di Guida^{a,d,2}, F. Fabozzi^{a,c}, A.O.M. Iorio^{a,b}, L. Lista^a, S. Meola^{a,d,2}, M. Merola^a, P. Paolucci^{a,2}

INFN Sezione di Padova ^a, Università di Padova ^b, Università di Trento (Trento) ^c, Padova, Italy

P. Azzi^a, N. Bacchetta^a, D. Bisello^{a,b}, A. Branca^{a,b}, R. Carlin^{a,b}, P. Checchia^a, M. Dall'Osso^{a,b}, T. Dorigo^a, M. Galanti^{a,b}, F. Gasparini^{a,b}, U. Gasparini^{a,b}, P. Giubilato^{a,b}, F. Gonella^a, A. Gozzelino^a, K. Kanishchev^{a,c}, S. Lacaprara^a, M. Margoni^{a,b}, A.T. Meneguzzo^{a,b}, F. Montecassiano^a, J. Pazzini^{a,b}, N. Pozzobon^{a,b}, P. Ronchese^{a,b}, F. Simonetto^{a,b}, E. Torassa^a, M. Tosi^{a,b}, P. Zotto^{a,b}, A. Zucchetta^{a,b}

INFN Sezione di Pavia ^a, Università di Pavia ^b, Pavia, ItalyM. Gabusi^{a,b}, S.P. Ratti^{a,b}, C. Riccardi^{a,b}, P. Salvini^a, P. Vitulo^{a,b}**INFN Sezione di Perugia ^a, Università di Perugia ^b, Perugia, Italy**M. Biasini^{a,b}, G.M. Bilei^a, D. Ciangottini^{a,b}, L. Fanò^{a,b}, P. Lariccia^{a,b}, G. Mantovani^{a,b}, M. Menichelli^a, F. Romeo^{a,b}, A. Saha^a, A. Santocchia^{a,b}, A. Spiezia^{a,b,2}**INFN Sezione di Pisa ^a, Università di Pisa ^b, Scuola Normale Superiore di Pisa ^c, Pisa, Italy**K. Androsov^{a,25}, P. Azzurri^a, G. Bagliesi^a, J. Bernardini^a, T. Boccali^a, G. Broccolo^{a,c}, R. Castaldi^a, M.A. Ciocci^{a,25}, R. Dell'Orso^a, S. Donato^{a,c}, F. Fiori^{a,c}, L. Foà^{a,c}, A. Giassi^a, M.T. Grippo^{a,25}, F. Ligabue^{a,c}, T. Lomtadze^a, L. Martini^{a,b}, A. Messineo^{a,b}, C.S. Moon^{a,26}, F. Palla^{a,2}, A. Rizzi^{a,b}, A. Savoy-Navarro^{a,27}, A.T. Serban^a, P. Spagnolo^a, P. Squillacioti^{a,25}, R. Tenchini^a, G. Tonelli^{a,b}, A. Venturi^a, P.G. Verdini^a, C. Vernieri^{a,c,2}**INFN Sezione di Roma ^a, Università di Roma ^b, Roma, Italy**L. Barone^{a,b}, F. Cavallari^a, D. Del Re^{a,b}, M. Diemoz^a, M. Grassi^{a,b}, C. Jorda^a, E. Longo^{a,b}, F. Margaroli^{a,b}, P. Meridiani^a, F. Micheli^{a,b,2}, S. Nourbakhsh^{a,b}, G. Organtini^{a,b}, R. Paramatti^a, S. Rahatlou^{a,b}, C. Rovelli^a, F. Santanastasio^{a,b}, L. Soffi^{a,b,2}, P. Traczyk^{a,b}**INFN Sezione di Torino ^a, Università di Torino ^b, Università del Piemonte Orientale (Novara) ^c, Torino, Italy**N. Amapane^{a,b}, R. Arcidiacono^{a,c}, S. Argiro^{a,b,2}, M. Arneodo^{a,c}, R. Bellan^{a,b}, C. Biino^a, N. Cartiglia^a, S. Casasso^{a,b,2}, M. Costa^{a,b}, A. Degano^{a,b}, N. Demaria^a, L. Finco^{a,b}, C. Mariotti^a, S. Maselli^a, E. Migliore^{a,b}, V. Monaco^{a,b}, M. Musich^a, M.M. Obertino^{a,c,2}, G. Ortona^{a,b}, L. Pacher^{a,b}, N. Pastrone^a, M. Pelliccioni^a, G.L. Pinna Angioni^{a,b}, A. Potenza^{a,b}, A. Romero^{a,b}, M. Ruspa^{a,c}, R. Sacchi^{a,b}, A. Solano^{a,b}, A. Staiano^a, U. Tamponi^a**INFN Sezione di Trieste ^a, Università di Trieste ^b, Trieste, Italy**S. Belforte^a, V. Candelise^{a,b}, M. Casarsa^a, F. Cossutti^a, G. Della Ricca^{a,b}, B. Gobbo^a, C. La Licata^{a,b}, M. Marone^{a,b}, D. Montanino^{a,b}, A. Schizzi^{a,b,2}, T. Umer^{a,b}, A. Zanetti^a**Chonbuk National University, Chonju, Korea**

T.J. Kim

Kangwon National University, Chunchon, Korea

S. Chang, A. Kropivnitskaya, S.K. Nam

Kyungpook National University, Daegu, Korea

D.H. Kim, G.N. Kim, M.S. Kim, D.J. Kong, S. Lee, Y.D. Oh, H. Park, A. Sakharov, D.C. Son

Chonnam National University, Institute for Universe and Elementary Particles, Kwangju, Korea

J.Y. Kim, S. Song

Korea University, Seoul, Korea

S. Choi, D. Gyun, B. Hong, M. Jo, H. Kim, Y. Kim, B. Lee, K.S. Lee, S.K. Park, Y. Roh

University of Seoul, Seoul, Korea

M. Choi, J.H. Kim, I.C. Park, S. Park, G. Ryu, M.S. Ryu

Sungkyunkwan University, Suwon, Korea

Y. Choi, Y.K. Choi, J. Goh, D. Kim, E. Kwon, J. Lee, H. Seo, I. Yu

Vilnius University, Vilnius, Lithuania

A. Juodagalvis

National Centre for Particle Physics, Universiti Malaya, Kuala Lumpur, Malaysia

J.R. Komaragiri, M.A.B. Md Ali

Centro de Investigacion y de Estudios Avanzados del IPN, Mexico City, Mexico

H. Castilla-Valdez, E. De La Cruz-Burelo, I. Heredia-de La Cruz²⁸, R. Lopez-Fernandez, A. Sanchez-Hernandez

Universidad Iberoamericana, Mexico City, Mexico

S. Carrillo Moreno, F. Vazquez Valencia

Benemerita Universidad Autonoma de Puebla, Puebla, Mexico

I. Pedraza, H.A. Salazar Ibarguen

Universidad Autónoma de San Luis Potosí, San Luis Potosí, Mexico

E. Casimiro Linares, A. Morelos Pineda

University of Auckland, Auckland, New Zealand

D. Krofcheck

University of Canterbury, Christchurch, New Zealand

P.H. Butler, S. Reucroft

National Centre for Physics, Quaid-I-Azam University, Islamabad, Pakistan

A. Ahmad, M. Ahmad, Q. Hassan, H.R. Hoorani, S. Khalid, W.A. Khan, T. Khurshid, M.A. Shah, M. Shoaib

National Centre for Nuclear Research, Swierk, Poland

H. Bialkowska, M. Bluj, B. Boimska, T. Frueboes, M. Górski, M. Kazana, K. Nawrocki, K. Romanowska-Rybinska, M. Szleper, P. Zalewski

Institute of Experimental Physics, Faculty of Physics, University of Warsaw, Warsaw, Poland

G. Brona, K. Bunkowski, M. Cwiok, W. Dominik, K. Doroba, A. Kalinowski, M. Konecki, J. Krolikowski, M. Misiura, M. Olszewski, W. Wolszczak

Laboratório de Instrumentação e Física Experimental de Partículas, Lisboa, Portugal

P. Bargassa, C. Beirão Da Cruz E Silva, P. Faccioli, P.G. Ferreira Parracho, M. Gallinaro, F. Nguyen, J. Rodrigues Antunes, J. Seixas, J. Varela, P. Vischia

Joint Institute for Nuclear Research, Dubna, Russia

P. Bunin, M. Gavrilenko, I. Golutvin, A. Kamenev, V. Karjavin, V. Konoplyanikov, A. Lanev, A. Malakhov, V. Matveev²⁹, P. Moisenz, V. Palichik, V. Perelygin, M. Savina, S. Shmatov, S. Shulha, N. Skatchkov, V. Smirnov, A. Zarubin

Petersburg Nuclear Physics Institute, Gatchina (St. Petersburg), Russia

V. Golovtsov, Y. Ivanov, V. Kim³⁰, P. Levchenko, V. Murzin, V. Oreshkin, I. Smirnov, V. Sulimov, L. Uvarov, S. Vavilov, A. Vorobyev, An. Vorobyev

Institute for Nuclear Research, Moscow, Russia

Yu. Andreev, A. Dermenev, S. Gninenko, N. Golubev, M. Kirsanov, N. Krasnikov, A. Pashenkov, D. Tlisov, A. Toropin

Institute for Theoretical and Experimental Physics, Moscow, Russia

V. Epshteyn, V. Gavrilov, N. Lychkovskaya, V. Popov, G. Safronov, S. Semenov, A. Spiridonov, V. Stolin, E. Vlasov, A. Zhokin

P.N. Lebedev Physical Institute, Moscow, Russia

V. Andreev, M. Azarkin, I. Dremin, M. Kirakosyan, A. Leonidov, G. Mesyats, S.V. Rusakov, A. Vinogradov

Skobeltsyn Institute of Nuclear Physics, Lomonosov Moscow State University, Moscow, Russia

A. Belyaev, E. Boos, V. Bunichev, M. Dubinin³¹, L. Dudko, A. Ershov, A. Gribushin, V. Klyukhin, O. Kodolova, I. Lokhtin, S. Obraztsov, S. Petrushanko, V. Savrin

State Research Center of Russian Federation, Institute for High Energy Physics, Protvino, Russia

I. Azhgirey, I. Bayshev, S. Bitioukov, V. Kachanov, A. Kalinin, D. Konstantinov, V. Krychkin, V. Petrov, R. Ryutin, A. Sobol, L. Tourtchanovitch, S. Troshin, N. Tyurin, A. Uzunian, A. Volkov

University of Belgrade, Faculty of Physics and Vinca Institute of Nuclear Sciences, Belgrade, Serbia

P. Adzic³², M. Ekmedzic, J. Milosevic, V. Rekovic

Centro de Investigaciones Energéticas Medioambientales y Tecnológicas (CIEMAT), Madrid, Spain

J. Alcaraz Maestre, C. Battilana, E. Calvo, M. Cerrada, M. Chamizo Llatas, N. Colino, B. De La Cruz, A. Delgado Peris, D. Domínguez Vázquez, A. Escalante Del Valle, C. Fernandez Bedoya, J.P. Fernández Ramos, J. Flix, M.C. Fouz, P. Garcia-Abia, O. Gonzalez Lopez, S. Goy Lopez, J.M. Hernandez, M.I. Josa, G. Merino, E. Navarro De Martino, A. Pérez-Calero Yzquierdo, J. Puerta Pelayo, A. Quintario Olmeda, I. Redondo, L. Romero, M.S. Soares

Universidad Autónoma de Madrid, Madrid, Spain

C. Albajar, J.F. de Trocóniz, M. Missiroli, D. Moran

Universidad de Oviedo, Oviedo, Spain

H. Brun, J. Cuevas, J. Fernandez Menendez, S. Folgueras, I. Gonzalez Caballero, L. Lloret Iglesias

Instituto de Física de Cantabria (IFCA), CSIC-Universidad de Cantabria, Santander, Spain

J.A. Brochero Cifuentes, I.J. Cabrillo, A. Calderon, J. Duarte Campderros, M. Fernandez, G. Gomez, A. Graziano, A. Lopez Virto, J. Marco, R. Marco, C. Martinez Rivero, F. Matorras, F.J. Munoz Sanchez, J. Piedra Gomez, T. Rodrigo, A.Y. Rodríguez-Marrero, A. Ruiz-Jimeno, L. Scodellaro, I. Vila, R. Vilar Cortabitarte

CERN, European Organization for Nuclear Research, Geneva, Switzerland

D. Abbaneo, E. Auffray, G. Auzinger, M. Bachtis, P. Baillon, A.H. Ball, D. Barney, A. Benaglia, J. Bendavid, L. Benhabib, J.F. Benitez, C. Bernet⁷, G. Bianchi, P. Bloch, A. Bocci, A. Bonato, O. Bondu, C. Botta, H. Breuker, T. Camporesi, G. Cerminara, S. Colafranceschi³³, M. D'Alfonso, D. d'Enterria, A. Dabrowski, A. David, F. De Guio, A. De Roeck, S. De Visscher, M. Dobson, M. Dordevic, N. Dupont-Sagorin, A. Elliott-Peisert, J. Eugster, G. Franzoni, W. Funk, D. Gigi, K. Gill, D. Giordano, M. Girone, F. Glege, R. Guida, S. Gundacker, M. Guthoff, J. Hammer, M. Hansen, P. Harris, J. Hegeman, V. Innocente, P. Janot, K. Kousouris, K. Krajczar, P. Lecoq, C. Lourenço, N. Magini, L. Malgeri, M. Mannelli, J. Marrouche, L. Masetti, F. Meijers, S. Mersi, E. Meschi, F. Moortgat, S. Morovic, M. Mulders, P. Musella, L. Orsini, L. Pape, E. Perez, L. Perrozzi, A. Petrilli, G. Petrucciani, A. Pfeiffer, M. Pierini, M. Pimiä, D. Piparo, M. Plagge, A. Racz, G. Rolandi³⁴, M. Rovere, H. Sakulin, C. Schäfer, C. Schwick, A. Sharma, P. Siegrist, P. Silva, M. Simon, P. Sphicas³⁵, D. Spiga, J. Steggemann, B. Stieger, M. Stoye, D. Treille, A. Tsiros, G.I. Veres¹⁷, J.R. Vlimant, N. Wardle, H.K. Wöhri, H. Wollny, W.D. Zeuner

Paul Scherrer Institut, Villigen, Switzerland

W. Bertl, K. Deiters, W. Erdmann, R. Horisberger, Q. Ingram, H.C. Kaestli, S. König, D. Kotlinski, U. Langenegger, D. Renker, T. Rohe

Institute for Particle Physics, ETH Zurich, Zurich, Switzerland

F. Bachmair, L. Bäni, L. Bianchini, P. Bortignon, M.A. Buchmann, B. Casal, N. Chanon, A. Deisher, G. Dissertori, M. Dittmar, M. Donegà, M. Dünser, P. Eller, C. Grab, D. Hits, W. Lustermann, B. Mangano, A.C. Marini, P. Martinez Ruiz del Arbol, D. Meister, N. Mohr, C. Nägeli³⁶, F. Nessi-Tedaldi, F. Pandolfi, F. Pauss, M. Peruzzi, M. Quittnat, L. Rebane, M. Rossini, A. Starodumov³⁷, M. Takahashi, K. Theofilatos, R. Wallny, H.A. Weber

Universität Zürich, Zurich, Switzerland

C. Amsler³⁸, M.F. Canelli, V. Chiochia, A. De Cosa, A. Hinzmann, T. Hreus, B. Kilminster, B. Millan Mejias, J. Ngadiuba, P. Robmann, F.J. Ronga, S. Taroni, M. Verzetti, Y. Yang

National Central University, Chung-Li, Taiwan

M. Cardaci, K.H. Chen, C. Ferro, C.M. Kuo, W. Lin, Y.J. Lu, R. Volpe, S.S. Yu

National Taiwan University (NTU), Taipei, Taiwan

P. Chang, Y.H. Chang, Y.W. Chang, Y. Chao, K.F. Chen, P.H. Chen, C. Dietz, U. Grundler, W.-S. Hou, K.Y. Kao, Y.J. Lei, Y.F. Liu, R.-S. Lu, D. Majumder, E. Petrakou, Y.M. Tzeng, R. Wilken

Chulalongkorn University, Faculty of Science, Department of Physics, Bangkok, Thailand

B. Asavapibhop, N. Srimanobhas, N. Suwonjandee

Cukurova University, Adana, Turkey

A. Adiguzel, M.N. Bakirci³⁹, S. Cerci⁴⁰, C. Dozen, I. Dumanoglu, E. Eskut, S. Girgis, G. Gokbulut, E. Gurpinar, I. Hos, E.E. Kangal, A. Kayis Topaksu, G. Onengut⁴¹, K. Ozdemir, S. Ozturk³⁹, A. Polatoz, K. Sogut⁴², D. Sunar Cerci⁴⁰, B. Tali⁴⁰, H. Topakli³⁹, M. Vergili

Middle East Technical University, Physics Department, Ankara, Turkey

I.V. Akin, B. Bilin, S. Bilmis, H. Gamsizkan, G. Karapinar⁴³, K. Ocalan, S. Sekmen, U.E. Surat, M. Yalvac, M. Zeyrek

Bogazici University, Istanbul, Turkey

E. Gülmez, B. Isildak⁴⁴, M. Kaya⁴⁵, O. Kaya⁴⁵

Istanbul Technical University, Istanbul, Turkey

H. Bahtiyar⁴⁶, E. Barlas, K. Cankocak, F.I. Vardarli, M. Yücel

National Scientific Center, Kharkov Institute of Physics and Technology, Kharkov, Ukraine

L. Levchuk, P. Sorokin

University of Bristol, Bristol, United Kingdom

J.J. Brooke, E. Clement, D. Cussans, H. Flacher, R. Frazier, J. Goldstein, M. Grimes, G.P. Heath, H.F. Heath, J. Jacob, L. Kreczko, C. Lucas, Z. Meng, D.M. Newbold⁴⁷, S. Paramesvaran, A. Poll, S. Senkin, V.J. Smith, T. Williams

Rutherford Appleton Laboratory, Didcot, United Kingdom

K.W. Bell, A. Belyaev⁴⁸, C. Brew, R.M. Brown, D.J.A. Cockerill, J.A. Coughlan, K. Harder, S. Harper, E. Olaiya, D. Petyt, C.H. Shepherd-Themistocleous, A. Thea, I.R. Tomalin, W.J. Womersley, S.D. Worm

Imperial College, London, United Kingdom

M. Baber, R. Bainbridge, O. Buchmuller, D. Burton, D. Colling, N. Cripps, M. Cutajar, P. Dauncey, G. Davies, M. Della Negra, P. Dunne, W. Ferguson, J. Fulcher, D. Futyan, A. Gilbert,

G. Hall, G. Iles, M. Jarvis, G. Karapostoli, M. Kenzie, R. Lane, R. Lucas⁴⁷, L. Lyons, A.-M. Magnan, S. Malik, B. Mathias, J. Nash, A. Nikitenko³⁷, J. Pela, M. Pesaresi, K. Petridis, D.M. Raymond, S. Rogerson, A. Rose, C. Seez, P. Sharp[†], A. Tapper, M. Vazquez Acosta, T. Virdee

Brunel University, Uxbridge, United Kingdom

J.E. Cole, P.R. Hobson, A. Khan, P. Kyberd, D. Leggat, D. Leslie, W. Martin, I.D. Reid, P. Symonds, L. Teodorescu, M. Turner

Baylor University, Waco, USA

J. Dittmann, K. Hatakeyama, A. Kasmi, H. Liu, T. Scarborough

The University of Alabama, Tuscaloosa, USA

O. Charaf, S.I. Cooper, C. Henderson, P. Rumerio

Boston University, Boston, USA

A. Avetisyan, T. Bose, C. Fantasia, A. Heister, P. Lawson, C. Richardson, J. Rohlf, D. Sperka, J. St. John, L. Sulak

Brown University, Providence, USA

J. Alimena, E. Berry, S. Bhattacharya, G. Christopher, D. Cutts, Z. Demiragli, A. Ferapontov, A. Garabedian, U. Heintz, G. Kukartsev, E. Laird, G. Landsberg, M. Luk, M. Narain, M. Segala, T. Sinthuprasith, T. Speer, J. Swanson

University of California, Davis, Davis, USA

R. Breedon, G. Breto, M. Calderon De La Barca Sanchez, S. Chauhan, M. Chertok, J. Conway, R. Conway, P.T. Cox, R. Erbacher, M. Gardner, W. Ko, R. Lander, T. Miceli, M. Mulhearn, D. Pellett, J. Pilot, F. Ricci-Tam, M. Searle, S. Shalhout, J. Smith, M. Squires, D. Stolp, M. Tripathi, S. Wilbur, R. Yohay

University of California, Los Angeles, USA

R. Cousins, P. Everaerts, C. Farrell, J. Hauser, M. Ignatenko, G. Rakness, E. Takasugi, V. Valuev, M. Weber

University of California, Riverside, Riverside, USA

J. Babb, K. Burt, R. Clare, J. Ellison, J.W. Gary, G. Hanson, J. Heilman, M. Ivova Rikova, P. Jandir, E. Kennedy, F. Lacroix, H. Liu, O.R. Long, A. Luthra, M. Malberti, H. Nguyen, M. Olmedo Negrete, A. Shrinivas, S. Sumowidagdo, S. Wimpenny

University of California, San Diego, La Jolla, USA

W. Andrews, J.G. Branson, G.B. Cerati, S. Cittolin, R.T. D'Agnolo, D. Evans, A. Holzner, R. Kelley, D. Klein, M. Lebourgeois, J. Letts, I. Macneill, D. Olivito, S. Padhi, C. Palmer, M. Pieri, M. Sani, V. Sharma, S. Simon, E. Sudano, M. Tadel, Y. Tu, A. Vartak, C. Welke, F. Würthwein, A. Yagil, J. Yoo

University of California, Santa Barbara, Santa Barbara, USA

D. Barge, J. Bradmiller-Feld, C. Campagnari, T. Danielson, A. Dishaw, K. Flowers, M. Franco Sevilla, P. Geffert, C. George, F. Golf, L. Gouskos, J. Incandela, C. Justus, N. Mccoll, J. Richman, D. Stuart, W. To, C. West

California Institute of Technology, Pasadena, USA

A. Apresyan, A. Bornheim, J. Bunn, Y. Chen, E. Di Marco, J. Duarte, A. Mott, H.B. Newman, C. Pena, C. Rogan, M. Spiropulu, V. Timciuc, R. Wilkinson, S. Xie, R.Y. Zhu

Carnegie Mellon University, Pittsburgh, USA

V. Azzolini, A. Calamba, T. Ferguson, Y. Iiyama, M. Paulini, J. Russ, H. Vogel, I. Vorobiev

University of Colorado at Boulder, Boulder, USA

J.P. Cumalat, W.T. Ford, A. Gaz, E. Luiggi Lopez, U. Nauenberg, J.G. Smith, K. Stenson, K.A. Ulmer, S.R. Wagner

Cornell University, Ithaca, USA

J. Alexander, A. Chatterjee, J. Chu, S. Dittmer, N. Eggert, N. Mirman, G. Nicolas Kaufman, J.R. Patterson, A. Ryd, E. Salvati, L. Skinnari, W. Sun, W.D. Teo, J. Thom, J. Thompson, J. Tucker, Y. Weng, L. Winstrom, P. Wittich

Fairfield University, Fairfield, USA

D. Winn

Fermi National Accelerator Laboratory, Batavia, USA

S. Abdullin, M. Albrow, J. Anderson, G. Apollinari, L.A.T. Bauerdick, A. Beretvas, J. Berryhill, P.C. Bhat, K. Burkett, J.N. Butler, H.W.K. Cheung, F. Chlebana, S. Cihangir, V.D. Elvira, I. Fisk, J. Freeman, Y. Gao, E. Gottschalk, L. Gray, D. Green, S. Grünendahl, O. Gutsche, J. Hanlon, D. Hare, R.M. Harris, J. Hirschauer, B. Hooberman, S. Jindariani, M. Johnson, U. Joshi, K. Kaadze, B. Klima, B. Kreis, S. Kwan, J. Linacre, D. Lincoln, R. Lipton, T. Liu, J. Lykken, K. Maeshima, J.M. Marraffino, V.I. Martinez Outschoorn, S. Maruyama, D. Mason, P. McBride, K. Mishra, S. Mrenna, Y. Musienko²⁹, S. Nahn, C. Newman-Holmes, V. O'Dell, O. Prokofyev, E. Sexton-Kennedy, S. Sharma, A. Soha, W.J. Spalding, L. Spiegel, L. Taylor, S. Tkaczyk, N.V. Tran, L. Uplegger, E.W. Vaandering, R. Vidal, A. Whitbeck, J. Whitmore, F. Yang

University of Florida, Gainesville, USA

D. Acosta, P. Avery, D. Bourilkov, M. Carver, T. Cheng, D. Curry, S. Das, M. De Gruttola, G.P. Di Giovanni, R.D. Field, M. Fisher, I.K. Furic, J. Hugon, J. Konigsberg, A. Korytov, T. Kypreos, J.F. Low, K. Matchev, P. Milenovic⁴⁹, G. Mitselmakher, L. Muniz, A. Rinkevicius, L. Shchutska, N. Skhirtladze, M. Snowball, J. Yelton, M. Zakaria

Florida International University, Miami, USA

S. Hewamanage, S. Linn, P. Markowitz, G. Martinez, J.L. Rodriguez

Florida State University, Tallahassee, USA

T. Adams, A. Askew, J. Bochenek, B. Diamond, J. Haas, S. Hagopian, V. Hagopian, K.F. Johnson, H. Prosper, V. Veeraraghavan, M. Weinberg

Florida Institute of Technology, Melbourne, USA

M.M. Baarmand, M. Hohlmann, H. Kalakhety, F. Yumiceva

University of Illinois at Chicago (UIC), Chicago, USA

M.R. Adams, L. Apanasevich, V.E. Bazterra, D. Berry, R.R. Betts, I. Bucinskaite, R. Cavanaugh, O. Evdokimov, L. Gauthier, C.E. Gerber, D.J. Hofman, S. Khalatyan, P. Kurt, D.H. Moon, C. O'Brien, C. Silkworth, P. Turner, N. Varelas

The University of Iowa, Iowa City, USA

E.A. Albayrak⁴⁶, B. Bilki⁵⁰, W. Clarida, K. Dilsiz, F. Duru, M. Haytmyradov, J.-P. Merlo, H. Mermerkaya⁵¹, A. Mestvirishvili, A. Moeller, J. Nachtman, H. Ogul, Y. Onel, F. Ozok⁴⁶, A. Penzo, R. Rahmat, S. Sen, P. Tan, E. Tiras, J. Wetzel, T. Yetkin⁵², K. Yi

Johns Hopkins University, Baltimore, USA

B.A. Barnett, B. Blumenfeld, S. Bolognesi, D. Fehling, A.V. Gritsan, P. Maksimovic, C. Martin, M. Swartz

The University of Kansas, Lawrence, USA

P. Baringer, A. Bean, G. Benelli, C. Bruner, J. Gray, R.P. Kenny III, M. Malek, M. Murray, D. Noonan, S. Sanders, J. Sekaric, R. Stringer, Q. Wang, J.S. Wood

Kansas State University, Manhattan, USA

A.F. Barfuss, I. Chakaberia, A. Ivanov, S. Khalil, M. Makouski, Y. Maravin, L.K. Saini, S. Shrestha, I. Svintradze

Lawrence Livermore National Laboratory, Livermore, USA

J. Gronberg, D. Lange, F. Rebassoo, D. Wright

University of Maryland, College Park, USA

A. Baden, A. Belloni, B. Calvert, S.C. Eno, J.A. Gomez, N.J. Hadley, R.G. Kellogg, T. Kolberg, Y. Lu, M. Marionneau, A.C. Mignerey, K. Pedro, A. Skuja, M.B. Tonjes, S.C. Tonwar

Massachusetts Institute of Technology, Cambridge, USA

A. Apyan, R. Barbieri, G. Bauer, W. Busza, I.A. Cali, M. Chan, L. Di Matteo, V. Dutta, G. Gomez Ceballos, M. Goncharov, D. Gulhan, M. Klute, Y.S. Lai, Y.-J. Lee, A. Levin, P.D. Luckey, T. Ma, C. Paus, D. Ralph, C. Roland, G. Roland, G.S.F. Stephans, F. Stöckli, K. Sumorok, D. Velicanu, J. Veverka, B. Wyslouch, M. Yang, M. Zanetti, V. Zhukova

University of Minnesota, Minneapolis, USA

B. Dahmes, A. Gude, S.C. Kao, K. Klapoetke, Y. Kubota, J. Mans, N. Pastika, R. Rusack, A. Singovsky, N. Tambe, J. Turkewitz

University of Mississippi, Oxford, USA

J.G. Acosta, S. Oliveros

University of Nebraska-Lincoln, Lincoln, USA

E. Avdeeva, K. Bloom, S. Bose, D.R. Claes, A. Dominguez, R. Gonzalez Suarez, J. Keller, D. Knowlton, I. Kravchenko, J. Lazo-Flores, S. Malik, F. Meier, G.R. Snow

State University of New York at Buffalo, Buffalo, USA

J. Dolen, A. Godshalk, I. Iashvili, A. Kharchilava, A. Kumar, S. Rappoccio

Northeastern University, Boston, USA

G. Alverson, E. Barberis, D. Baumgartel, M. Chasco, J. Haley, A. Massironi, D.M. Morse, D. Nash, T. Orimoto, D. Trocino, R.j. Wang, D. Wood, J. Zhang

Northwestern University, Evanston, USA

K.A. Hahn, A. Kubik, N. Mucia, N. Odell, B. Pollack, A. Pozdnyakov, M. Schmitt, S. Stoynev, K. Sung, M. Velasco, S. Won

University of Notre Dame, Notre Dame, USA

A. Brinkerhoff, K.M. Chan, A. Drozdetskiy, M. Hildreth, C. Jessop, D.J. Karmgard, N. Kellams, K. Lannon, W. Luo, S. Lynch, N. Marinelli, T. Pearson, M. Planer, R. Ruchti, N. Valls, M. Wayne, M. Wolf, A. Woodard

The Ohio State University, Columbus, USA

L. Antonelli, J. Brinson, B. Bylsma, L.S. Durkin, S. Flowers, C. Hill, R. Hughes, K. Kotov, T.Y. Ling, D. Puigh, M. Rodenburg, G. Smith, C. Vuosalo, B.L. Winer, H. Wolfe, H.W. Wulsin

Princeton University, Princeton, USA

O. Driga, P. Elmer, P. Hebda, A. Hunt, S.A. Koay, P. Lujan, D. Marlow, T. Medvedeva, M. Mooney, J. Olsen, P. Piroué, X. Quan, H. Saka, D. Stickland², C. Tully, J.S. Werner, S.C. Zenz, A. Zuranski

University of Puerto Rico, Mayaguez, USA

E. Brownson, H. Mendez, J.E. Ramirez Vargas

Purdue University, West Lafayette, USA

E. Alagoz, V.E. Barnes, D. Benedetti, G. Bolla, D. Bortoletto, M. De Mattia, Z. Hu, M.K. Jha, M. Jones, K. Jung, M. Kress, N. Leonardo, D. Lopes Pegna, V. Maroussov, P. Merkel, D.H. Miller, N. Neumeister, B.C. Radburn-Smith, X. Shi, I. Shipsey, D. Silvers, A. Svyatkovskiy, F. Wang, W. Xie, L. Xu, H.D. Yoo, J. Zablocki, Y. Zheng

Purdue University Calumet, Hammond, USA

N. Parashar, J. Stupak

Rice University, Houston, USA

A. Adair, B. Akgun, K.M. Ecklund, F.J.M. Geurts, W. Li, B. Michlin, B.P. Padley, R. Redjimi, J. Roberts, J. Zabel

University of Rochester, Rochester, USA

B. Betchart, A. Bodek, R. Covarelli, P. de Barbaro, R. Demina, Y. Eshaq, T. Ferbel, A. Garcia-Bellido, P. Goldenzweig, J. Han, A. Harel, A. Khukhunaishvili, G. Petrillo, D. Vishnevskiy

The Rockefeller University, New York, USA

R. Ciesielski, L. Demortier, K. Goulianos, G. Lungu, C. Mesropian

Rutgers, The State University of New Jersey, Piscataway, USA

S. Arora, A. Barker, J.P. Chou, C. Contreras-Campana, E. Contreras-Campana, D. Duggan, D. Ferencek, Y. Gershtein, R. Gray, E. Halkiadakis, D. Hidas, A. Lath, S. Panwalkar, M. Park, R. Patel, S. Salur, S. Schnetzer, S. Somalwar, R. Stone, S. Thomas, P. Thomassen, M. Walker

University of Tennessee, Knoxville, USA

K. Rose, S. Spanier, A. York

Texas A&M University, College Station, USA

O. Bouhali⁵³, R. Eusebi, W. Flanagan, J. Gilmore, T. Kamon⁵⁴, V. Khotilovich, V. Krutelyov, R. Montalvo, I. Osipenkov, Y. Pakhotin, A. Perloff, J. Roe, A. Rose, A. Safonov, T. Sakuma, I. Suarez, A. Tatarinov

Texas Tech University, Lubbock, USA

N. Akchurin, C. Cowden, J. Damgov, C. Dragoiu, P.R. Duderu, J. Faulkner, K. Kovitangoon, S. Kunori, S.W. Lee, T. Libeiro, I. Volobouev

Vanderbilt University, Nashville, USA

E. Appelt, A.G. Delannoy, S. Greene, A. Gurrola, W. Johns, C. Maguire, Y. Mao, A. Melo, M. Sharma, P. Sheldon, B. Snook, S. Tuo, J. Velkovska

University of Virginia, Charlottesville, USA

M.W. Arenton, S. Boutle, B. Cox, B. Francis, J. Goodell, R. Hirosky, A. Ledovskoy, H. Li, C. Lin, C. Neu, J. Wood

Wayne State University, Detroit, USA

R. Harr, P.E. Karchin, C. Kottachchi Kankanamge Don, P. Lamichhane, J. Sturdy

University of Wisconsin, Madison, USA

D.A. Belknap, D. Carlsmith, M. Cepeda, S. Dasu, S. Duric, E. Friis, R. Hall-Wilton, M. Herndon, A. Hervé, P. Klabbers, A. Lanaro, C. Lazaridis, A. Levine, R. Loveless, A. Mohapatra, I. Ojalvo, T. Perry, G.A. Pierro, G. Polese, I. Ross, T. Sarangi, A. Savin, W.H. Smith, N. Woods

†: Deceased

- 1: Also at Vienna University of Technology, Vienna, Austria
- 2: Also at CERN, European Organization for Nuclear Research, Geneva, Switzerland
- 3: Also at Institut Pluridisciplinaire Hubert Curien, Université de Strasbourg, Université de Haute Alsace Mulhouse, CNRS/IN2P3, Strasbourg, France
- 4: Also at National Institute of Chemical Physics and Biophysics, Tallinn, Estonia
- 5: Also at Skobeltsyn Institute of Nuclear Physics, Lomonosov Moscow State University, Moscow, Russia
- 6: Also at Universidade Estadual de Campinas, Campinas, Brazil
- 7: Also at Laboratoire Leprince-Ringuet, Ecole Polytechnique, IN2P3-CNRS, Palaiseau, France
- 8: Also at Joint Institute for Nuclear Research, Dubna, Russia
- 9: Also at Suez University, Suez, Egypt
- 10: Also at British University in Egypt, Cairo, Egypt
- 11: Also at Fayoum University, El-Fayoum, Egypt
- 12: Now at Ain Shams University, Cairo, Egypt
- 13: Also at Université de Haute Alsace, Mulhouse, France
- 14: Also at Brandenburg University of Technology, Cottbus, Germany
- 15: Also at The University of Kansas, Lawrence, USA
- 16: Also at Institute of Nuclear Research ATOMKI, Debrecen, Hungary
- 17: Also at Eötvös Loránd University, Budapest, Hungary
- 18: Also at University of Debrecen, Debrecen, Hungary
- 19: Also at University of Visva-Bharati, Santiniketan, India
- 20: Now at King Abdulaziz University, Jeddah, Saudi Arabia
- 21: Also at University of Ruhuna, Matara, Sri Lanka
- 22: Also at Isfahan University of Technology, Isfahan, Iran
- 23: Also at Sharif University of Technology, Tehran, Iran
- 24: Also at Plasma Physics Research Center, Science and Research Branch, Islamic Azad University, Tehran, Iran
- 25: Also at Università degli Studi di Siena, Siena, Italy
- 26: Also at Centre National de la Recherche Scientifique (CNRS) - IN2P3, Paris, France
- 27: Also at Purdue University, West Lafayette, USA
- 28: Also at Universidad Michoacana de San Nicolas de Hidalgo, Morelia, Mexico
- 29: Also at Institute for Nuclear Research, Moscow, Russia
- 30: Also at St. Petersburg State Polytechnical University, St. Petersburg, Russia
- 31: Also at California Institute of Technology, Pasadena, USA
- 32: Also at Faculty of Physics, University of Belgrade, Belgrade, Serbia
- 33: Also at Facoltà Ingegneria, Università di Roma, Roma, Italy
- 34: Also at Scuola Normale e Sezione dell'INFN, Pisa, Italy
- 35: Also at University of Athens, Athens, Greece
- 36: Also at Paul Scherrer Institut, Villigen, Switzerland
- 37: Also at Institute for Theoretical and Experimental Physics, Moscow, Russia
- 38: Also at Albert Einstein Center for Fundamental Physics, Bern, Switzerland
- 39: Also at Gaziosmanpasa University, Tokat, Turkey
- 40: Also at Adiyaman University, Adiyaman, Turkey
- 41: Also at Cag University, Mersin, Turkey
- 42: Also at Mersin University, Mersin, Turkey
- 43: Also at Izmir Institute of Technology, Izmir, Turkey
- 44: Also at Ozyegin University, Istanbul, Turkey
- 45: Also at Kafkas University, Kars, Turkey

46: Also at Mimar Sinan University, Istanbul, Istanbul, Turkey

47: Also at Rutherford Appleton Laboratory, Didcot, United Kingdom

48: Also at School of Physics and Astronomy, University of Southampton, Southampton, United Kingdom

49: Also at University of Belgrade, Faculty of Physics and Vinca Institute of Nuclear Sciences, Belgrade, Serbia

50: Also at Argonne National Laboratory, Argonne, USA

51: Also at Erzincan University, Erzincan, Turkey

52: Also at Yildiz Technical University, Istanbul, Turkey

53: Also at Texas A&M University at Qatar, Doha, Qatar

54: Also at Kyungpook National University, Daegu, Korea